1992

Modeling of Circulation and Transport in Terrebonne Bay, Louisiana and Its Implications for Oyster Harvesting Management.

Ellen J. Prager
Louisiana State University and Agricultural & Mechanical College

Order Number 9302921

Modeling of circulation and transport in Terrebonne Bay, Louisiana and its implications for oyster harvesting management

Prager, Ellen J., Ph.D.

The Louisiana State University and Agricultural and Mechanical Col., 1992

U·M·I
300 N. Zeeb Rd.
Ann Arbor, MI 48106

MODELING OF CIRCULATION AND TRANSPORT IN TERREBONNE BAY, LOUISIANA AND ITS IMPLICATIONS FOR OYSTER HARVESTING MANAGEMENT

A Dissertation

Submitted to the Graduate Faculty of
Louisiana State University and
Agricultural and Mechanical College
in partial fulfillment of the
requirements for the degree of
Doctor of Philosophy

in

The Department of Geology and Geophysics

by
Ellen J. Prager
B.A., Wesleyan University, 1984
M.S., University of Miami, 1987
August 1992

ACKNOWLEDGMENTS

I wish to thank Dr. Harry Roberts as my main advisor and as a source of optimistic support throughout my doctoral work. Thanks also goes to Dr. Bill Wiseman and Dr. Masamichi Inoue for their very helpful advice, insight, and encouragement as well as careful review of my dissertation manuscript. Additional appreciation is extended to Dr. Ralph Portier for his never ending energy and support, as well as to Dr. Steve Murray and Dr. Bill Herke for their comments on the manuscript.

Gratitude goes to the field support crew of the Coastal Studies Institute for their assistance in the field, as well as to David Wilensky for his computer wisdom and humor. Small funds provided by the Coastal Studies Institute are greatly appreciated, as is the use of data from the following agencies: Oyster-Water Monitoring Program, Office of Public Health, State of Louisiana (Mr. Ken Hemphill); Louisiana Office of State Climatology (Mr. John Grymes); and from the United States Geological Survey, Wetland's Loss Project, Contract #14-08-0001-23411.

Appreciation is extended to the staff and faculty of the Department of Geology and Geophysics for their assistance throughout my studies at Louisiana State University. My sincere thanks also goes to all of my friends who provided support, optimism, and especially humor during the more difficult periods. And finally, I must thank my family for their steadfast encouragement and friendship during my doctoral pursuit.

TABLE OF CONTENTS

LIST OF FIGURES

LIST OF TABLES

ABSTRACT

Contamination of oyster-rich waters in south Louisiana by sewage-related wastes is believed to occur on a seasonally varying basis, and pose a serious threat to both human welfare and the local economy. Fluctuations in the meteorologic and oceanographic conditions in the region are believed to be responsible for the variability observed in bacterial concentrations. To gain a better understanding of the relationship between transport processes, environmental forcing, and the potential for contamination, a combined program of in situ measurements and numerical modeling was conducted in the nearshore waters of Terrebonne Bay, Louisiana.

A finite element model based on the vertically integrated equations of motion and continuity was used to simulate flow under various environmental regimes. Wind, tides, and runoff were incorporated based on real-time measurements within the study area. Observations of large-scale circulation were used to calibrate and verify the ability of the model to realistically simulate flow. Lagrangian-type particle tracking was employed to specifically examine tidal advection and residual transport in the pollution-prone northwestern region of the bay.

Results indicate that the patterns of transport within the nearshore waters of Terrebonne Bay are highly complex and depend on the interactions of tides, wind, runoff, and changes in mean sea level within the bay. Residual flow of particulate materials within the bay is commonly seaward at a rate of 0.8 to 5.0

cm/s depending on location and environmental conditions occurring during the time of release. Even under the strongest of transport regimes, the residence time within the oyster-rich upper reaches of the bay appears to be on the order of 2 or more days. Rising sea level within the bay, daily landward advection by the incoming tide, and several wind/tide combinations produce transport patterns conducive to contamination. Consequently, the likelihood for contamination of oyster-rich waters is not a function of season or any one environmental parameter. Present management strategies for oyster harvesting are not supported by these results, and efforts towards more effective treatment of wastewater prior to discharge, and the use of depuration processes post-harvest are recommended.

CHAPTER 1

INTRODUCTION

The estuaries and bays along the northern Gulf Coast comprise one of the most productive and fertile environments worldwide. Approximately 20% of the United State's total fisheries are believed to come from within a narrow, 400 mile stretch along the Gulf coast, referred to as the "Fertile Fisheries Cresent" (Fig. 1; Gunter, 1963; 1967). Louisiana's entire coastline lies within this zone, and contains an estimated 41% of the Nation's wetlands. As a result of its highly productive coastal zone, the residents of south Louisiana rely heavily on its marine resources for both sustenance and economic revenue. However, as man continues to capitalize on Louisiana's fertile waters and coastal populations continue to grow, negative impacts on the environment are becoming increasingly apparent. Because of emphasis by the media, chemical spills and coastal erosion are the most widely recognized environmental problems along the Gulf Coast. However, recent publicity and concern has addressed another very serious problem affecting nearshore waters in the area. Water quality, marine productivity, and human health are being threatened daily by the effects of sewage discharge and polluted stormwater runoff. The release of poorly treated wastes and overflow from treatment facilities following heavy rains can cause contamination of oyster-growing

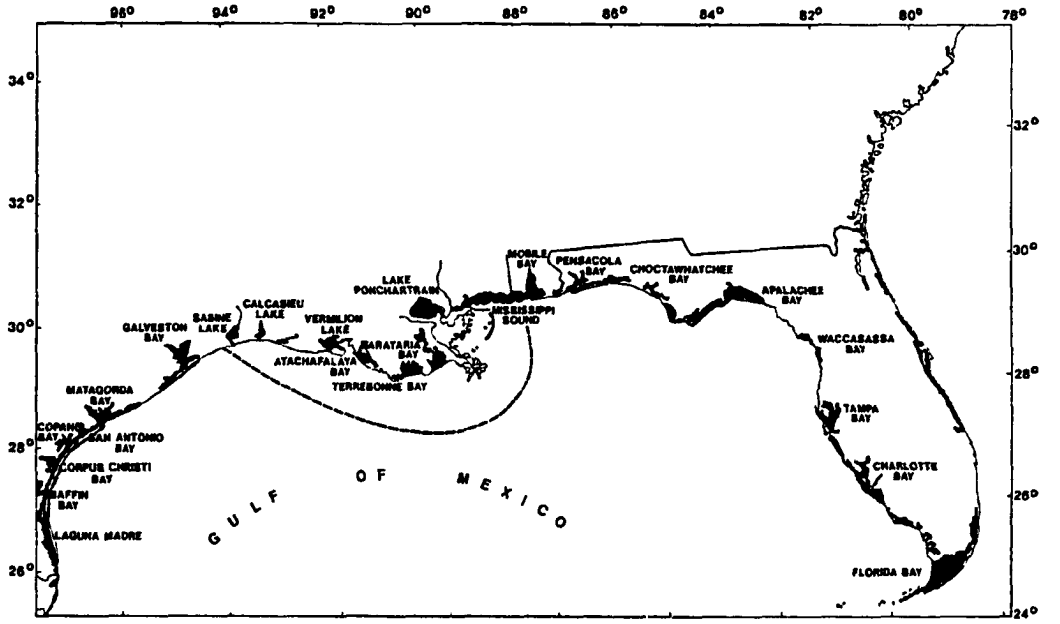

Figure 1: Bays along the Gulf Coast, the dashed line refers to the "Fertile Fisheries Crescent" (Gunter, 1967).

waters and has led to serious illness in those consuming tainted shellfish. With recognition of this problem, its continued threat, and the importance of nearshore oyster-beds, environmental management of estuarine waters in Louisiana has become a necessity. However, the ability of the State of Louisiana to effectively manage oyster-harvesting has been limited by the lack of knowledge regarding pollutant transport processes within Louisiana's coastal bay systems.

Sewage-related wastes enter nearshore waters primarily in suspension or adsorbed onto particulate material. Buoyancy and turbulence within the water column tend to prevent water-borne materials, such as sewage, from settling until the velocity of flow decreases to a point where the effects of gravity prevail. While wastes remain in suspension, filter-feeding organisms can extract bacteria and viruses associated with sewage, and over time accumulate them within their internal organs or muscle tissue. Though not necessarily harmful to the oyster, accumulated pathogens may act as a toxin to man when consumed uncooked as part of the host shellfish. Therefore, it is crucial to understand the pathways by which discharged wastes travel in oyster-inhabited waters to delineate probable areas of contamination.

Once discharged and in suspension, the principal factors controlling sewage transport and dispersal are the spatial and temporal patterns of water movement within the receiving water body. Particulate materials are advected by the main flow of water and may be dispersed due to spatial variations within the velocity field. Within estuaries, dispersion is primarily a function of

circulation driven by tidal interactions with bathymetry, wind-driven flow, and density differences between fresh and ocean water (Fischer, 1974). Within south Louisiana, patterns of nearshore water movement, particularly within coastal bays, are thought to be most strongly influenced by tides and wind, with additional forcing provided by freshwater inflow, and fluctuations in the coastal ocean (Murray, 1976; Kjerfve, 1975; Wiseman et. al., 1990). However, the relationship between these environmental factors and transport patterns within oyster-growing waters is not known.

The use of mathematical models to simulate flow has proven successful in numerous coastal bays (Leendertse, 1970; Wang and Connor, 1975; Christensen, 1983). When combined with a minimum of in situ measurements, numerical modeling techniques offer a cost-effective and accurate means of evaluating transport processes and residence times within nearshore waters. Additionally, these techniques can provide a better understanding of the interactions between environmental forcing mechanisms, such as tide, wind, and runoff, as well as the actual predictability of contamination by water-borne pollutants.

The objective of this study is to use numerical modeling techniques, calibrated and tested with real-time measurements, to simulate pollutant transport patterns in the highly productive, oyster-rich waters of a coastal bay in south Louisiana. Results from this effort will be used to evaluate present-day oyster-harvesting strategies and recommend adjustments in management practices as findings warrant. The research and results from this study will be described in three main chapters: 1) an introduction containing

historical and background information relative to the oyster-bed contamination problem in Louisiana's coastal waters, and a description of the area chosen for study, 2) a section on circulation modeling containing descriptions of the numerical model used, the input and calibration of the model, and the resulting simulated circulation patterns, as well as an examination of the model's accuracy as compared to in situ measurements, and lastly 3) a chapter detailing transport modeling methods and results, and the discussion of findings and their implications to oyster-harvesting management. The final section of this paper will provide the author's conclusions and recommendations for future directions in environmental management within Louisiana's coastal bay areas.

State of Louisiana's Shellfish Industry

The history of oyster harvesting in Louisiana dates back to the early French settlers in the 18th century. Since then, Louisiana has become the predominant supplier of oysters nationwide, with an estimated revenue from harvesting of 18 million dollars annually since 1981 (Gulf States Marine Fisheries Commission, unpub. manuscript). More than 1.3 million acres within Louisiana's coastal waters are leased and worked for the production of the eastern oyster (*Crassostrea virginica*). Unfortunately, within the last decade the oyster industry and even human welfare have been seriously threatened by sewage pollution. Ingestion of contaminated shellfish has caused outbreaks of hepatitis, gastroenteritis, and food poisoning (Sobsey et al., 1980). In 1982 approximately 500 cases of

oyster-associated viral gastroenteritis were reported in Louisiana (Gulf States Marine Fisheries Commission, unpub. manuscript). As a result of this outbreak at least 500,000 acres of productive oyster grounds in Terrebonne Parish (Fig. 2) were immediately closed. Analysis of water samples revealed that fecal coliform bacteria in the overlying waters, commonly used as a measure of sewage pollution, were above levels considered safe for consumption (Kilgen and Kilgen, 1990). Further studies in Terrebonne in 1983 found enteric viruses also present in waters overlying oyster reefs (Kilgen et al., 1985). In the fall of 1983 over 95% of the oyster-growing waters in Terrebonne Parish were closed to harvest again due to excessive levels of fecal coliform bacteria. Restrictions on harvesting also occurred in the fall of 1984 and winter of 1985. Although the winter months had historically exhibited peak oyster sales, due to contamination only the summer months were becoming safe for widespread harvesting. Local fisherman and the State began to take note; revenue from oyster sales was greatly diminishing.

The oyster, like other filter-feeding organisms, can concentrate bacteria and viruses from the surrounding water during normal feeding activities (Perkins et al., 1980). Though not normally hazardous to the oyster itself, when high bio-accumulation occurs and the oyster is consumed uncooked, serious illness in humans is likely (Berg, 1973). Following the 1982 contamination and widespread illness, a two part initiative was put forth by the State of Louisiana to study sewage pollution in its coastal waters. A water quality monitoring program was established in which oyster

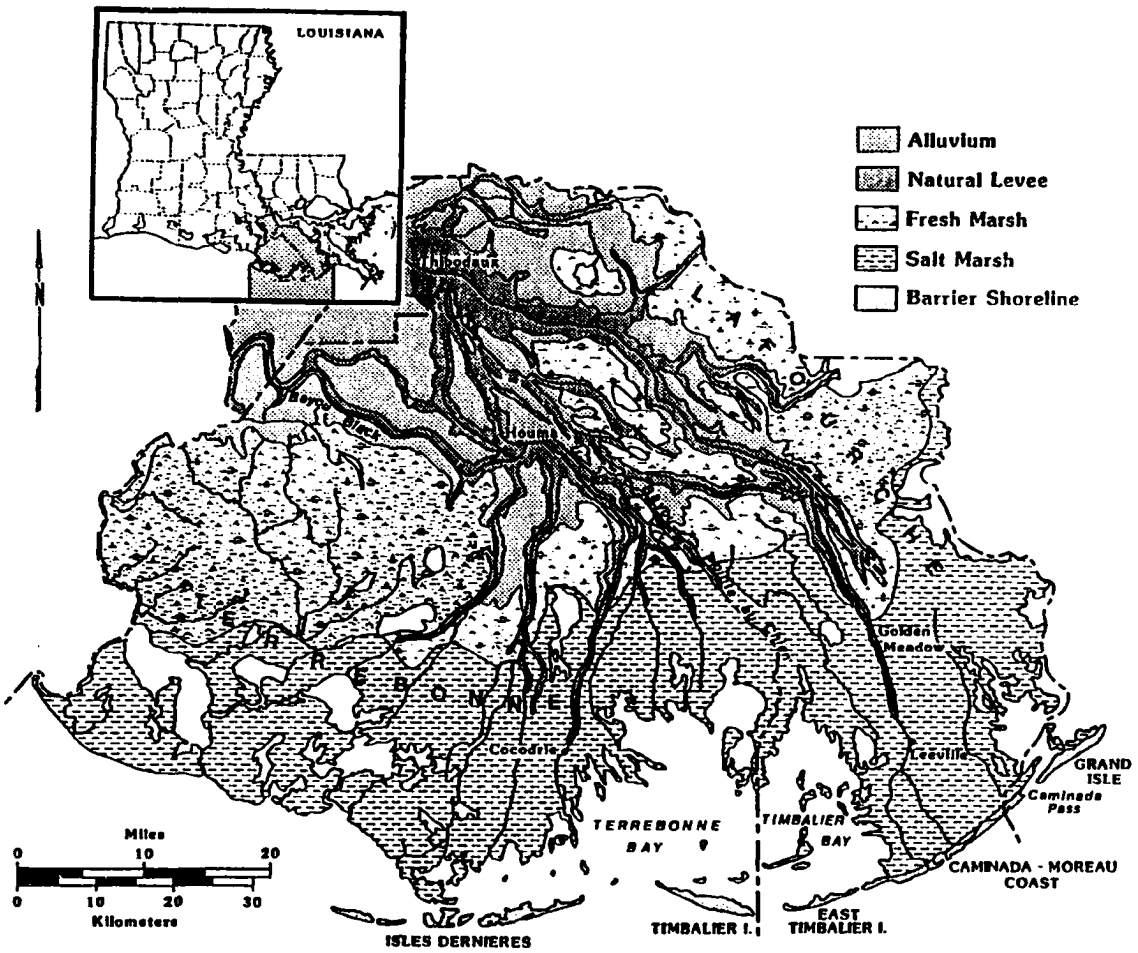

Figure 2: Location and description of the Terrebonne Parish area in south Louisiana.

growing waters would be regularly tested for fecal coliform levels and an initiative was made to fund basic research on the source of sewage pollution as well as the factors that control its variability. For over ten years the State has collected one sample per month in Terrebonne areas which are heavily harvested and sites of potential contamination (Fig. 3). At first, several stations were each tested continuously over a tidal cycle and many sites were monitored more frequently than once per month. But in more recent years, the sampling frequency has often become less than once per month. The underlying cause is probably a lack of funds and personnel, as well as the logistical difficulties in covering a large sampling region on as synoptic a time scale as possible. Due to inadequate funding and the complexity of the problem, monitoring programs and research have had limited success in understanding the contamination problem.

Whereas fecal coliform are used as an indicator of sewage pollution in both the monitoring program and research, it is necessary at this point to briefly discuss the advantages and disadvantages of this measure. Fecal coliform concentration is the most commonly accepted and used means of detecting near-source sewage contamination in water (Bonde, 1974; APHA, 1980). The National Shellfish Sanitation Program (NSSP) has established a standard of 14 MPN/100 ml (Most Probable Number) for shellfish harvesting waters. A threshold of 230 fecal coliforms/100 g of shellfish meat has also been given as a guide for safe consumption. Techniques used to measure fecal coliforms are both convenient and economical, and studies reveal a strong correlation between

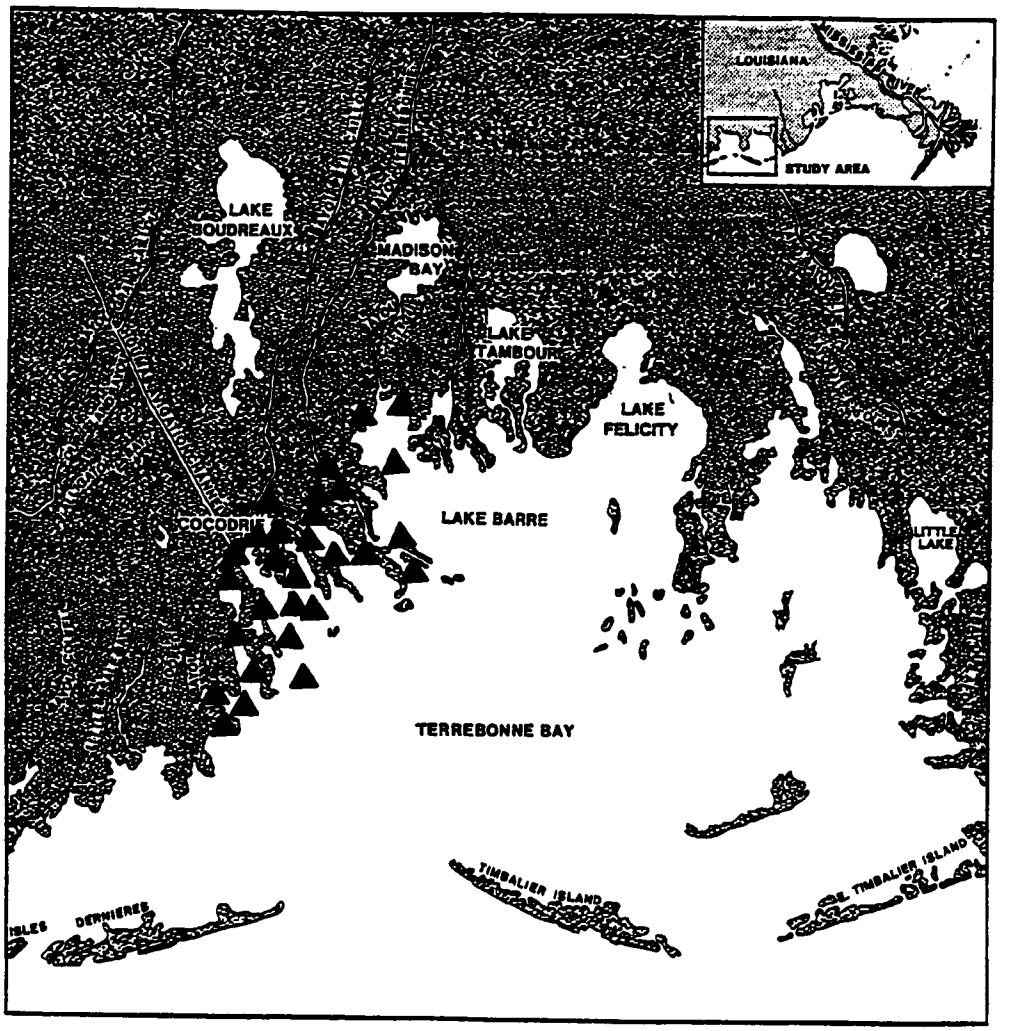

Figure 3: A portion of the sampling sites within the Terrebonne Bay area for The State of Louisiana oyster-water monitoring program.

moderate to excessive sewage pollution and fecal coliform levels (Metcalf, 1974). The disadvantages of using coliforms as an indicator include the lack of information provided regarding enteric viruses which may also be associated with sewage, and the inability of tests to distinguish between bacteria from human sewage and those which may occur naturally in coastal waters. Until more economical and efficient means are developed, fecal coliforms will continue to be the indicator of choice for the detection of sewage pollution in coastal waters.

Based on the statistical analysis of data from the State's monitoring program and the results of scientific research performed thus far, the following somewhat tentative conclusions have been reached (Kilgen and Kilgen, 1990). Pollution occurs as a result of both point and non-point sources such as domestic waste discharges, landfill and agricultural runoff, and stormwater drainage. There is a relationship between rainfall and the bacteriological quality of local waters, but the timing of event-increased concentrations of bacteria is not well understood. Specific weather patterns, particularly frontal gulf return, show a consistently positive correlation with high fecal coliform levels. Temperature consistently exhibits a negative correlation with coliform concentrations, however, the relationship between river stage or tidal phase and bacterial levels is poorly defined. No statistical differences occur in near-bottom versus surface water concentrations of coliform bacteria. Within Terrebonne Bay and the surrounding waters, both the northwest and northeast quadrants generally exhibit the worst intrusions of contaminated waters,

though seasonal trends are unclear. In general, the final outcome of the Kilgen and Kilgen report (1990) was that the bacteriological quality of oyster-growing waters is the product of interacting environmental factors, including tide, wind, river runoff, sewage discharge, and rainfall. Additionally, these forces seem to produce patterns that are unpredictable based on statistical analyses. Furthermore, the authors stated that predictive models based on statistical analysis of historical data, such as that conducted by the state, were inadequate for use in predicting coliform levels (Kilgen and Kilgen, 1990).

Based on these findings and gross trends in water quality provided by long-term monitoring (Fig. 4), the State has established the following management plan. The Louisiana Shellfish program is

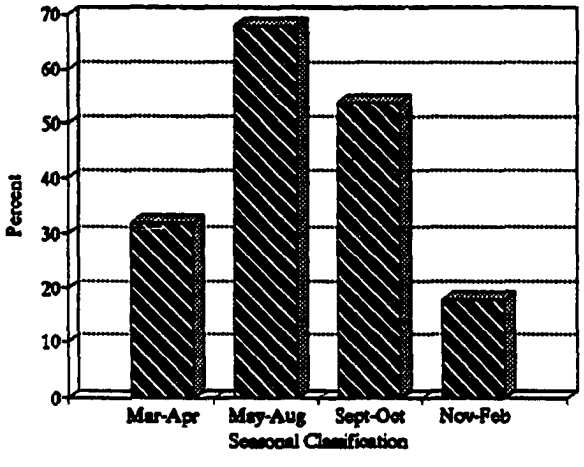

Figure 4: Percent stations with acceptable water quality based on the results of monitoring from 1980 - 1989, (Kilgen and Kilgen, 1990).

divided into four seasonal periods: 1) March 1 to April 30, 2) May 1 to August 31, 3) September 1 to October 31, and 4) November 1 to February 28. Using the results of statistical analyses over the last

decade, areas in which 10% of the samples consistently exceed the NSSP standard within a given season are closed to harvest during that season. The spatial extent of these restrictions is somewhat nebulous, defined by landforms which are recognizable by local fisherman (Figs. 5 - 6). Because data analyses show a trend toward higher coliform levels during the colder months of the year and enteric viruses are more persistent in cold water (Kilgen and Kilgen, 1990), harvesting is most restricted during the cold-water months (November - February). Because of their frequency within the winter, it is suspected that transport patterns resulting from cold-front passage may ultimately be responsible for the relatively high contamination levels observed during the cold-water months.

Where discharge of waters potentially containing sewage is strongly controlled by river stage, e.g., the Atchafalaya River, harvesting is managed on a conditional basis. This management plan has been in effect since 1984, and no outbreaks like that of 1982 have since been reported in Louisiana. However, contamination is still occurring as evidenced by high levels measured by the state (unpub. data, Louisiana Oyster Water Monitoring Program). Serious concerns by both scientists and the public exist regarding the safety of shellfish consumption, particularly in light of the ongoing illegal harvest of oysters from closed leases. Furthermore, the relationship between coliform bacteria as indicators and the true threat of illness from bacteria and enteric viruses in general remains poorly understood (Ellender et al., 1980; Cole et al., 1986). In order to further understand the problem several remaining questions must be addressed, 1) what is

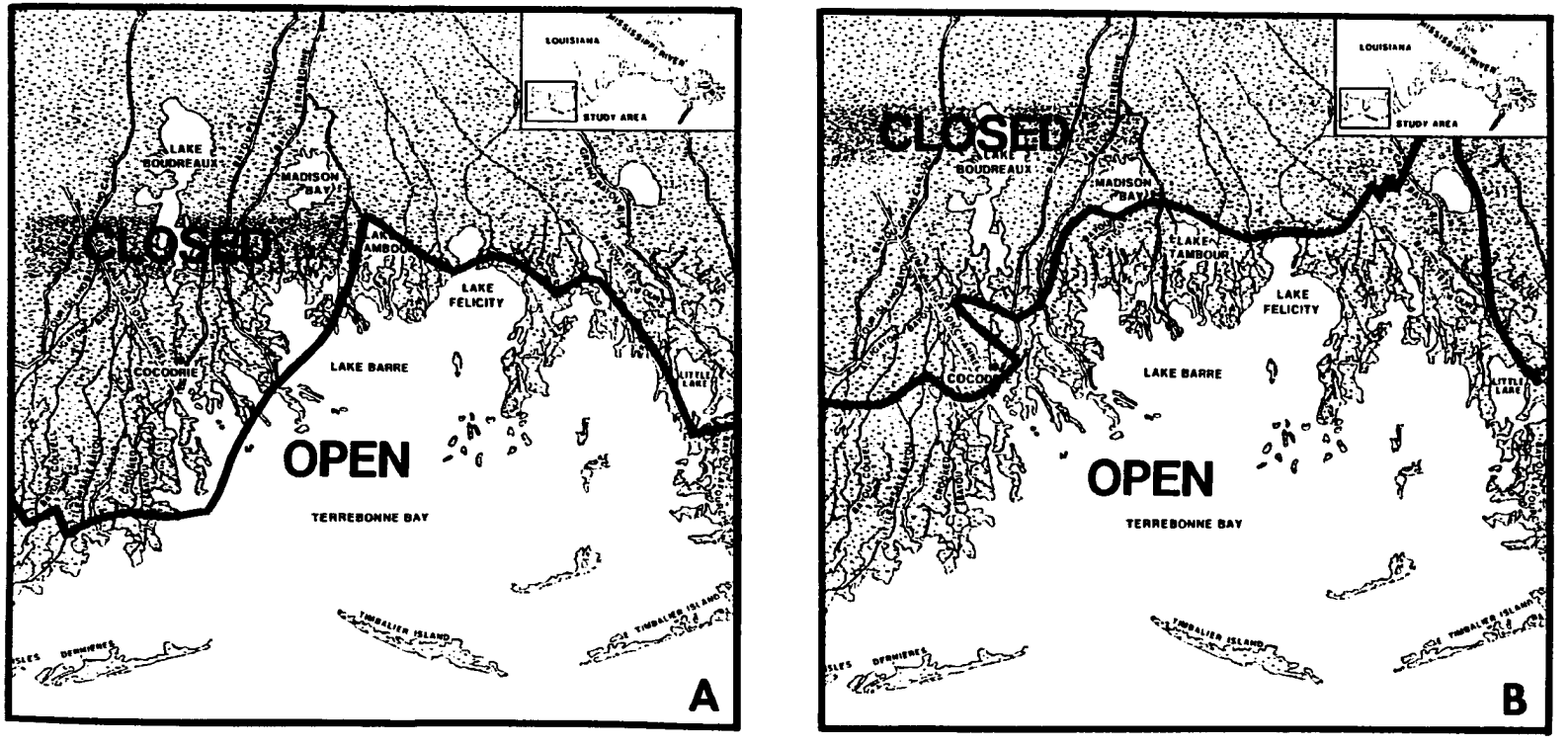

Figure 5: State restrictions on areas for oyster harvesting during (A) November through February and (B) March through April of 1990 (Kilgen and Kilgen, 1990).

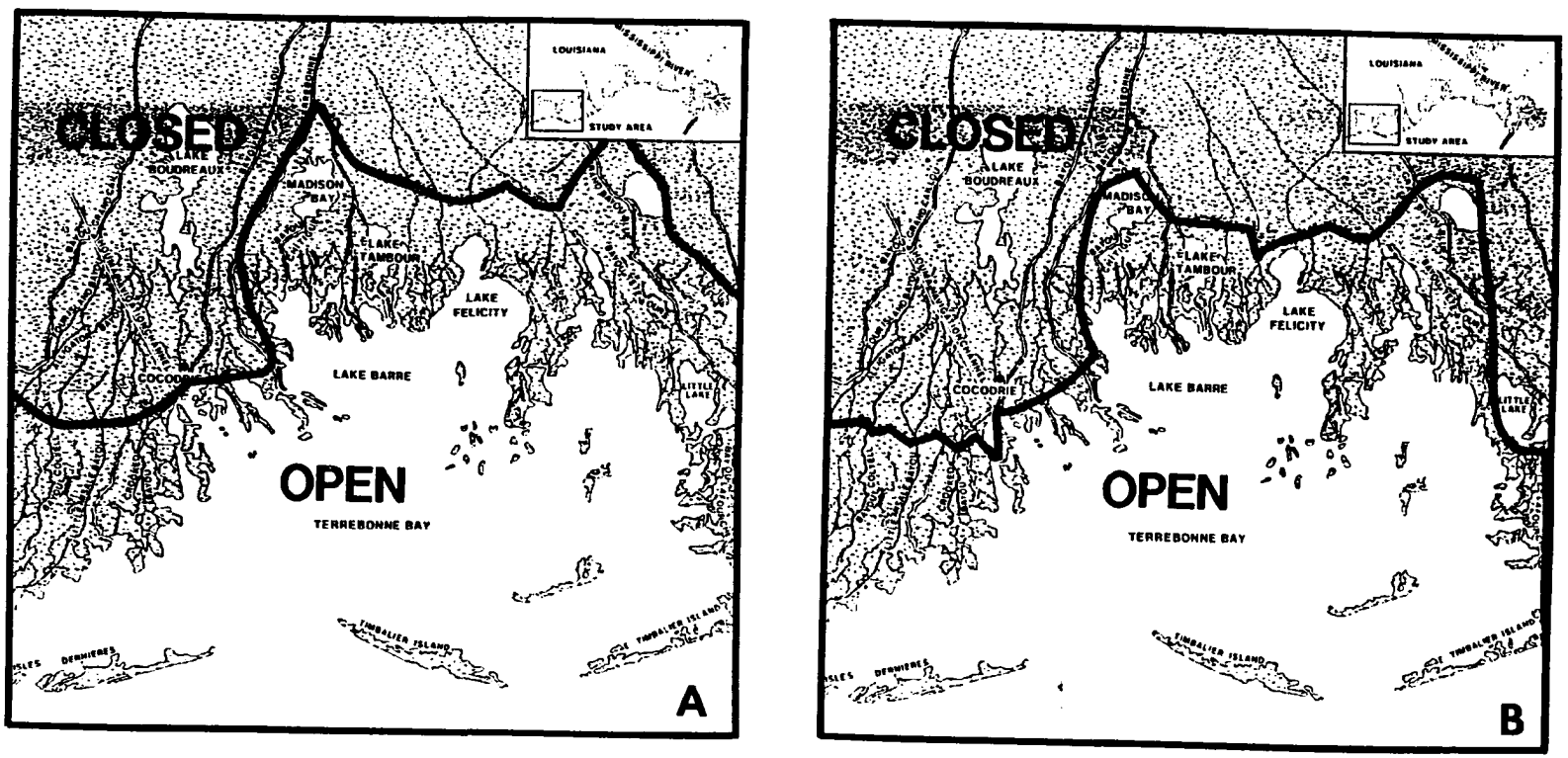

Figure 6: State restrictions on areas for oyster harvesting during (A) May through August and (B) September through October of 1990 (Kilgen and Kilgen, 1990).

the nature of the relationship between tides, wind, and runoff with patterns of sewage dispersal, and 2) what is the residence time of water-borne contaminants in bay waters under various environmental conditions. Attempting to synoptically sample coastal bay waters on a regular basis and for extended periods of time, e.g., over a complete tidal cycle, is logistically difficult as well as extremely expensive. Clearly, some other means of addressing the nature of the relationship between sewage dispersal, contamination, and environmental forcing is needed.

Because oysters are sessile, filter-feeding organisms, it is the concentration and residence time of contaminants in the water column overlying oyster beds which determines the degree to which biologic uptake occurs. Residence time being defined as the amount of time detrimental concentrations of bacteria or viruses remain within the water column of a given region. Previous research suggests that maximum accumulation levels within oysters may be reached within six hours, and that increased exposure time increases the percent of the population which reaches this state (Perkins et al., 1980). Consequently, because enteric bacteria and viruses are known to survive within estuarine and coastal waters (Colwell and Kaper, 1978), uptake and contamination within coastal bay waters is principally a function of transport and dispersal via water movement. The distribution of these organisms may also be affected by dilution due to dispersal, predators, or die-off. Die-off results from adverse physico-chemical water conditions such as high salinities or temperature, low nutrients, or high levels of light (Anderson et al., 1979; Faust et al., 1975). Although the rate of

survival is highly variable, it is water circulation and residual flow transporting materials in suspension on a time scale of hours to days which is most critical to the oyster-contamination problem.

Numerical modeling techniques simulating physical transport have been shown to give conservative, yet realistic estimates of bacterial distributions (Munro, 1974; Christensen, 1973). In order to simplify the process, such modeling techniques normally simulate the spread of waste-water effluent as a neutrally buoyant plume. In situ measurements of current flow, tracer concentrations, and fecal coliform are commonly employed to compare model output with actual conditions (Cederwall et al., 1974). Because the Terrebonne Bay area appears to be both an important source of oysters in south Louisiana and particularly susceptible to the effects of sewage-related wastes, especially within its northwest quadrant, it was chosen as the site for study. Additionally, real-time observations of currents and tides were available for comparison with results from computer simulations.

Study Site

The Terrebonne and Timbalier Bay area is located approximately 90 km west of the Mississippi River mouth, extending between 29°03' and 29°19' N latitudes, and 90°50' to 90°15' W longitudes along Louisiana's southern coast (refer to Fig. 1). It is a complex coastal system comprised of two major bays, and several smaller lakes. The formation of the Terrebonne/Timbalier system is thought to have begun when the focus of deposition from

the Mississippi was located in the vicinity of the present-day bay complex, historically referred to as the Lafourche lobe (Kolb and Van Lopik, 1958; Fig. 7).

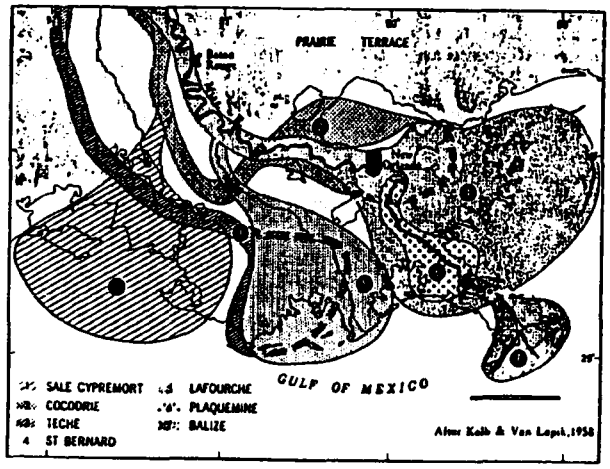

Figure 7: Holocene delta lobes of the Mississippi River, note the position of the Laforche Lobe over the present-day Terrebonne-Timbalier Bay complex.

As the Mississippi changed course and fewer sediments were deposited in the region, sediment compaction and subsidence became dominant and the bays began to form. Continued subsidence plus the effects of erosion by waves, and storm energy combined to enlarge the bays, and eventually produce the configuration as seen today. Though originally separated by a natural levee, erosion by wave action (Waldron, 1963) merged the two major water bodies. Now being freely connected, they may be considered one body of water, henceforth the bay complex will be referred to here simply as Terrebonne Bay.

The morphology of Terrebonne Bay is that of a bar-built estuary, where several offshore barrier islands restrict exchange between the open Gulf waters and the Bay. Saline water from the

Gulf of Mexico enters the Bay primarily through the largest tidal inlet, a combination of Wine Island and Cat Island Passes; flow also occurs through Little Pass Timbalier and Whiskey Pass (Fig. 8). Little, if any, water from the Mississippi now flows directly into Terrebonne Bay, and freshwater runoff is determined principally by precipitation over the catchment basin (Fig. 9). The major contributors of runoff are thought to be Bayous Terrebonne, Petit Caillou, DuLarge, Grand Caillou, Penchant, Blue, and Grand Bayou Blue (Kilgen and Kilgen, 1990). These bayous average approximately 40 km in length, 2 to 3 meters in depth, and range from less than 9 meters to over 200 meters in width (Table 1). Houma Navigation Canal which enters the Bay in its upper northwest quadrant is also a major source of flow and the site of local boating activity. The canal runs from the northwest corner of

Table 1: Dimensions of main bayous entering Terrebonne Bay

BAYOUS/CANALS	LENGTH (km)	WIDTH (m)	AVG. DEPTH (m)
Terrebonne	72	38	2.3
Petit Caillou	48	18	1.4
DuLarge	40	24	1.2
Grand Caillou	40	30 - 457	1.8 - 6.1
Penchant	40	76	2.1
Blue	32	9	1.4
Grand Bayou Blue	32	61	3.2

(Kilgen and Kilgen, 1990)

the bay to Cat Island Pass, and is dredged periodically to maintain an approximate depth of 5 to 6 meters. Except for the canal and tidal passes, Terrebonne Bay averages approximately 1 to 2 meters in depth. The morphology of the shoreline surrounding Terrebonne Bay is highly irregular due to the interfingering of numerous

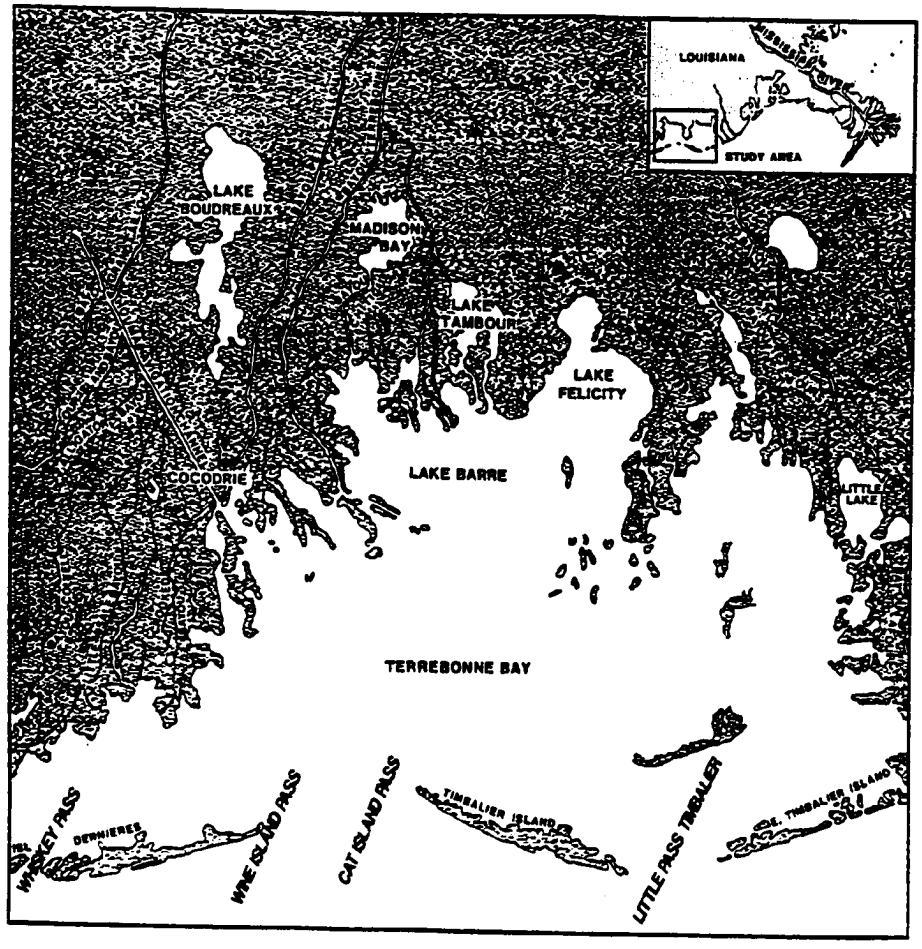

Figure 8: Terrebonne Bay and the main tidal passes connecting bay waters with the Gulf of Mexico.

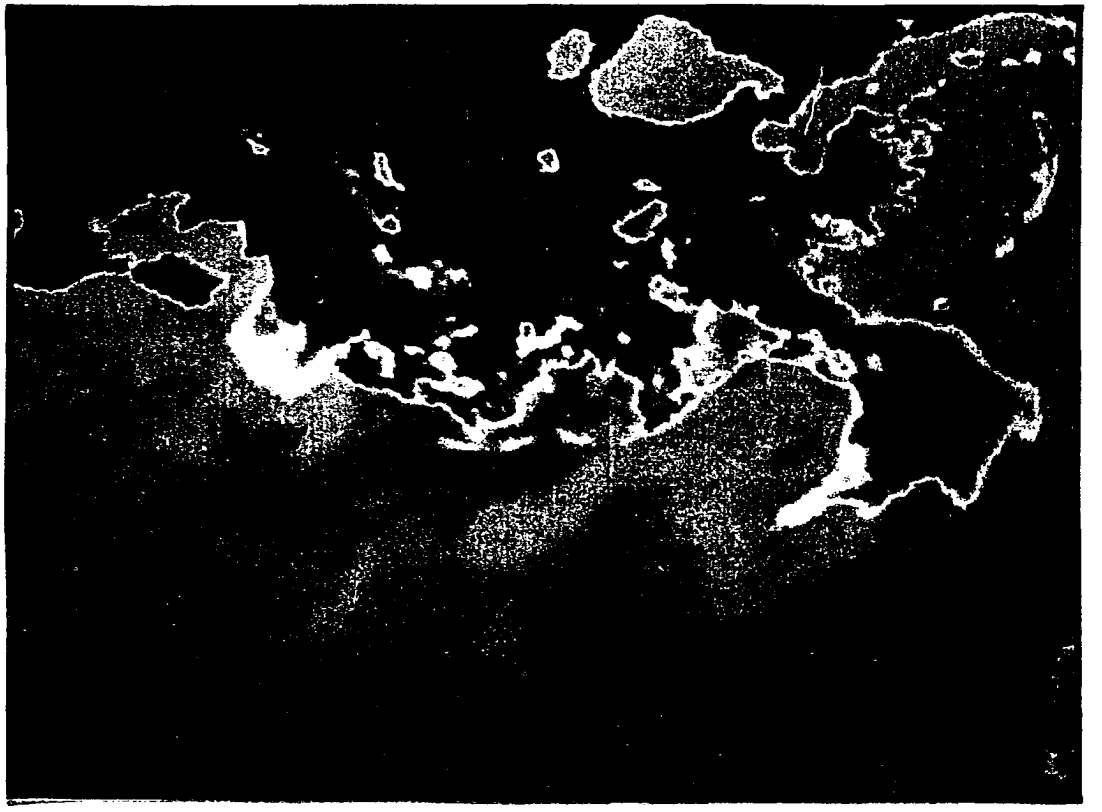

Figure 9: Infrared satellite image of coastal Louisiana, April 1, 1989; arrow indicates Terrebonne Bay. Taken following high discharge of the Mississippi River (light blue - white in color), thus depicting the lack of river input into the Terrebonne Bay system.

bayous, large areas of salt-marsh, and the continued erosion of the coastal sediments.

Meteorology

The climate of Louisiana is principally influenced by its subtropical latitude and proximity to the Gulf of Mexico (NOAA, 1982). In southern Louisiana, the average annual temperature is approximately 21°C, though during the summer months the temperature may often exceed 35°C and fall below freezing in the winter months. Two pressure ridges dominate weather conditions within coastal Louisiana and produce winds with an easterly component (Kilgen and Kilgen, 1990). The "Bermuda high", centered over the Bermuda-Azores region of the Atlantic prevails during summer months, while the "Mexican heat low", centered over Texas, dominates during the winter. During the fall and winter months winds are predominantly out of the northeast, while in the spring and summer winds from the southeast prevail (Fig. 10).

Much of the time in the fall and winter months northeasterly winds bring cool, dry air to Louisiana. However, when cold fronts approach from the west transiting the relatively warm air overlying coastal Louisiana and the Gulf of Mexico, rapid and distinct changes in the ambient environment can occur. The intensity of the front's pressure system and speed of movement (controlling the duration of wind forcing) influence the extent to which these changes occur (Roberts et al., 1989). As a front advances towards the Louisiana coast, moist Gulf of Mexico winds tend to blow from a south to southeasterly direction. When these winds blow for an extended period of time or with great enough strength, water-levels may be

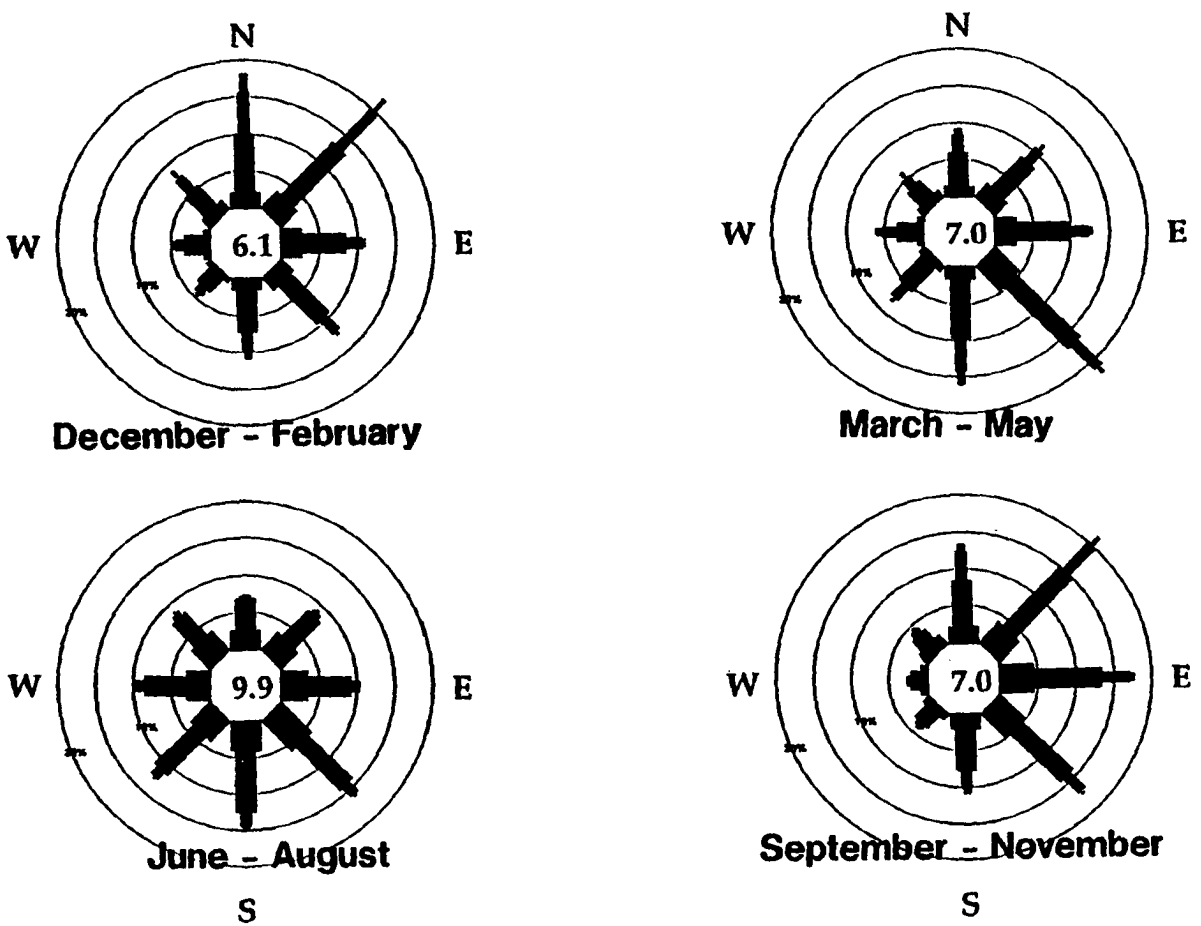

Figure 10: Seasonal wind patterns based on data from Boothville, Louisiana, 1975 - 1988 (Louisiana Office of State Climatology). Center numbers refer to percent calm, and rings are in increments of 5 knots.

set-up against the coast and strong wave attack on the shore occurs. Bay water levels may be elevated by as much as 0.6 m during this pre-frontal phase (Roberts et al., 1989). As the front passes, barometric pressure drops, and intense but generally short-lived squalls occur along the coast. Strong winds and rainfall often accompany these squalls. Following frontal passage, barometric pressure increases, winds dramatically shift to the north, and air temperature and humidity drop. Previously set-up water is driven seaward, flushing suspended particulate matter out into bay waters and the Gulf of Mexico (Roberts et al., 1987). The sequence of events associated with cold-front passage is an important process by which sediments are transported offshore, and has been hypothesized (Kilgen and Kilgen, 1990) as a major factor contributing to the episodic contamination of oyster-growing waters by sewage during the winter and fall seasons.

During the spring and summer months, southeasterly winds bring warm, humid air from the Gulf of Mexico to coastal Louisiana. Afternoon thunderstorms occur almost daily as a result of the moist air driven landward. Heavier rains and winds which accompany tropical storms and hurricanes also occasionally influence the region (June to November).

Records from two climate stations just north of Terrebonne Bay, Houma and Galliano, indicate that over a five-year period, mean annual precipitation in the area is reasonably high, averaging approximately 162 cm (Kilgen and Kilgen, 1990). The maximum rainfall often occurs during August and the minimum during April,

November or December (Fig. 11). Exceptionally heavy precipitation is likely to occur during the summer months associated with

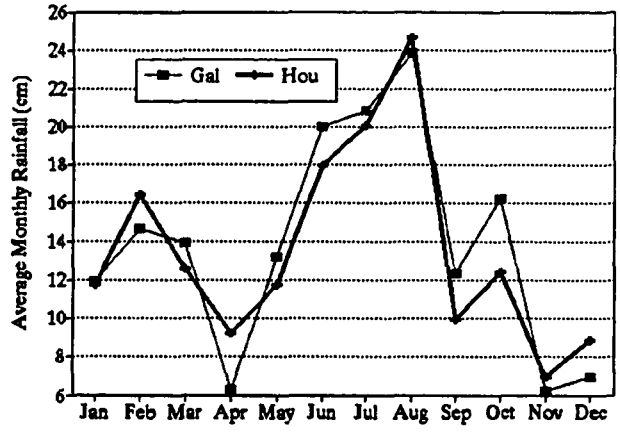

Figure 11: Monthly rainfall based on a five year average of data collected at Houma and Galliano climate stations (Kilgen and Kilgen, 1990).

tropical storms and hurricanes or accompanying cold-front passage in the winter.

Oceanography

Tides within the Terrebonne Bay area are principally diurnal, with a weakly semi-diurnal component. The tidal range varies over a fortnightly cycle with the strongest tropic tides producing a water level variation of approximately 0.7 - 0.8 m, and the weaker, equatorial tides producing a range of less than 0.4 m (LUMCON, 1989). During equatorial tidal periods, the semi-diurnal component may become predominant over the diurnal. Tidal measurements along Louisiana's coast indicate an eastward propagation direction along the coast in the Terrebonne Bay area (NOAA, 1990). Strong tidal currents are produced as the tides pass into coastal bays through relatively narrow inlets. These tidal

currents, combined with wind-driven flow are thought to control circulation within the shallow bays of Louisiana.

Typically estuaries are classified by either their morphological configuration, e.g., drowned river valley, or by the physical processes associated with the movement and mixing of water within their confines. The physical processes which commonly drive estuarine circulation are 1) tidal forcing through inlets, 2) local wind stress, 3) density-induced pressure gradients, 4) locally forced water level variations in the coastal ocean, and 5) non-local events. Previous research suggests that circulation within bar-built estuaries such as Terrebonne Bay is predominantly controlled by wind-driven flow (Pritchard, 1967). However, in the shallow bays of south Louisiana, studies indicates that tides and wind may both play an equally important role in controlling estuarine circulation. In Caminada Bay, similar in configuration to Terrebonne, water-level dynamics and surface water slopes correlate to forcing through tidal passages and fair-weather wind stress (Kjerfve, 1973; 1975). In a recent study of flow through Calcasieu Pass (west of Terrebonne Bay), the exchange between Gulf waters and more restricted bay waters was shown to be primarily barotropic in nature, driven by wind-stress and tidal forcing (Lee et al., 1990). In addition to local wind stress, regional-scale winds have also been shown to cause Ekman-type forcing and drive flow into and out of Gulf estuaries (Kjerfve, 1975; Schroeder and Wiseman, 1986) Non-local forcing and water level variations in the coastal ocean due to the propagation of low salinity Mississippi River water downcoast or

seasonal temperature effects may also affect bay-wide water movement (Smith, 1977; Dinnel and Wiseman, 1986).

Because of their shallow depths, bays in south Louisiana are thought to be rapidly mixed as a result of wind and tidally-driven flow. However, following periods of heavy rainfall or river runoff, stratification of the water column may occur. Preliminary results of an ongoing study in Terrebonne Bay suggest that stratification occurs only on an infrequent basis, principally during summer periods of strong runoff and weak winds (Mckee, unpubl. data; Wiseman, pers. comm.). Overall, tide and wind-driven flow are thought to be the dominant driving mechanisms behind circulation in the shallow bays of south Louisiana, like the Terrebonne-Timbalier complex.

CHAPTER 2

MODELING

Methods

Since the early use of numerical methods to study hydrodynamic processes (Dronkers, 1964; Leendertse, 1967; Reid and Bodine, 1968), two types of modeling schemes have become widely accepted; the finite difference and finite element methods. Each technique seeks to represent a complex physical system and those forces governing the hydrodynamics within that system through a simplified mathematical formulation. When used to simulate flow in coastal bays, both schemes rely on the equations governing conservation of fluid mass (continuity) and momentum (motion). In the finite difference approach, the solution to these equations is approximated by a difference calculation between nearby points. In contrast, in the finite element method, an integral approximation of the equations is made and a solution to that approximation at particular points is found. Because of its advantages in representing an irregular shoreline, and its successful use in the past, a finite element formulation by Wang and Connor (1975) was chosen for this study. The following discussion will include important concepts in finite element modeling and the basic equations pertaining to Wang and Connor's

model, called CAFE. For a more comprehensive review of the development of numerical modeling techniques and equations, readers are referred to Dronkers (1964), Pritchard (1971), or Wang and Connor (1975); and for information regarding the finite element method Zienkewicz (1971) or Brebbia (1973).

In their full forms the equations of motion and continuity consider variations in both the horizontal and vertical planes. A vertically integrated approach appropriate for shallow-water was derived in 1960 to simplify the problem and increase the efficiency of computations (Pritchard, 1971). The term "shallow water" has been given to this set of equations to denote a water mass in which little variation of properties occurs over depth. Clearly, the assumption of vertical homogeneity is a simplification in all but rare instances. However, where variations in variables such as temperature, salinity, sediment concentration, or velocity are minor with respect to their frequency and predominance in the forcing of flow, the use of the shallow water equations is acceptable. Use of the vertically integrated approach was deemed reasonable based on the strong vertical mixing by tides and wind previously found to occur in shallow Louisiana bays.

The depth integrated equations of motion and continuity developed to describe circulation in shallow bays are as follows (Pritchard, 1971; Wang, 1978):

$$\frac{\partial \eta}{\partial t} + \frac{\partial q_x}{\partial x} + \frac{\partial q_y}{\partial y} = q, \qquad \text{continuity} \qquad (1)$$

$$\frac{\partial q_x}{\partial t} + \frac{\partial (uq_x)}{\partial x} + \frac{\partial (vq_x)}{\partial y} = fq_y - gH\frac{\partial \eta}{\partial x} + \frac{\tau_x^s}{\rho} - \frac{1}{2}\frac{gH^2}{\rho}\frac{\partial \Delta\rho}{\partial x} - \frac{1}{\rho}H\frac{\partial p^a}{\partial x}$$

$$- C_f \frac{(q_x^2 + q_y^2)^{1/2} q_x}{H} + \frac{\partial F_{xx}}{\partial x} + \frac{F_{yx}}{\partial y}, \quad x \text{ - momentum} \quad (2)$$

$$\frac{\partial q_y}{\partial t} + \frac{\partial (uq_y)}{\partial x} + \frac{\partial (vq_y)}{\partial y} = -fq_x - gH\frac{\partial \eta}{\partial y} + \frac{\tau_y^s}{\rho} - \frac{1}{2}\frac{gH^2}{\rho}\frac{\partial \Delta\rho}{\partial y} - \frac{1}{\rho}H\frac{\partial p^a}{\partial y}$$

$$- C_f \frac{(q_x^2 + q_y^2)^{1/2} q_y}{H} + \frac{\partial F_{xy}}{\partial x} + \frac{F_{yy}}{\partial y}, \quad y \text{ - momentum} \quad (3)$$

where η = surface displacement, $H = h + \eta$ = total depth, h = bottom depth referred to a datum ($z = 0$), q_x and q_y are discharges per unit width in the x and y directions, respectively, u and v are depth-averaged velocities, q = a volume source, $f = 2\omega\sin\theta$ is the Coriolis parameter, ω = angular velocity of the Earth's rotation (in radians), θ = latitude, τ^s = surface shear stress, ρ = density, $\Delta\rho$ = the density anomaly, p^a = atmospheric pressure, and F_{xx}, F_{xy}, and F_{yy} are the internal stress terms. Bottom friction C_f is incorporated using a quadratic law based on Manning's bottom roughness n, gravitational acceleration g, and depth H [$C_f = (n^2/H^{1/3})g$]. An assumption of incompressibility is assumed in deriving the continuity equation (1), from the conservation of mass equation. Two further assumptions are relied upon in the latter two equations: 1) pressure variations are small, thus the

hydrostatic pressure assumption may be used, and 2) the density anomaly $\Delta\rho$ may be ignored except in the determination of the pressure gradient (Boussinesq approximation). Wind stress (τ^s) is simulated as a function of velocity, U, 10 meters above the surface, the density of air (ρ_a) and an empirically derived drag coefficient C_D:

$$\tau^s = C_D \rho_a U^2$$

Based on previous studies a drag coefficient of $C_D = (1.1 + 0.0536 U) * 0.001$ is employed, where U is in meters per second (Wang, 1978).

Using the depth integrated approach, turbulence or velocity shear which is normally generated internally within a flow is neglected. However, the concept of eddy viscosity is used in the internal stress terms to represent the momentum flux generated by turbulence. The internal stresses may then be estimated as a function of flow velocities, grid spacing and the eddy viscosities:

$$F_{xx} = E_{xx} \left(\frac{\partial q_x}{\partial x}\right)$$
$$F_{xy} = E_{xy} \left(\frac{\partial q_x}{\partial qy} + \frac{\partial q_y}{\partial qx}\right)$$
$$F_{yy} = E_{yy} \left(\frac{\partial q_y}{\partial qy}\right)$$

Within the model these internal stress terms have been found to provide a means of controlling small-scale numerically generated noise (Wang and Connor, 1975).

In the finite element method, the area of interest is subdivided into elements, in the model CAFE they are triangular in shape. Each element is defined by the position of its nodal points, located at the intersection of the element sides. Boundary conditions at all nodal points on the perimeter of a grid are specified. These boundary conditions consist of either a specified water level variation at the open boundaries, or a discharge, e.g., river input at the head of a bay. The common no-slip condition is used along solid lateral boundaries, where tangential discharge at the boundary nodes is set to 0.

As mentioned earlier, an integral approximation of the real equations often called the weak form, is used in the finite element method. The method of weighted residuals is used to develop these equations. This method minimizes the residual error between the true equations and the approximate equations. If a residual is defined as $R = Lu_a - f_o$, for the differential equation $Lu = f_o$, where L is a differential operator, u is the exact solution, u_a is an approximate solution and f_o is the data or inhomogeneous term, then applying a weighting function w to the residual and summing over the entire domain leads to $WR = \int_\Omega Rw\partial\omega = \int_\Omega (Lu_a - f_o)w\partial\omega$. Requiring the summed weighted residual, WR, to vanish yields the integral equation on which a finite element solution is based (Wang and Connor, 1975).

The next step is to modify the equations to coincide with the shape of the elements within the grid. Given a grid composed of triangular elements, an interpolation function is used to convert coordinates originally in a rectangular system to one that is

triangular. If this interpolation function, sometimes called the shape function, has also been used as the weighting function in the previously described step, it is commonly referred to as the Galerkin Method. After the coordinate system has been modified, the equations are then approximated by a piecewise polynomial at each element [$f(x) = \phi_1 + \phi_2 x + \phi_3 x$], where x is the shape function and ϕ a matrix of the unknowns at each of the three nodal points (i.e. q_x, q_y, η). The piecewise polynomials are then substituted into the weak equations and summed over all the elements to give the system equations. Using the boundary conditions, these equations are then solved and a time stepping function is added.

Time integration is performed using the trapezoidal rule modified by a "split-time" method (Wang, 1978). Commonly used in finite difference modeling, the split-time method integrates alternating time steps using a central differencing scheme to increase computational efficiency. Stability during the iterative process is achieved by adhering to the well-known Courant-Friedrichs-Lewy (CFL) condition $\Delta t \leq \Delta s / \sqrt{2gh}$, where Δt is less than or equal to the critical time step, Δs is grid spacing, g gravitational acceleration, and h is depth.

Another of the advantages of using this model is that it readily allows for computer generated drogue tracking which will be employed to examine transport processes in the Bay. These methods will be discussed in greater detail later in the section on transport. The conditions used as input for the model are a function of the study area.

Input and Calibration

A grid of 866 nodal points and 1425 triangular elements was constructed to represent Terrebonne Bay (Fig. 12). Grid boundaries were determined principally from bathymetric charts. However, where available, recent aerial photographs were used to better delineate the land/water interface in regions which have been subject to recent erosion. The size of triangular elements within the grid ranges from about 1000 m mid-bay to 400 m in the northwest quadrant. Depths specified at each nodal point were estimated based on standard bathymetric charts of the region. Because of the dynamic nature of the region and the importance of bathymetry in modeling, depths in the vicinity of the bay's mouth and Houma Navigation Canal were measured. Using a small boat and fathometer, four parallel and three perpendicular bathymetric profiles were measured within the major tidal pass (Wine Island and Cat Island Passes combined; Fig. 13). Six profiles were also measured across the Navigation Canal ranging in position from near Cat Island Pass to near the canal's entrance into the northwest region of the bay. Additionally, other areas in which bathymetric charts appeared questionable were inspected. A tide gage was placed in the bay during profiling, however due to equipment failure, data were unretrievable. Consequently, the predicted tides were used to remove tidal variations and obtain an estimate of mean low water depth. Given the conditions present during profiling, strong tropic tides and

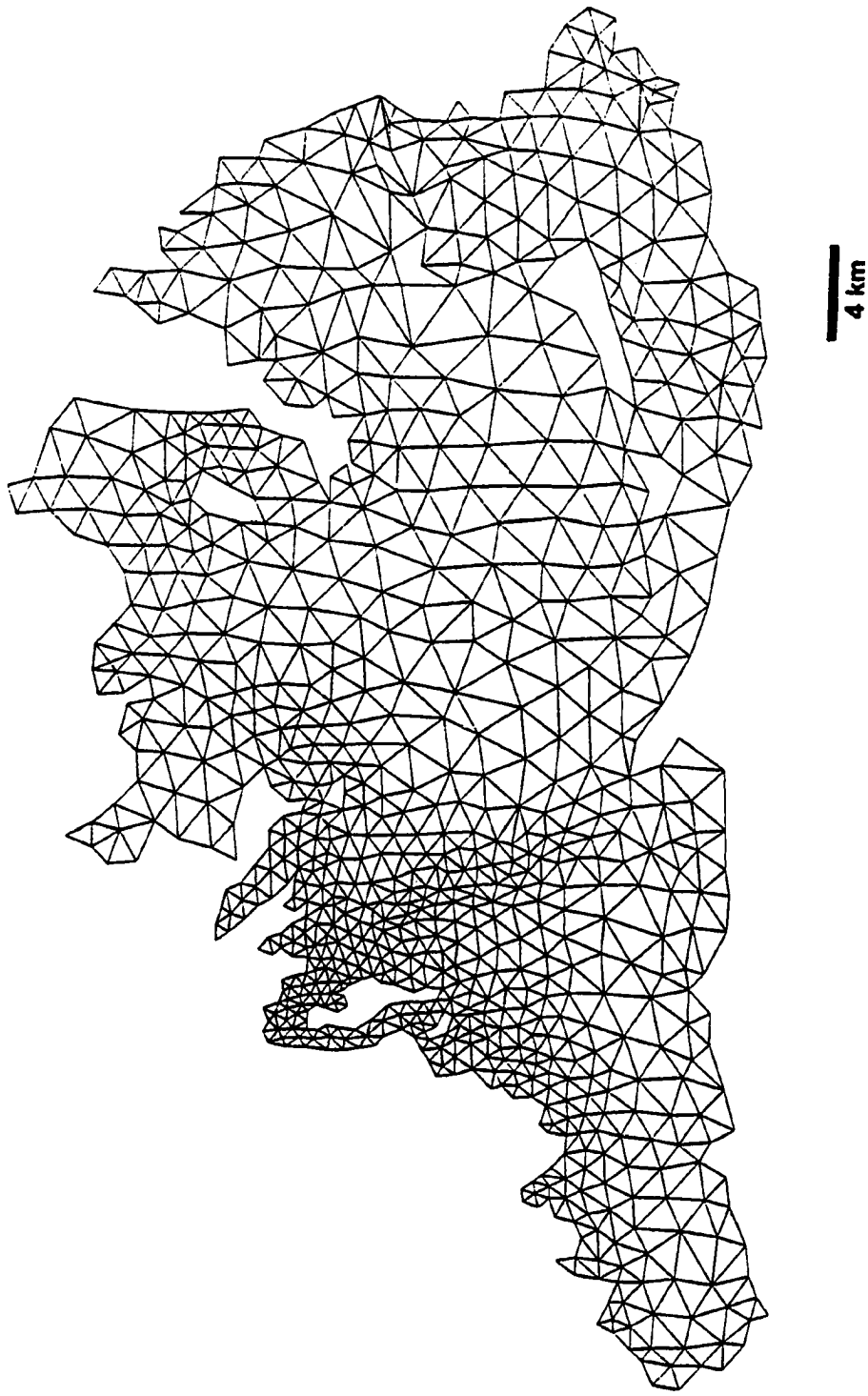

Figure 12: Triangular grid constructed to represent Terrebonne Bay for finite element modeling.

Figure 13: Bathymetric transects and profiles measured in Terrebonne Bay. Profiles are shown as diagrammatic sketches only, (A) crossing the Navigation Canal and (B) transecting the main tidal pass.

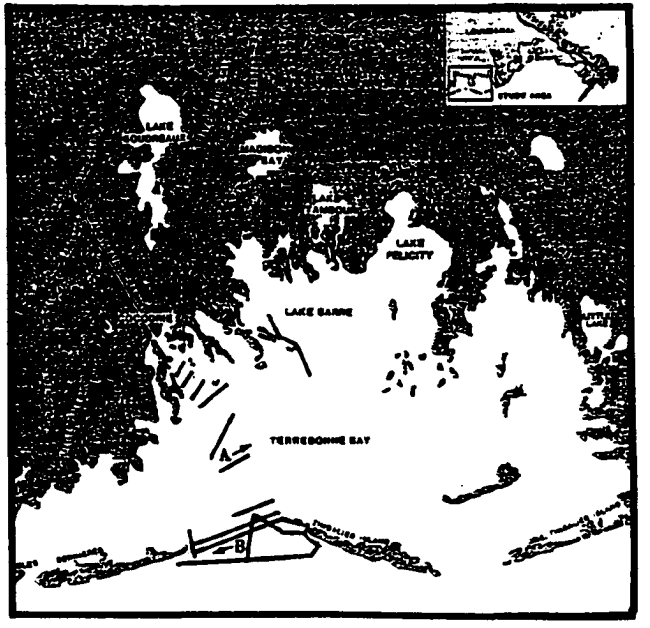

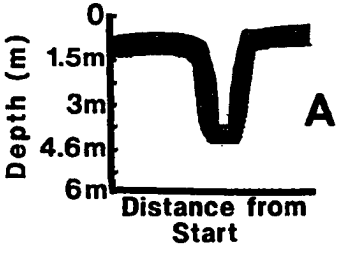

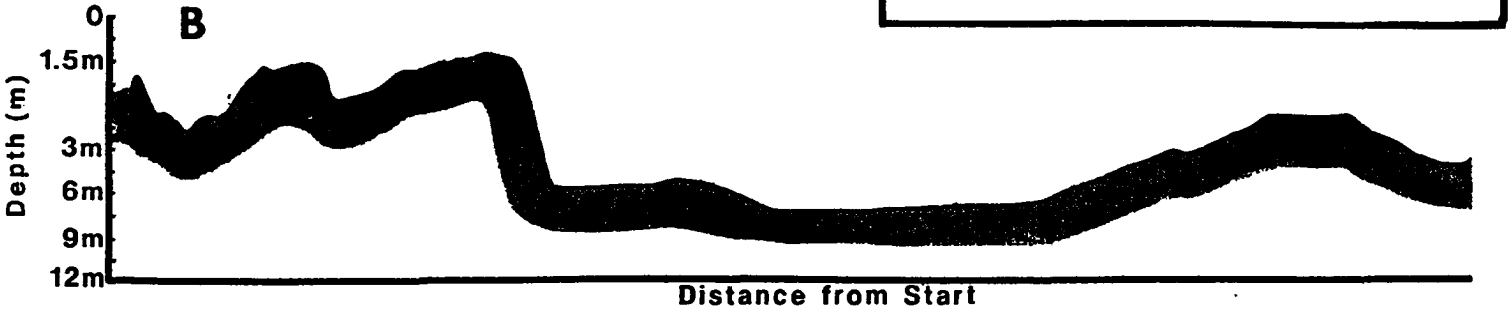

light winds, predicted tides may be relatively accurate in representing the actual tidal variations (Fig. 14).

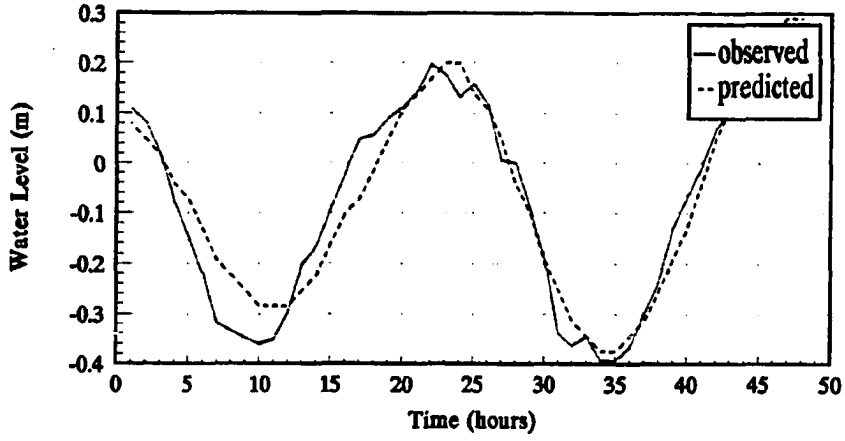

Figure 14: Predicted versus observed tides at Cat Island Pass with a tropic tidal range and weak, southeasterly winds.

Results of depth profiling showed significant deviations from the charted bathymetry at the bay's mouth. Few differences from charted depths mid-bay near the Navigation Canal were found. However, just south of the Canal's outlet, depths were shallower than expected. It is suspected that this is the result of spoil recently dumped during maintenance dredging operations in the area. Where dredging was thought not to have affected the area, depth measurements from the field were incorporated into model bathymetry. However where dredging is known to have been conducted after the periods being modeled, chart depths were used. In order to resolve the rapid and relatively narrow bathymetric changes associated with the Navigation Canal, the size of the elements in the vicinity of the canal was reduced.

The year 1990 was chosen for simulations based on the availability of in situ measurements in the study area. Tides,

currents, and wind within the Terrebonne area were recorded in situ as part of a wetland's loss study conducted by Louisiana State University's Coastal Studies Institute and funded by the United States Geologic Survey. Four 10 to 12 day periods were randomly chosen for simulation from each of the 1990 seasons as prescribed by the State's oyster-water monitoring program. Each of these periods was subdivided into 3 to 4 day increments for data management purposes and efficiency while running on the computer (Table 2). Care was taken to ensure that all phases of

Table 2: Seasonal modeling periods (1990)

MODELING PERIODS	3 - 4 DAY INCREMENTS
March 24 - April 4	3/24-3/27, 3/28-4/31, 4/1-4/4
June 25 - July 7	6/25-6/27, 6/27-6/30, 7/1-7/5, 7/4-7/8
September 8 - 22	9/8-9/12, 9/12-9/16, 9/16-9/20, 9/18-9/22
December 5 - 17	12/5-12/9, 12/9-12/13, 12/13-12/18
April 25 - 29 (Cold front passage)	4/25-4/29

the fortnightly tidal cycle were incorporated during each of the chosen weeks per season. Additional conditions representing events thought to play a significant role in particulate transport were also used, i.e., cold front passage.

Tides are incorporated within the model through the specification of time-varying changes in the water level at open boundaries. Each tidal pass, as described earlier, was represented as an open boundary. The phase and range of tides used in each modeling run were based on real-time measurements taken near the major tidal inlet, Cat Island Pass. A SeaGauge water level recorder was mounted approximately 5 m below the surface on a pipe attached to an oil well platform. Data from the gage was

logged in situ every 15 minutes on a cassette tape and later read in the laboratory for processing. To allow for data retrieval and maintenance, the tide gage was deployed for four, approximately three month periods: 1) March 13 to May 29, 2) June 4 to August 2, 3) August 3 to October 16, and 4) October 16 to January 3 (1991). Data were converted from pressure readings to depth (Appendix A), and a mean water level calculated. This mean was then subtracted out of the time series to obtain the tidal signal. Because no true datum was used during deployments, variations in the absolute water level could not be determined from the data, however observations provide the range and phase of tidal variations as needed for model input (Figs. 15 - 16).

The time lag of tidal forcing within the passes of Terrebonne Bay were estimated based on the following simplifications. The speed of tidal propagation may be approximated by a shallow-water wave, and the direction of movement may be taken as essentially alongshore in the eastward direction. The shallow-water wave approximation is based on the magnitude of the tidal wavelength, thousands of kilometers, shelf depth (less than 10 m), and the definition of a shallow-water wave, depth being less than one twentieth of the wavelength. The velocity of the tidal wave may then be estimated using the simplified form $C = (gh)^{1/2}$, where g is gravitational acceleration and h is depth. Given the velocity of wave passage and evaluating the distance between tidal inlets, a lag time was estimated. Though the actual tidal propagation in this area is more complex, the standard tidal predictions (NOAA, 1990) indicate that there is an easterly trend

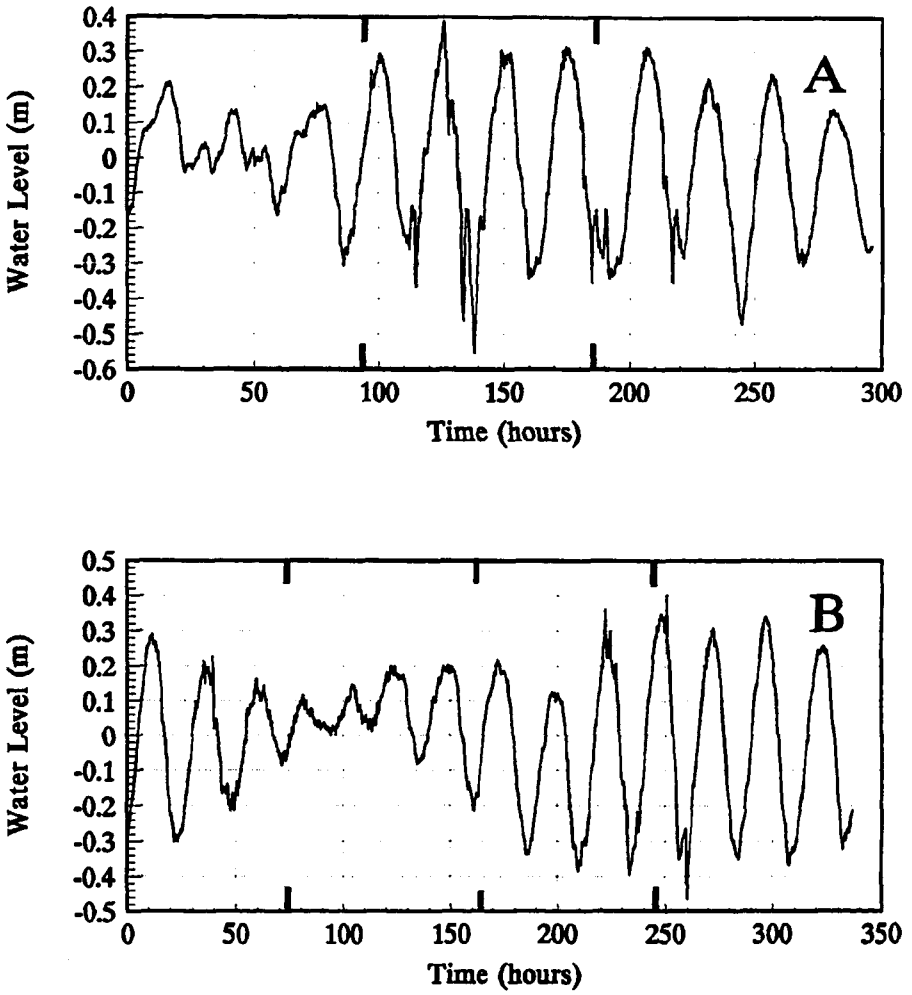

Figure 15: Tidal records from Cat Island Pass (A) March 24 - April 4, 1990, and (B) June 25 - July 8, 1990. Subdivisions represent incremental modeling periods, refer to Table 2 for dates.

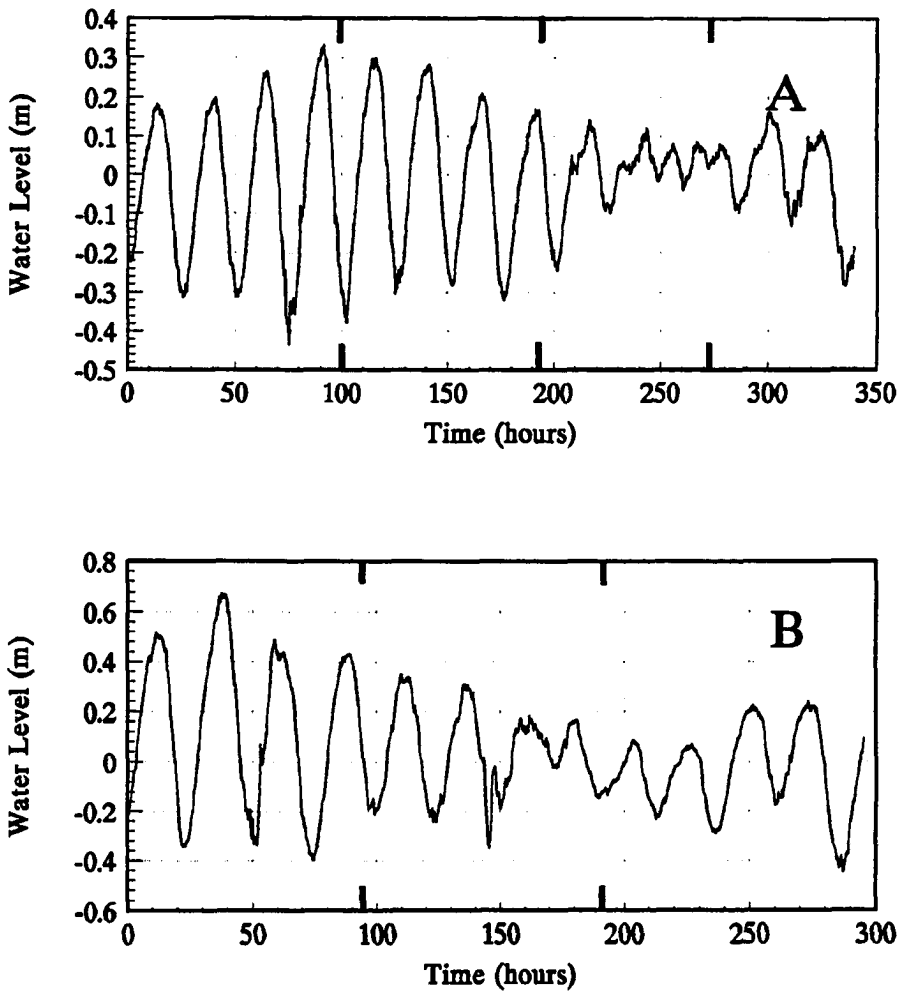

Figure 16: Tidal records from Cat Island Pass (A) September 8 - 22, 1990, and (B) December 5 - 17, 1990. Subdivisions represent incremental modeling periods, refer to Table 2 for dates.

in its flow (Table 3). Consequently, the observed tides in Cat Island pass were taken as time zero, and a negative lag calculated for Whiskey pass and positive lags calculated for Little Pass Timbalier and a small, unnamed pass further east (Table 4). To determine if these estimated lags were of the correct order of magnitude, similar calculations were performed using standard tidal prediction tables for passes within the region. Results suggest that the method described above produces time lags that are compatible with those found in the standard tide tables (refer to Tables 3 and 4).

Table 3: Phase lag of tides as predicted by standard tide tables (NOAA, 1990).

STATION	LAT.	LONG.	PREDICTED LAG HIGH (min.)*	PREDICTED LAG LOW (min.)*	ESTIMATED DISTANCE (km)*	ESTIMATED LAG (min.)*
Racoon Point	29°04'	90°58'	0	0	0	0
Caillou Boca	29°04'	90°48'	43	8	16	33
Wine Island	29°05'	90°37'	71	82	38	79

* Relative to Racoon Point

Table 4: Calculated lag time between passes in Terrebonne Bay using a tidal propagation speed of 8 - 9 m/s.

TIDAL PASS	EST. DISTANCE TO REFERENCE PASS (km)	CALCULATED LAG (s)
Cat Island/Wine Island	0	0
Whiskey Pass	16.5	-2062
Little Pass Timbalier	22	2444
Un-named Pass	34	3777

Tidal observations were also available approximately 2 kilometers northwest of the bay at the Louisiana Universities Marine Consortium Laboratory (LUMCON; NOAA, unpub. data). Comparison between tides at the mouth of Terrebonne Bay and at

LUMCON reveal that a lag of less than one to two hours commonly occurs between stations (Fig. 17). Data from the LUMCON tide gage was also used to calibrate the order of magnitude of water level variations near the landward boundaries of the grid. These data provided another means of qualitatively comparing real-time observations with simulated data for all modeling runs.

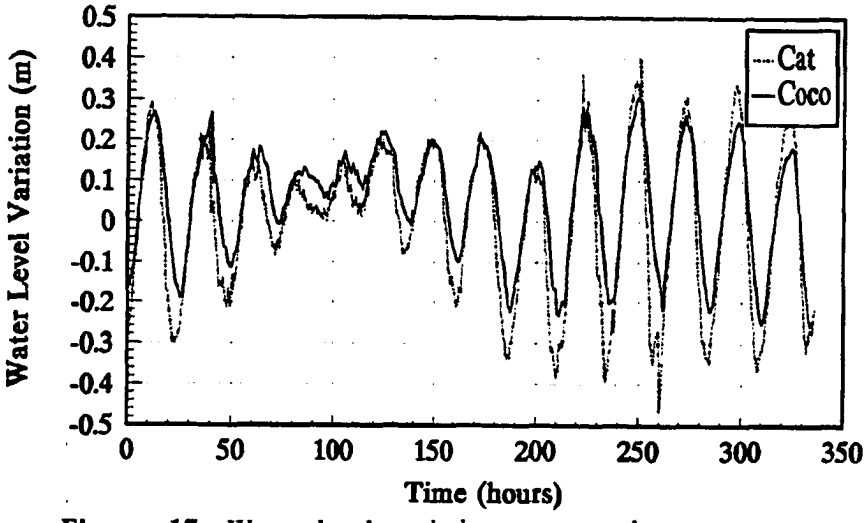

Figure 17: Water level variations measured at an up-estuary location, Cocodrie, and from within Cat Island Pass.

Winds used as model input for each numerical simulation were based on observations from a meteorological station located on Isles Dernieres in the southwest region of the Bay (refer to Fig. 2). To more realistically simulate wind forcing, modifications of the original CAFE program were made to allow for time varying winds. For each modeling period, observed winds (Figs. 18 - 21) were generally split into six intervals of average direction, magnitude and duration. The length of averaged periods was based on distinct changes in either direction or speed (Fig. 22).

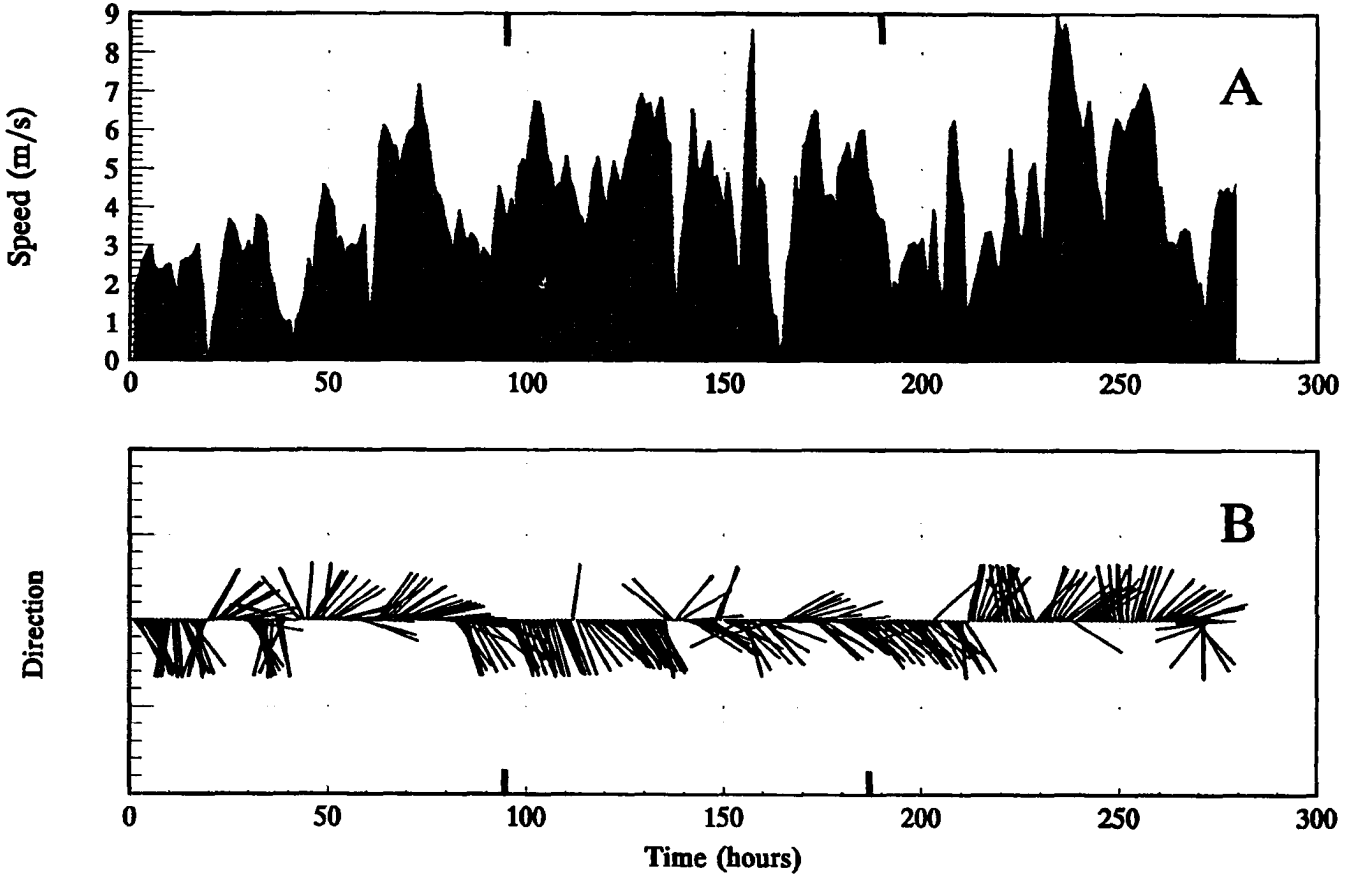

Figure 18: Observed wind speed (A) and direction (B) on Isles Dernieres March 24 - April 4, 1990. Subdivisions represent incremental modeling periods, refer to Table 2 for dates.

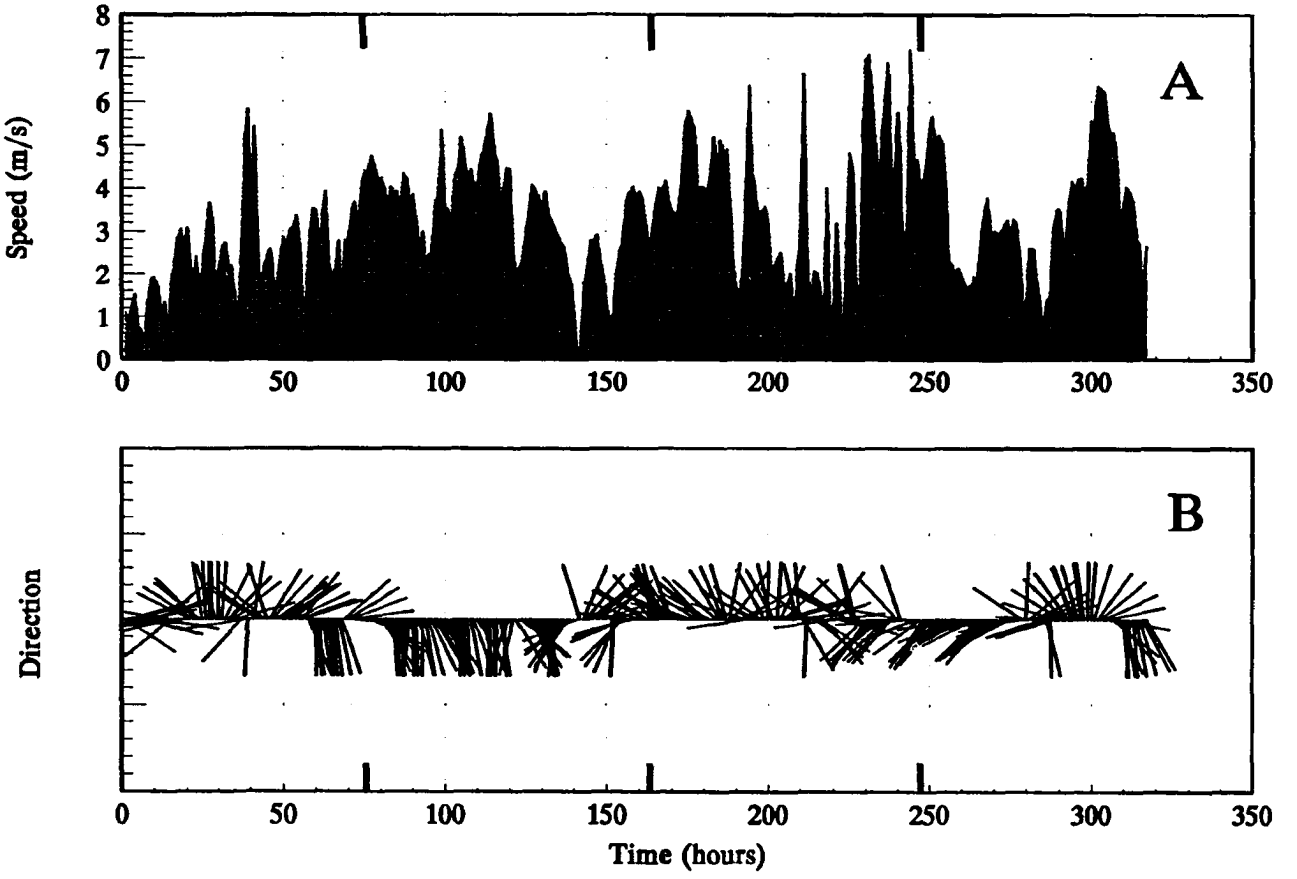

Figure 19: Observed wind speed (A) and direction (B) on Isles Dernieres June 25 - July 8, 1990. Subdivisions represent incremental modeling periods, refer to Table 2 for dates.

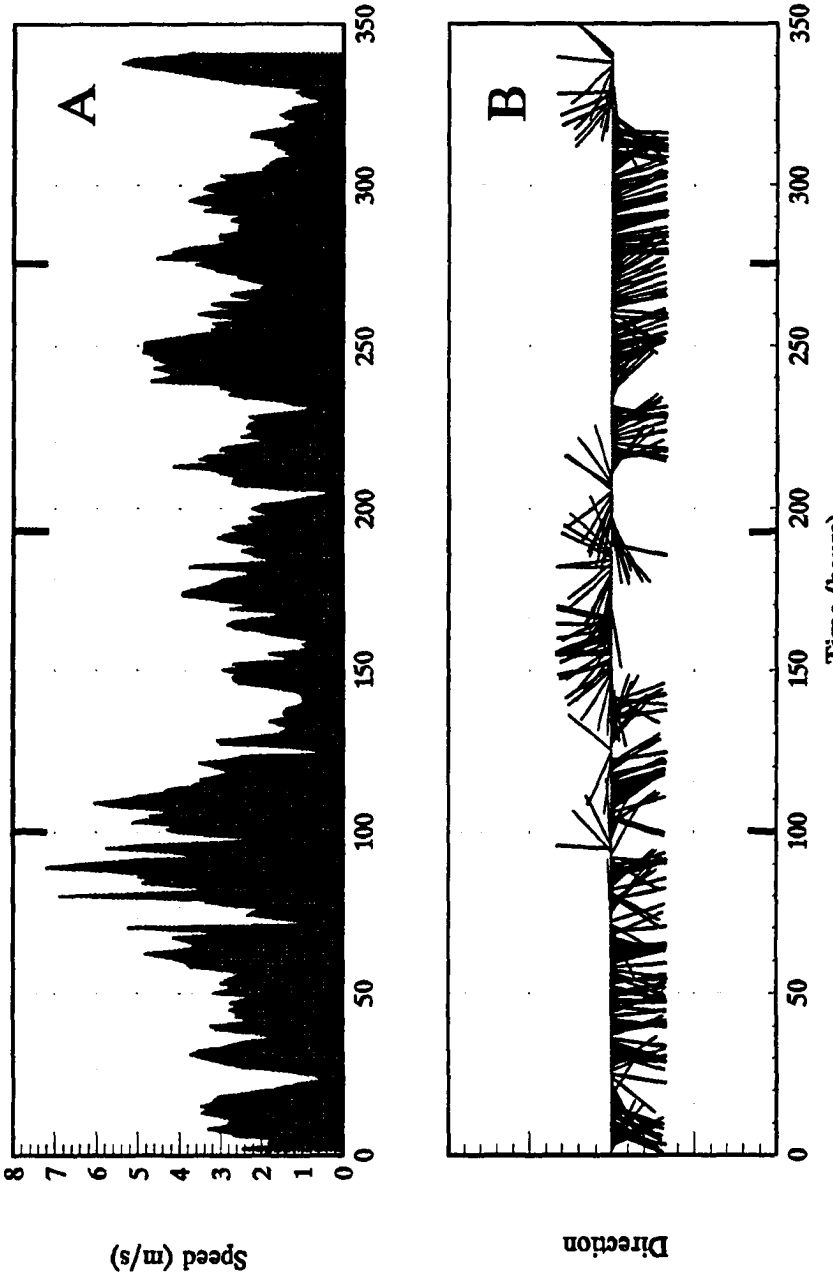

Figure 20: Observed wind speed (A) and direction (B) on Isles Dernieres September 8 - 22, 1990. Subdivisions represent incremental modeling periods, refer to Table 2 for dates.

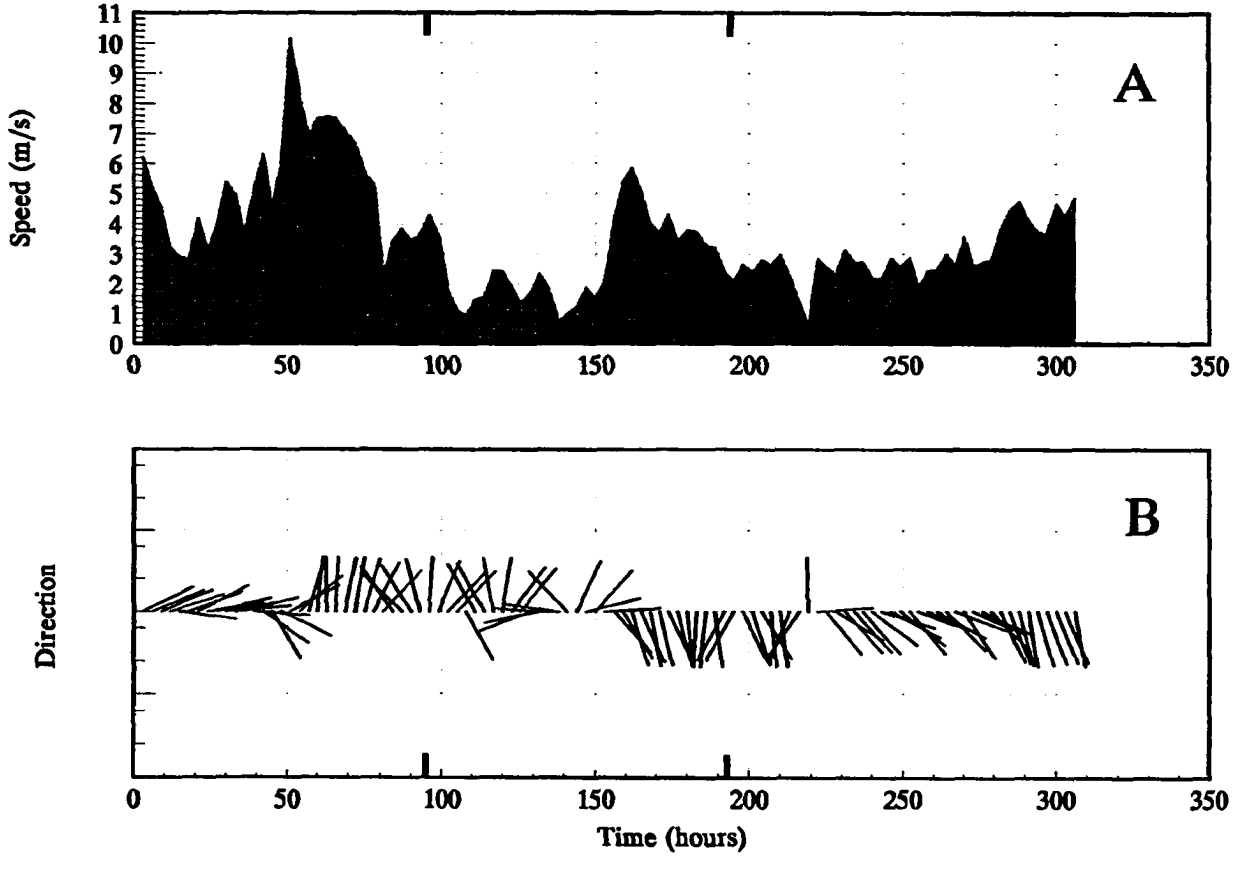

Figure 21: Observed wind speed (A) and direction (B) on Isles Dernieres December 5 - 17, 1990. Subdivisions represent incremental modeling periods, refer to Table 2 for dates.

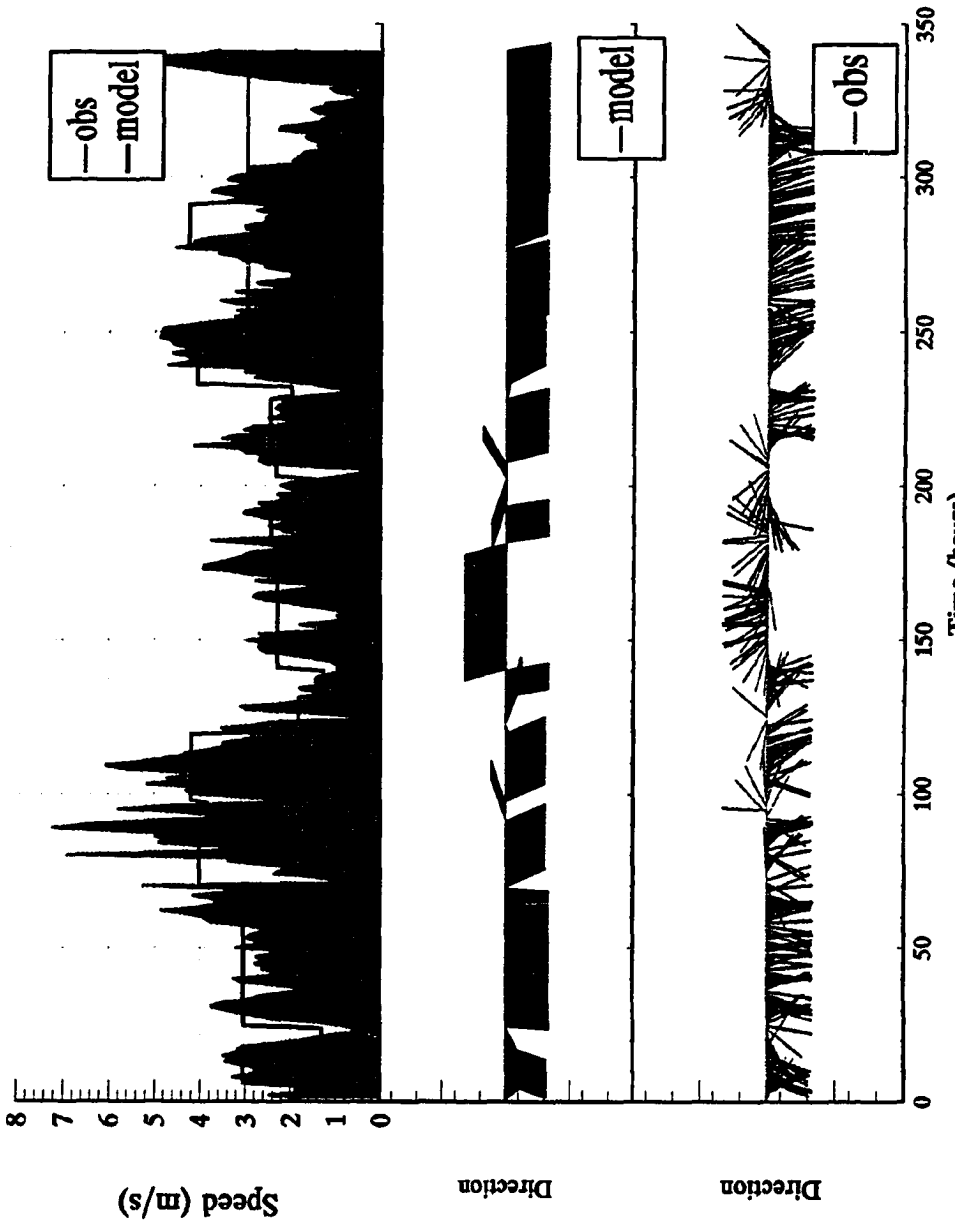

Figure 22: Observed versus modeled winds for September 8 - 22, 1990.

The significance of bayou discharge on forcing circulation within Terrebonne Bay is unknown. Not only is the amount and velocity of discharge from these bayous highly irregular, but relatively few in situ measurements in the area are available. Rather than neglect bayou flow, a means was sought to 1) characterize the variation and relative magnitude of discharge for modeling periods, and 2) incorporate these variations into computer simulations. As previously mentioned, bayou runoff into Terrebonne Bay is mainly a function of precipitation over the catchment area, thus a relationship should exist between rainfall and discharge. In order to examine this relationship more closely, an analysis of the climatic water budget was performed for the years 1988 to 1990 in the Terrebonne Bay area and compared to the discharge of 2 major bayous in the area over the same period.

The climatic water budget, first introduced by Thornwaite (1948), is based on mean monthly temperatures and precipitation data collected at regional climate stations. Two such stations are located in the vicinity of Terrebonne Bay, 1) Houma, just northwest of the bay, and 2) Galliano, just northeast of the bay. The two main components of the water budget analysis are potential evapotranspiration (PE) and actual evapotranspiration (AE). Potential evapotranspiration being defined as the amount of water that would evaporate and transpire from a landscape fully covered by a homogeneous stand of vegetation without any shortage of soil moisture within the rooting zone. Given large regions with similar vegetation and soil moisture conditions, Thornwaite derived a complex set of empirical equations for

estimating monthly PE from temperature and latitude. Evapotranspiration is taken then to represent the precipitation and soil moisture actually used by plants to meet the energy demands estimated by PE. In general, the average climatic water budget model can then be described by two interrelated equations: 1) P = AE + S, where P is precipitation and S is moisture surplus, and 2) PE = AE + D, where D refers to the moisture deficit. Because the area in question is principally composed of bayous and swamp lands, D is taken as zero, and PE equals AE. Thus the moisture surplus, which in this case will be considered runoff, is equal to P - PE. This simplification potentially results in a slight overestimation of runoff, but it will be a more realistic value than simply using rainfall data. Results of water budget analysis performed by the Louisiana State Office of Climatology indicate a seasonal variation in runoff within the Terrebonne Bay area (Fig. 23).

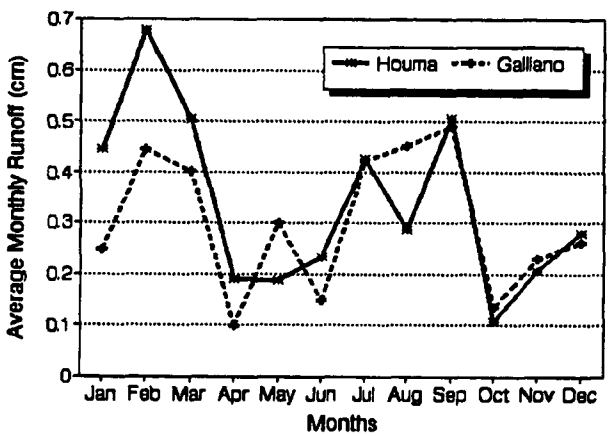

Figure 23: Seasonal pattern of results from water budget analyses for 1990.

Observations of daily discharge from Bayou Lafourche and Bayou Grand Caillou were used for comparisons with results of the water budget analysis (USGS, unpublished data). Qualitative analysis of the relationship between runoff and bayou discharge suggests that a strong correlation exists during the winter and early spring months (Fig. 24A). The relationship between summer and fall runoff with discharge is less clear (Fig. 24B). This difference may be explained by the contrasting means by which precipitation most commonly occurs during these seasons. In the winter and early spring the passage of large-scale fronts brings wide-spread rainfall, in contrast during the summer and fall months small-scale squalls and thunderstorms characteristically generate precipitation events that are highly variable in both space and time. Therefore, while results of water budget analyses based on data taken at discrete stations reflect precipitation events appropriately in the winter and early spring, the same may not be true in the summer and fall, with the exception of tropical storms or hurricanes.

Based on the qualitative evaluation of discharge variations, a baseline runoff of 0.02 m^2/s was chosen. During the winter and early spring periods of modeling, if discharge of either bayou increased with respect to a rainfall event, flow was proportionally increased. During summer and fall months, if discharge of both bayous increased respectively, then flow was proportionally increased.

Previous studies indicate that bayou flow within several kilometers of Terrebonne Bay is tidally dominated (Kilgen and

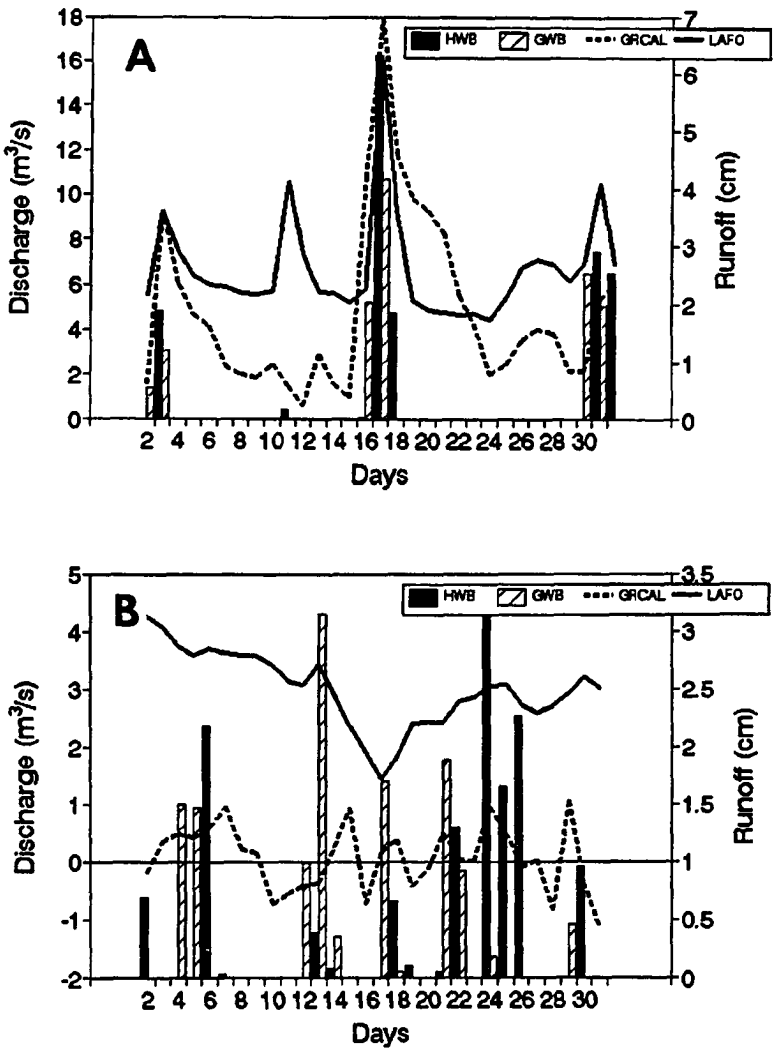

Figure 24: Estimated water budget runoff at Houma and Galliano stations as compared to discharge of Bayous Grand Caillou and Laforche for March (A) and July (B) 1990.

Kilgen, 1990). Because no actual measurements were available for bayou flow entering Terrebonne Bay, and because of boundary condition restrictions (two adjacent nodal points may not both be prescribed flow), each discharge was taken to represent flow for a given section of the bay (potentially more than one bayou). To simulate the variation of flow direction and velocity with regard to tidal forcing the following equation was used to specify flow at each discharge point:

$$Q = (Q_c * \sin(2\pi(T\text{-}lag)/P)) - (Q_b * H)$$

where Q is discharge per unit depth (m^3/s), Q_b is baseflow (m^2/s), Q_c is a calibrated discharge factor (m^3/s), T is time (s), P is the tidal period (s), and H is depth (m). Depths were based on bathymetric charts and a few in situ measurements. Because two adjacent nodes cannot both have prescribed discharges, each discharge often had to represent flow into and out of the bay for relatively broad up-estuary inlets. The calibrated discharge factor, Q_c, was used in the model to compensate for the varying amounts of flow needed in each area to produce realistic water level variations and movement over a given tidal cycle. During calibration runs, Q_c was adjusted such that variations in water level in close proximity to each discharge were within approximately 0.30 m of known tidal variations at Cocodrie. The values of Q_c per unit depth ranged from 0.80 m^2/s in the vicinity of the Houma Navigation Canal to 0.10 m^2/s in areas of lesser flow. Following calibration these values were kept constant for

the remainder of the modeling runs. A time lag of one hour was incorporated in the above equation to reflect the estimated tidal lag from the bay mouth to its head.

In addition to the discharge factor, both bottom friction and eddy viscosities were adjusted during calibration runs. Winds and tides for each calibration were chosen from within the first deployment period (March 13 to May 29). Initial values of both the bottom roughness and eddy viscosities were based on data presented in the literature (Limerinos, 1970; Callaway, 1974; Wang and Connor, 1975). Data from five current meter stations located within Terrebonne Bay (Fig. 25) were used to compare with simulated flow.

After calibration in the laboratory, Endeco 174 current meters were swivel mounted on vertical pipes attached to sturdy platforms within the bay. Meters were periodically checked and cleaned of organic growth to ensure free rotation with the tide. Data were recorded in situ at 10 minute intervals on a cassette tape. Tapes were recovered and processed in the laboratory. Three of the five stations were equipped with one current meter at mid-depth in the water column (approximately 2 meters). Originally two of the stations, the one at the mouth and one mid-bay, were equipped with both a near-bottom and near-surface meter. However, due to unforeseen difficulties, data from both meters at the mouth was lost. Additional data were lost during the later half of the first deployment period at one of the mid-bay stations. With this in mind, calibration runs were based on data collected during the first half of the first deployment period. For

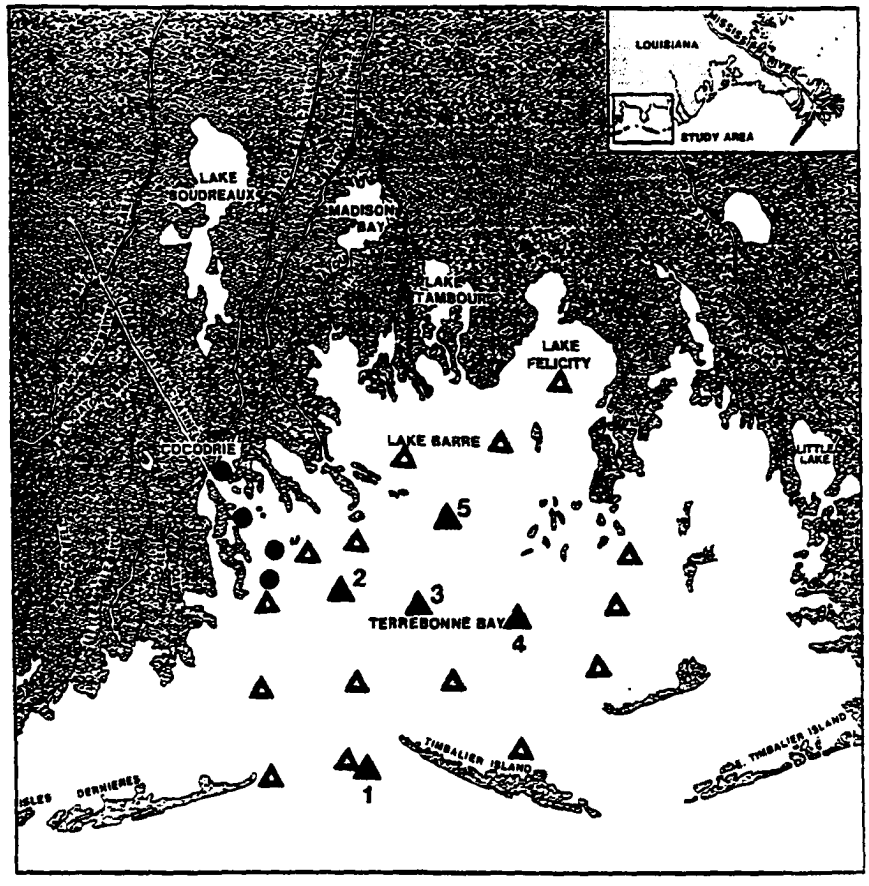

Figure 25: Location of in situ measurements within Terrebonne Bay, (▲) moored current meter stations, (▲) CTD survey sites, and (●) 24 - hour current monitoring experiment.

comparison with model output, both speed and direction were hourly averaged. Where plotted data appeared visibly suspect, unaveraged data were manually inspected. Laboratory calibrations indicated that the current meters are accurate to within 1 to 3 cm/s in speed and 7° in direction.

Modifications to the model were made over numerous independent calibration runs to obtain the closest fit between observed current velocity and computer generated velocity. Flow averaged within the element in which each current meter station was located was used for comparisons. Based on the outcome of calibration runs a bottom roughness value of 0.015 was chosen. This value results in bottom friction coefficients ranging from approximately 0.003 in shallow water (less than 1 m) to about 0.001 at greater depths (over 5 m). A value of 0.019 was originally chosen for bottom roughness based on the fine-grained nature of the sediments within the Terrebonne area. The lower value required may be a function of 1) the use of a constant bottom roughness value rather than a more realistic spatially varying term, and 2) to compensate for theoretically large eddy viscosities used to dampen out numerically generated noise.

Where eddy viscosity is usually taken to represent sub-grid scale turbulence, an initial value of approximately 0.5 m^2/s was used based on mixing length theory. Described by Okubo (1970), mixing length theory suggests that the effect of turbulence, as represented by an eddy viscosity term, is a function of the length scale of the system being investigated (Fig. 26). The use of a value within the range as expected from Okubo's work was

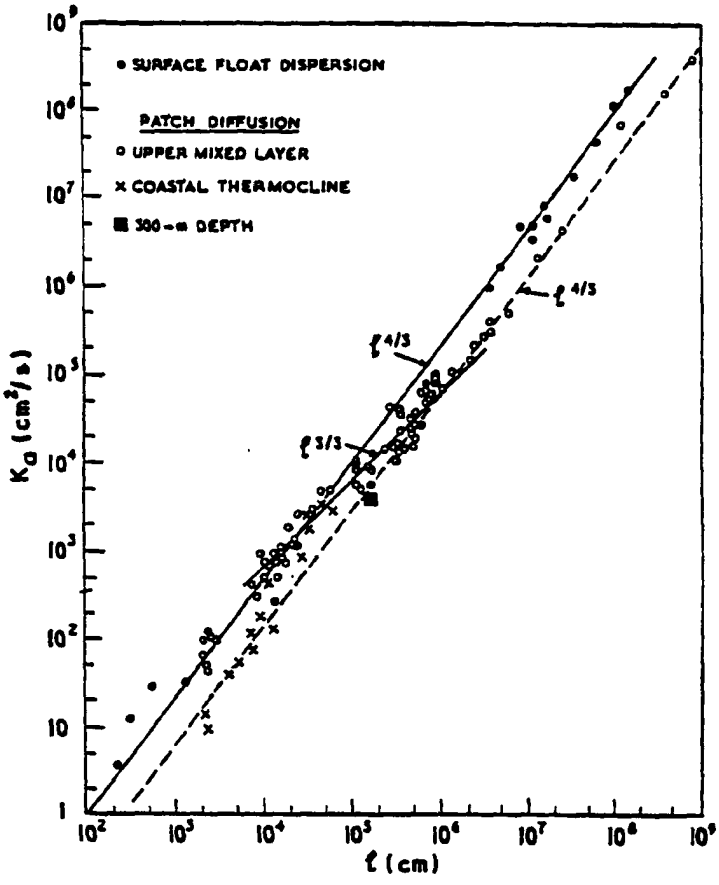

Figure 26: Okubo's (1975) diagram of patch diffusion and float dispersion with mixing length theory predictions superimposed.

incompatible with model stability. Subsequently, the value of the eddy viscosity terms was increased until the model became stable. Stability was achieved using a value of at least 100 m^2/s, increasing the value more than this had little effect on the model outcome. This value is consistent with the range of values Wang and Connor (1975) prescribe from previous use of the model 1 - 10^5 m^2/s.

Eddy viscosities within the model CAFE are used primarily to dampen out short-wave noise produced during numerical processing. This type of noise may have been generated by rapid changes in the size of neighboring elements within the grid, thereby requiring an eddy viscosity term greater than theoretically expected. Given the resolution of the grid, and the eddy viscosities incorporated, the model can be used only to examine the pattern of water movement over two or more grid points (> 400 m). In areas of the bay where the bathymetry changes on a scale less than that of the grid spacing, numerical diffusion will produce only an average picture of larger scale flow. The use of a no-slip lateral boundary condition and prescribed shallowing of depths near grid walls results in strong frictional effects (lateral shear) primarily within one element of the boundary. In some instances the effects of friction at a boundary may also be observed within two elements from the wall.

CHAPTER 3

CIRCULATION RESULTS

The general pattern of modeled circulation within Terrebonne Bay will be discussed here; more specific details on the response of water movement and residual flow to variations in meteorological and oceanographic forcing will be addressed in a following chapter on transport. Typical patterns of modeled water movement within Terrebonne Bay are shown in Figs. 27 - 30. For better graphical display and arrow resolution, slightly different horizontal and vertical length scales were used in figures containing an outline of the Bay's shoreline. Average flow within the Bay is generally between 5 to 20 cm/s, with increasing speeds of up to 50 cm/s or more in or near the main tidal pass. Weaker flow, less than 5 cm/s, generally occurs behind mid-bay islands and in the more sheltered, northern regions of the bay. Strong flow occurs during mid-ebb or flood, and weaker flow just following peak high or low water.

Though slight variations in direction and speed occur, the general pattern of water movement within the Bay is similar between simulations. During the flood tide, water enters primarily through Cat Island Pass and flows northward. Four main paths of flow commonly occur: 1) into the narrower, westward portion of the bay, 2) up-estuary within or near the

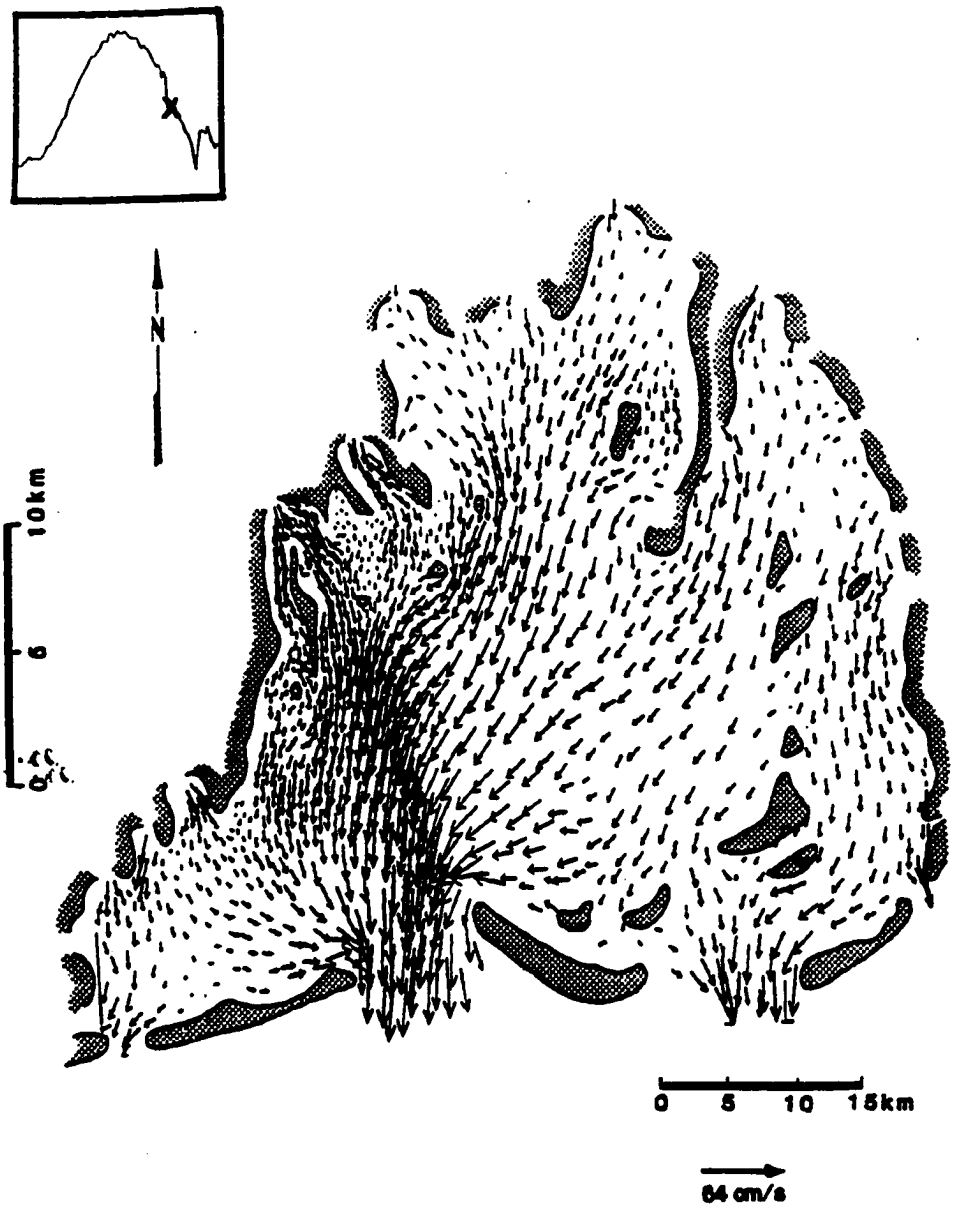

Figure 27: Typical pattern of simulated bay flow during ebb, the average current speed is 16 cm/s.

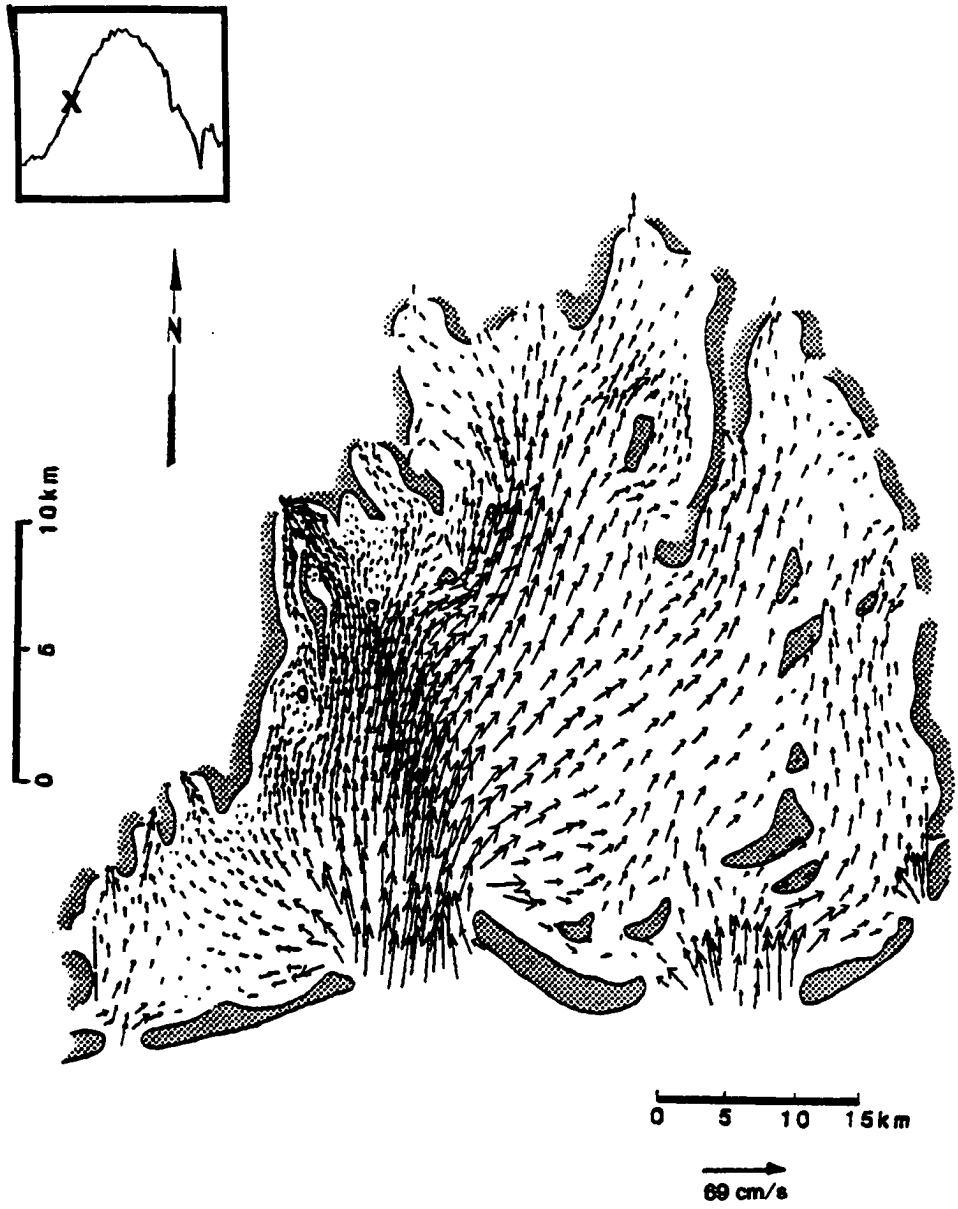

Figure 28: Typical pattern of simulated bay flow during flood, the average current speed is 17 cm/s.

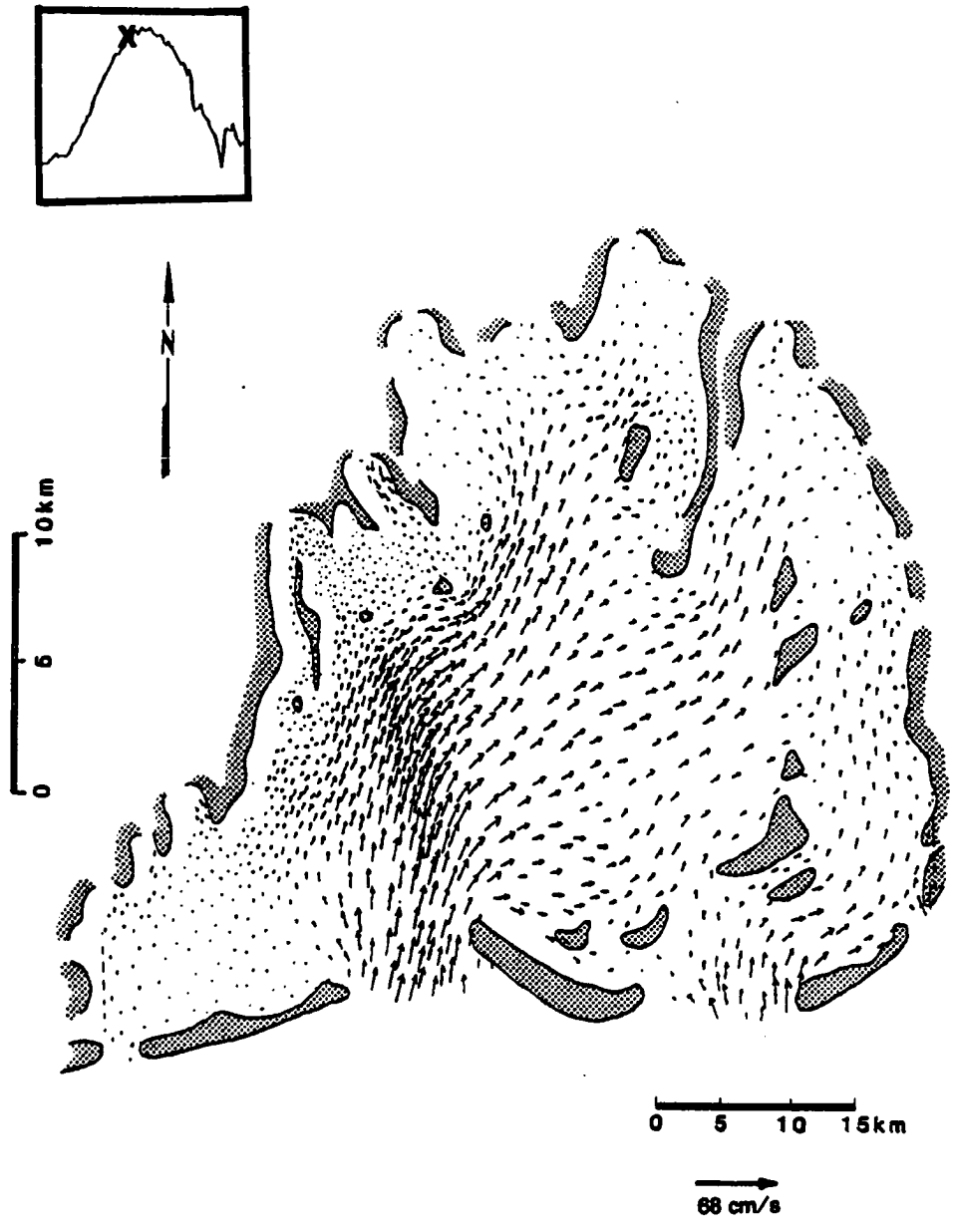

Figure 29: Typical pattern of simulated bay flow nearing high tide, the average current speed is 7 cm/s.

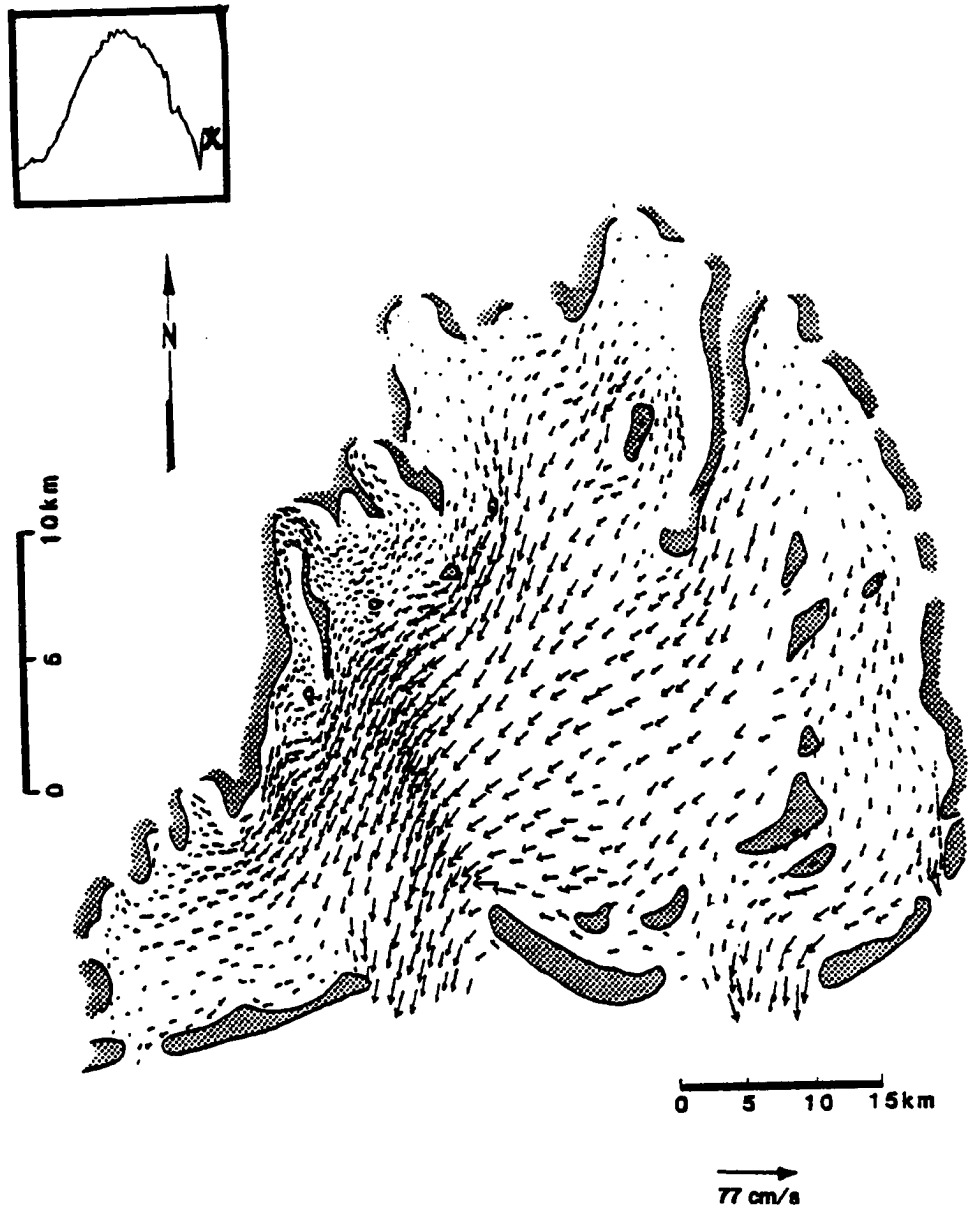

Figure 30: Typical pattern of simulated bay flow just prior to low water, the average current speed is 10 cm/s.

Houma Navigation Canal and out the northwest portion of the bay, 3) up-estuary and towards the east into Lake Barre, and 4) more directly eastward into the Timbalier Bay region. Flow during the outgoing tide is also largely controlled by Cat Island Pass. Ebb-tide currents move primarily to the south - southwest, with some flow directed southeast in the narrow western region of the bay. The magnitude of flow throughout the tidal cycle varies depending on the phase and range of the tide, as well as additional forcing provided by wind or discharge.

The effect of varying winds and runoff on current flow within Terrebonne Bay is depicted by the model runs shown in Figs. 31 - 33, and described in Table 5. Both the maximum and average speed of water movement within the Bay at a particular tidal stage are compared for several simulations. Each modeling run was performed using the same tidal curve (Fig. 34), but varying wind speed, direction, or runoff. As might be expected, the effects of wind are more obvious in the shallower regions of the bay (refer to Figs. 30 - 33).

Table 5: Modeled rate of flow given varied winds and runoff

	Maximum Speed (cm/s)				Average Speed (cm/s)			
Tidal Stage	No Wind	North Wind	South Wind	Added Runoff	No Wind	North Wind	South Wind	Added Runoff
high	12.77	18.88	14.39	19.21	3.04	3.56	2.96	3.19
mid-flood	46.70	50.04	49.24	45.82	14.46	14.02	14.63	13.84
mid-ebb	57.45	57.87	57.21	58.27	16.80	17.28	16.40	17.34
low	25.89	30.61	19.18	26.11	6.82	9.97	5.73	7.15

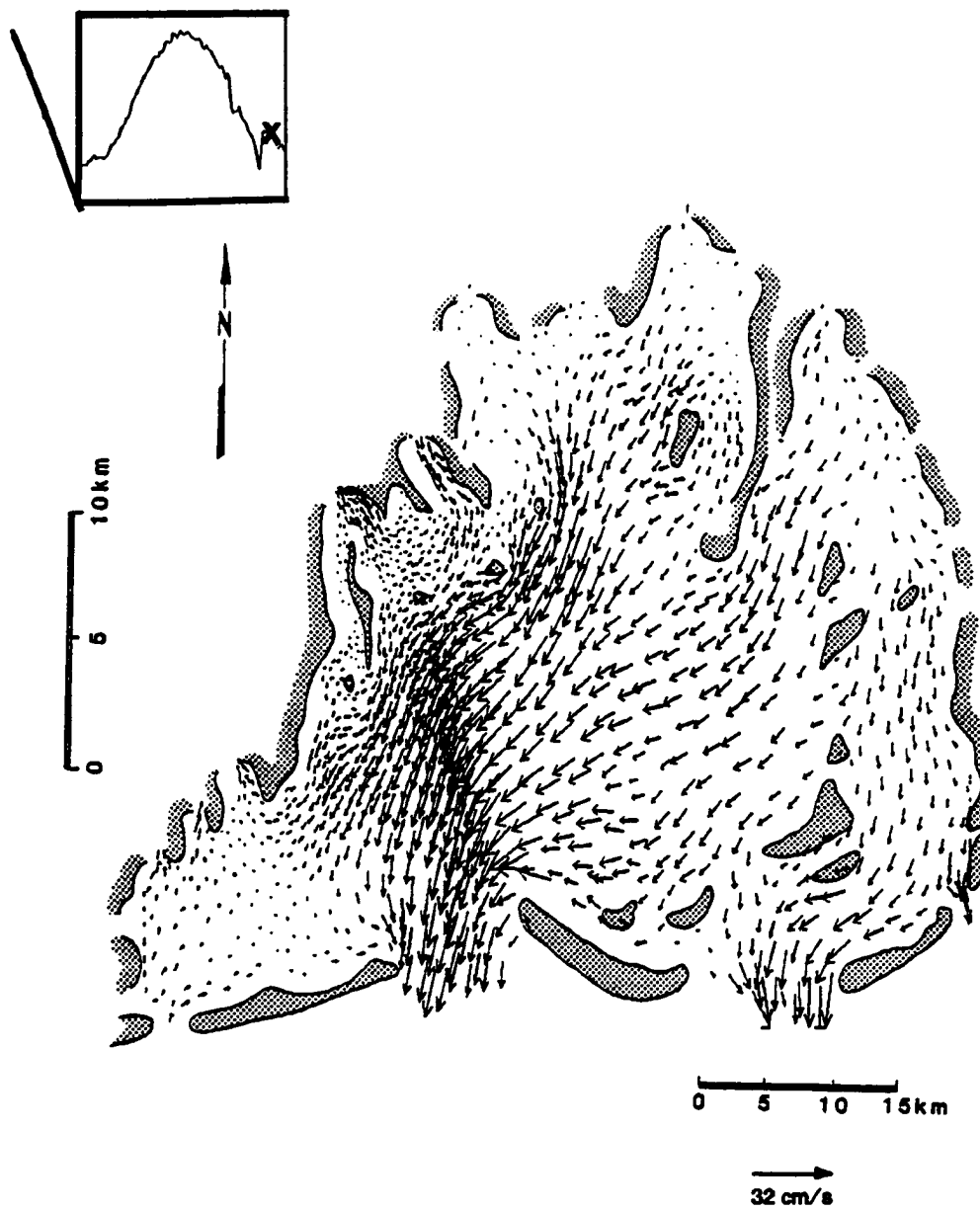

Figure 31: Simulated bay circulation near low tide in the absence of wind, incorporating the April 1 - 4 tidal variations.

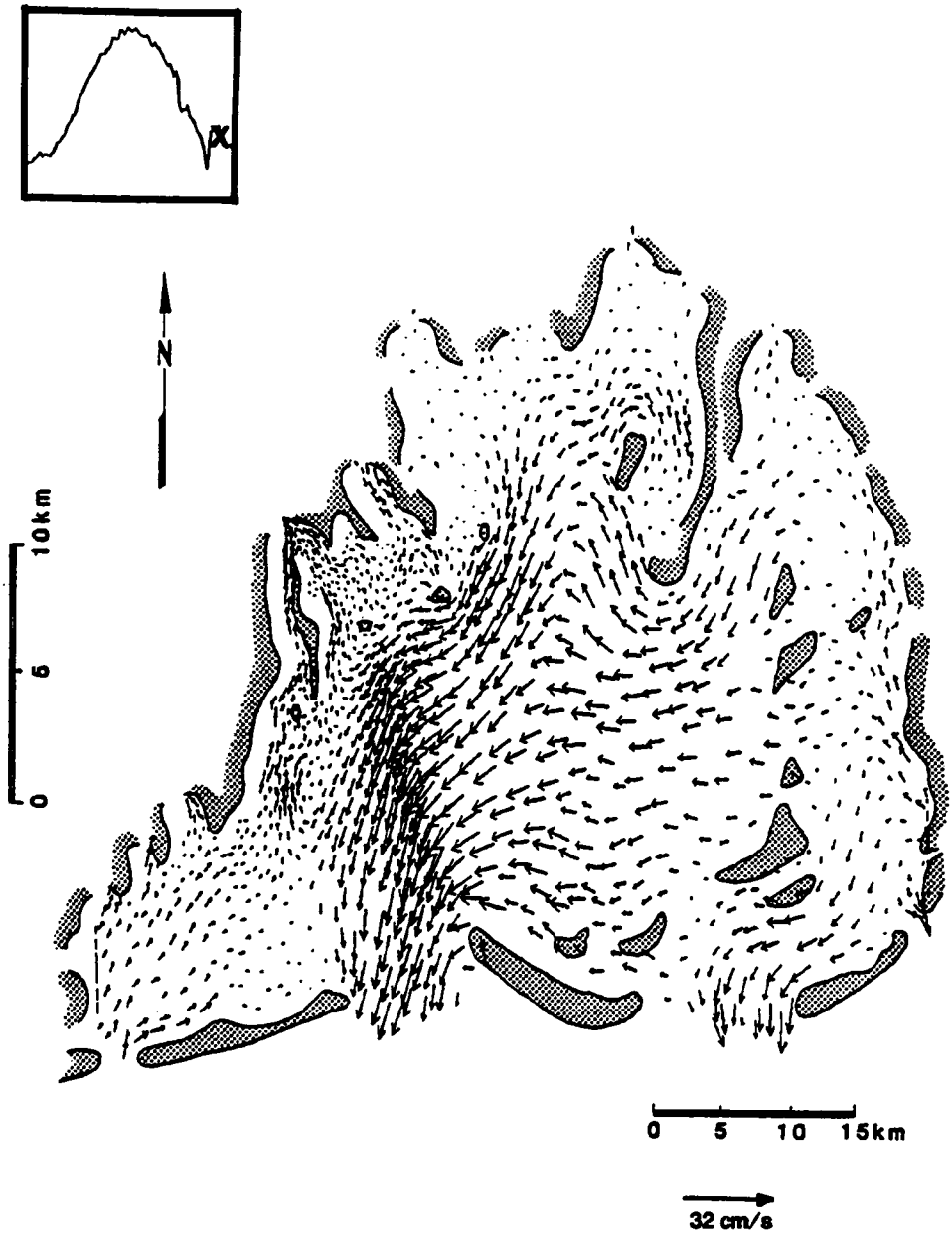

Figure 32: Simulated bay circulation near low tide with winds from the south and the April 1 - 4 tidal variations.

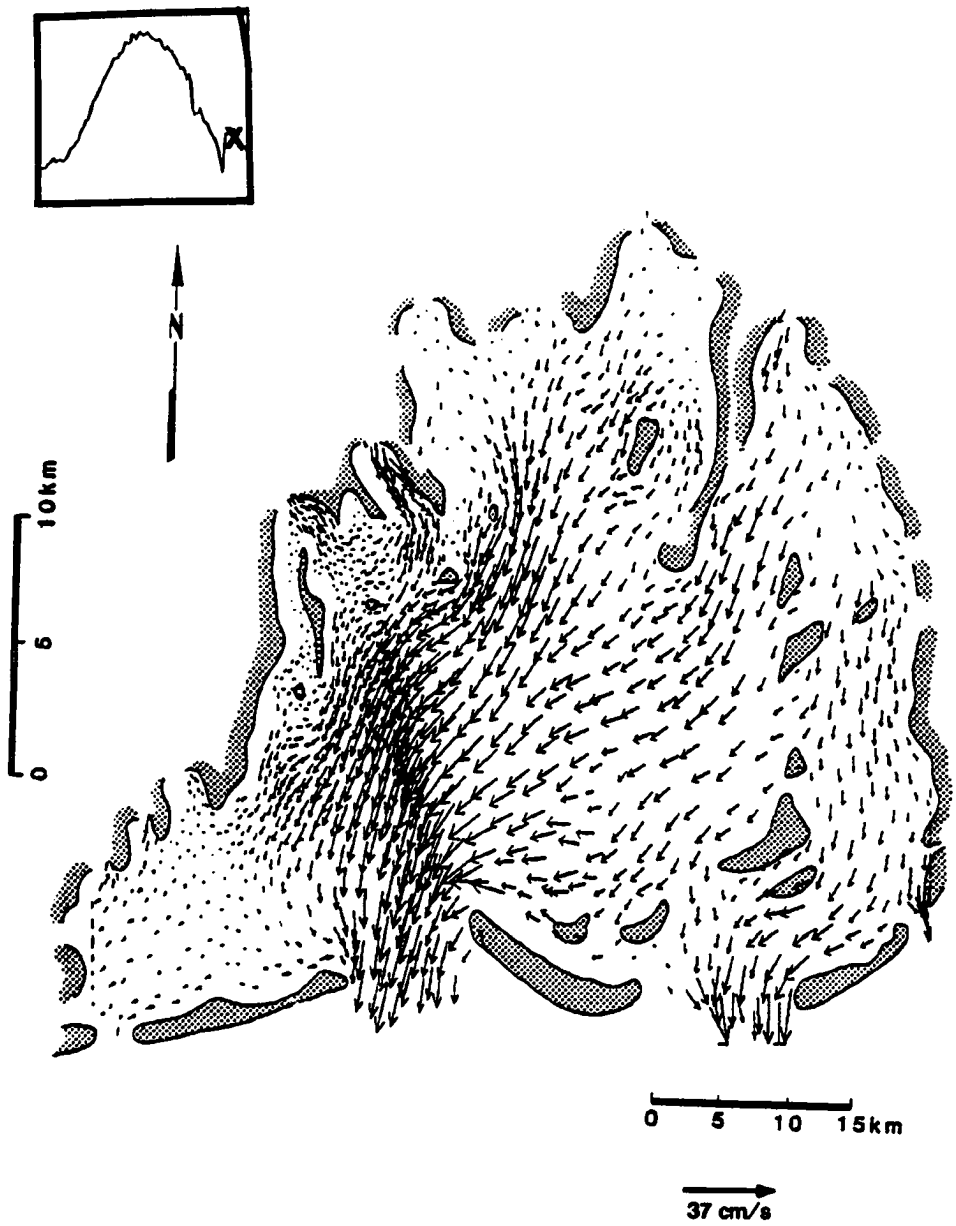

Figure 33: Simulated bay circulation near low tide with added runoff and the April 1 - 4 tidal variations.

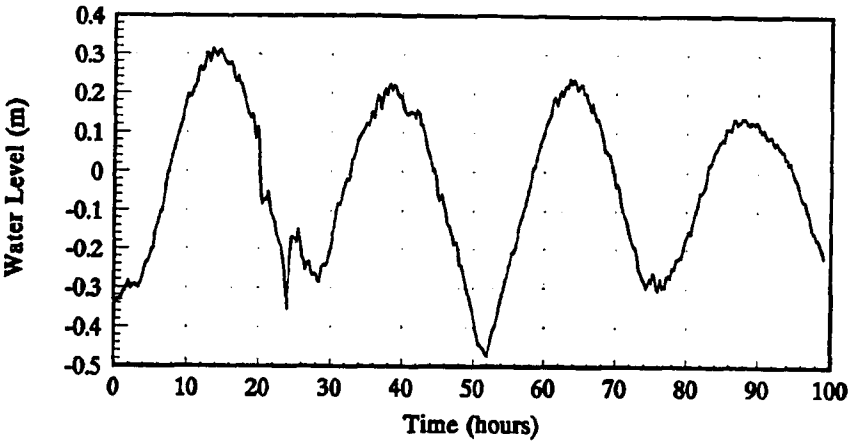

Figure 34: Water level variation at Cat Island Pass, April 1 - 4, 1990.

Results of circulation modeling within Terrebonne Bay generally show the expected variations in current flow in response to modified meteorologic and oceanographic conditions. Winds out of the north tend to augment flow southward during ebb, and decrease it northward during flood. Southerly winds, as would be expected, counteract flow during ebb, and increase it during flood. Stronger tidal currents appear to be generated by the increasing tidal range within the fortnightly cycle. Increased runoff has an effect similar to that of northerly winds, intensifying flow seaward. Particularly strong flow into the Gulf occurred during simulations of cold-front passage (Fig. 35). When varying tides, winds, and runoff are combined to simulate more realistic conditions in Terrebonne Bay, the effects on circulation are not as obvious as described above.

In order to evaluate transport patterns within the bay, advective water movement and residual flow are examined in detail using Lagrangian tracking techniques. Because these

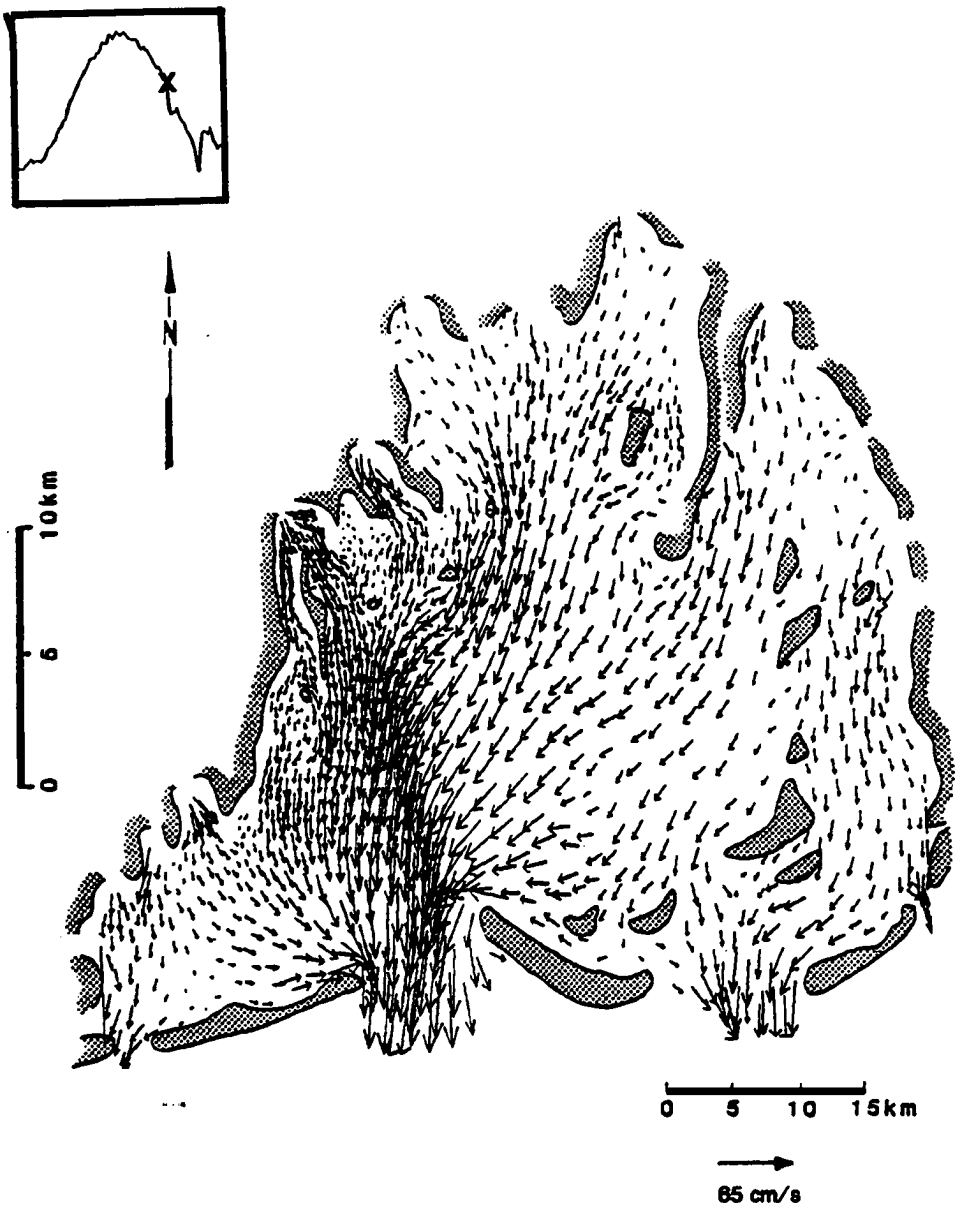

Figure 35: Simulated strong seaward flow at ebb following cold front passage, the average current speed is 19 cm/s.

transport patterns are a function of circulation, these methods offer not only a means of delineating the potential flow of sewage-related wastes, but also a means to better depict the response of water movement to realistically complex environmental conditions. With this in mind, modeled circulation patterns produced during the main modeling periods, as well as simulated cold-front passage, will not be discussed here, but in a following chapter with regard to transport processes within the Bay.

CHAPTER 4

MODEL ACCURACY

Two of the four simulation periods were chosen for comparison with real-time data, one during late March and a second during early September. The oceanographic and meteorologic conditions of the March period are representative of those prevalent during much of the year: varying wind speeds and direction, with a predominant easterly component. The September period is representative of less frequently occurring conditions: reasonably constant, weak winds from the south combined with periods of increased bay-wide runoff. The latter interval was chosen because it was expected that under these environmental conditions the model is least likely to duplicate the actual patterns of flow. Comparisons between model output and observations are based on water level variations up-estuary, current speed and direction at particular sites over time, and the mean Eulerian residual flow over one, two, and three tidal cycles.

Water Level Variations

Because the location from which up-estuary water level data were available is approximately 2 km north of the upper grid boundary, only qualitative comparisons with model output are possible. Hourly averages of Cocodrie water levels measured at

fifteen minute intervals are used, and a point two elements in from the northwest boundary near the Houma Navigation Canal was chosen from within the model. Comparisons between modeled water level fluctuations at this point with that measured at LUMCON visually show a good correlation (Fig. 36). Within the majority of simulation periods, water level variations at this position within the model are slightly greater (0.01 - 0.2 m) than the observed Cocodrie values, and the phase of the tide coincides most often within one hour or less. The model does not consistently lead nor lag the Cocodrie data, and the worst correlation appears to occur when an equatorial tidal range is present.

Results suggest that water-level variations up-estuary are reproduced well by the model in both phase and magnitude. The difference between the modeled and observed water level change may be a function of the locations from which values are being compared, the wall-like boundary conditions required by the model, and the real versus simulated effects of friction. Cocodrie tides are measured within a shallow embayment off a channel approximately 2 km north of the Bay. Hence, due to bottom friction there should be a short lag between the tidal phase at the Cocodrie location as compared to the model location. Amplitude of the tidal variation should, however, be similar. As tides propagate up-estuary, interactions with bifurcating channels and shoaling salt-marsh areas gradually dampen out tidal energy. However, numerical modeling techniques require a wall-like boundary, thus as tides reach the northern grid wall energy is damped, but may

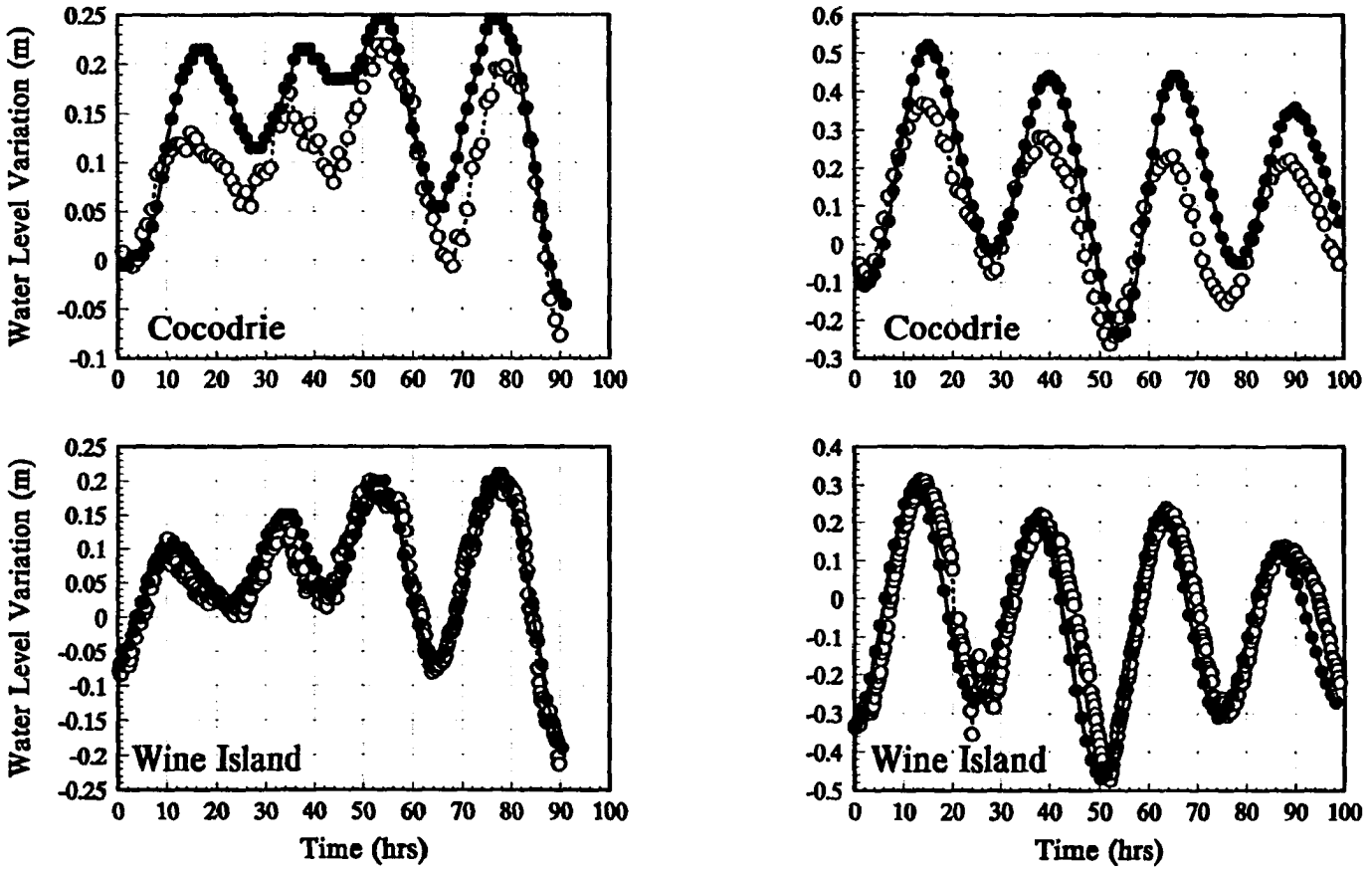

Figure 36: Observed (○) and modeled (●) water level variations up-estuary (Cocodrie) and at the mouth (Wine Island) under equatorial tides (A) and tropic tides (B). Note that the model location used for comparison at the Bay's mouth is several elements in from the specified open boundary input.

also be reflected. As a consequence the relatively greater range (0.01 - 0.20 m) of the up-estuary model tide as compared to that measured at Cocodrie is probably a function of reflection at the grid boundary. The variability observed in the phase correlation between model and observed data may also be a function of these conditions as well as the averaging of the observed values and the effects of simplifying bottom friction. Due to shoaling and an increasing abundance of plant growth, the effects of friction increase up-estuary. Since bottom roughness is simplified as a constant in the model, its effects are probably underestimated in the upper reaches of the bay. A stronger correlation could be obtained by extending the grid northward, however computational efficiency would be significantly diminished and the overall running time greatly increased. Decreasing accuracy in the reproduction of water level variations up-estuary during equatorial tides suggests that the model is less accurate when tidal forcing weakens. Given the purpose of this study, it is the author's opinion that the differences between the modeled and observed water level variations up-estuary are not large enough to have a significant effect on the results.

Velocity Field

The term error will be used here to describe the difference between the observed (current meter data) and predicted (model output) flow at particular locations and times within Terrebonne Bay. Comparisons will be based on both the speed and direction

of water movement measured at each current meter station and the numerically derived average from within the model element in which the current meter station is located. Average error will be used to describe the average difference between the observed and predicted speed ($U_o - U_p = D_u$) and direction ($D_o - D_p = D_d$) at particular points in time. Because current speed and direction are time varying, the use of a statistical parameter such as the root mean square error (Willmott et al., 1985), provides information only about the accuracy of tidally averaged flow, but reveals little regarding the correlation within a tidal period. Consequently, qualitative graphical methods will be employed to evaluate the accuracy of modeled flow as compared to that of real-time flow during successive tidal cycles. Because the goal of this project is to evaluate net displacement of pollutants after one or more tidal periods, quantitative measures of accuracy will also be based on the comparison of the mean Eulerian residual flow at the current meter stations ($\overline{U_o}$, $\overline{D_o}$) with those at corresponding model locations ($\overline{U_p}$, $\overline{D_p}$) over one, two, and three tidal cycles.

Due to equipment loss and failure, observations from station #1 are not suitable for comparison during either of the verification periods. Similar problems occurred at station #2 during the first deployment period, and station #5 in the later interval. Based on over 800 data point comparisons of instantaneous flow from the late March simulation, the average error between the observed speeds, and the modeled speeds is approximately 4 cm/s (Fig. 37A). Given that the average magnitude of flow is approximately 15 cm/s the model appears to

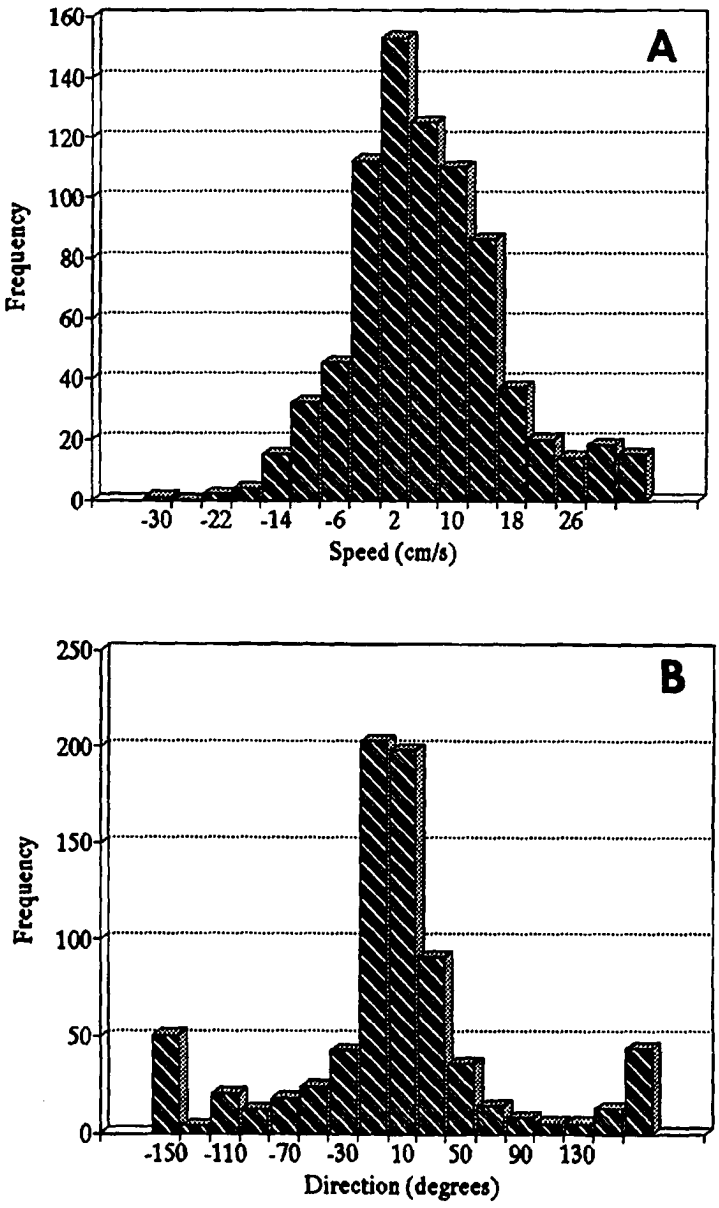

Figure 37: Difference between the unaveraged observed and modeled speed (A), and direction (B) of flow at current meter station locations, March 24 -April 4, 1990.

be generally within about 25% of the real current speed during this period (Table 6). The average error between the observed direction of flow at the stations and the direction of modeled flow at these same locations is approximately -10° to 10° (Fig. 37B). Whereas the manufacturer specifications of the current meters for accuracy are 2 cm/s in speed and 7° in direction, the simulated flow appears reasonably reliable. For purposes of discussion and comparison with the September modeling interval the error due to instrument accuracy will be ignored. Evaluation of the difference between the predicted and observed flow as a function of the observed speed shows little relationship between the magnitude of flow and error (Fig. 38); the same holds true for error as a function of direction. Within the March period, the

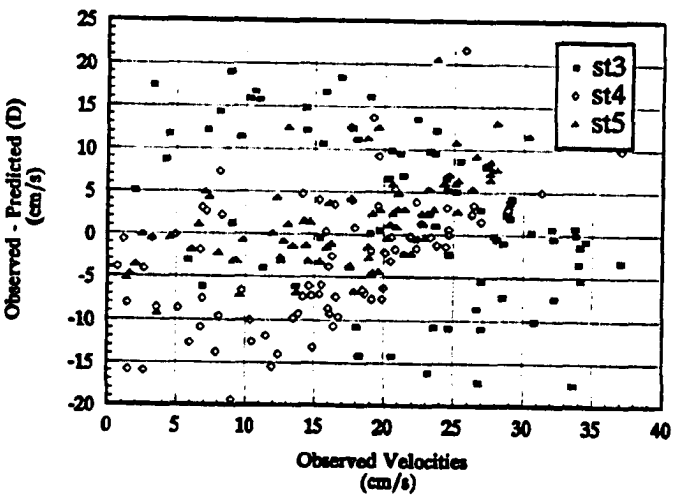

Figure 38: Model error as a function of velocity for the March simulation period.

alternation of the flood and ebb tidal flows is reproduced well by the model (Fig. 39). During the March 24th period, when tidal forcing was relatively weak, the correlation between model output

Table 6: Difference between the tidally averaged observed and modeled flow at current meter stations for the March simulation period.

1 Tide		Speed (cm/s)			Direction (degrees)		
Model run	Station	$\overline{U_p}$	$\overline{U_o}$	D_u	$\overline{D_p}$	$\overline{D_o}$	D_d
3/24	3	15.16	12.62	2.54	107	102	5
	4	11.96	7.91	4.04	113	102	10
	5	10.87	9.55	1.32	128	152	-23
3/28	3	21.68	19.49	2.19	116	144	-28
	4	16.75	13.39	3.44	111	124	-13
	5	14.4	15.11	-0.68	136	176	-40
4/1	3	23.19	20.13	3.18	122	149	-27
	4	17.97	14.14	3.83	126	167	-41
	5	15.01	16.06	-1.05	147	178	-31
Avg.		16.33	14.27	2.09	123	144	-21
Std. Dev.		3.86	3.83	1.77	12	27	17
2 Tides							
3/24	3	13.75	11.48	2.27	128	128	0
	4	10.93	7.06	3.83	130	117	13
	5	9.82	7.4	2.43	145	171	-26
3/28	3	23.54	21.71	1.8	128	154	-26
	4	18.24	15.05	3.19	122	142	-20
	5	15.30	17.01	-1.7	148	191	-43
4/1	3	23.30	20.41	2.89	129	156	-26
	4	18.21	14.20	4.0	128	161	-33
	5	15.08	17.07	-2.0	151	185	-34
Avg.		16.46	14.60	1.86	134	156	-22
Std. Dev.		4.58	4.89	2.09	10	23	17
3 Tides							
3/24	3	14.13	10.94	3.19	124	127	-3
	4	11.33	7.12	4.21	124	124	-0.45
	5	10.07	8.61	1.46	143	154	-11
3/28	3	24.38	22.35	2.04	130	151	-21
	4	19.01	15.83	3.18	124	139	-15
	5	15.70	17.98	-2.23	149	188	-39
4/1	3	24.28	22.14	2.14	135	154	-19
	4	19.03	16.51	2.52	132	158	-26
	5	15.60	19.06	-3.45	155	178	-23
Avg.		17.06	15.62	1.45	135	153	-17
Std. Dev.		4.80	5.26	2.43	11	20	11

($\overline{U_p}$ = tidally averaged model speed, $\overline{U_o}$ = tidally averaged observed speed, $D_u = U_p - U_o$, $\overline{D_p}$ = tidally averaged model direction, $\overline{D_o}$ = tidally averaged observed direction, and $D_d = D_p - D_o$)

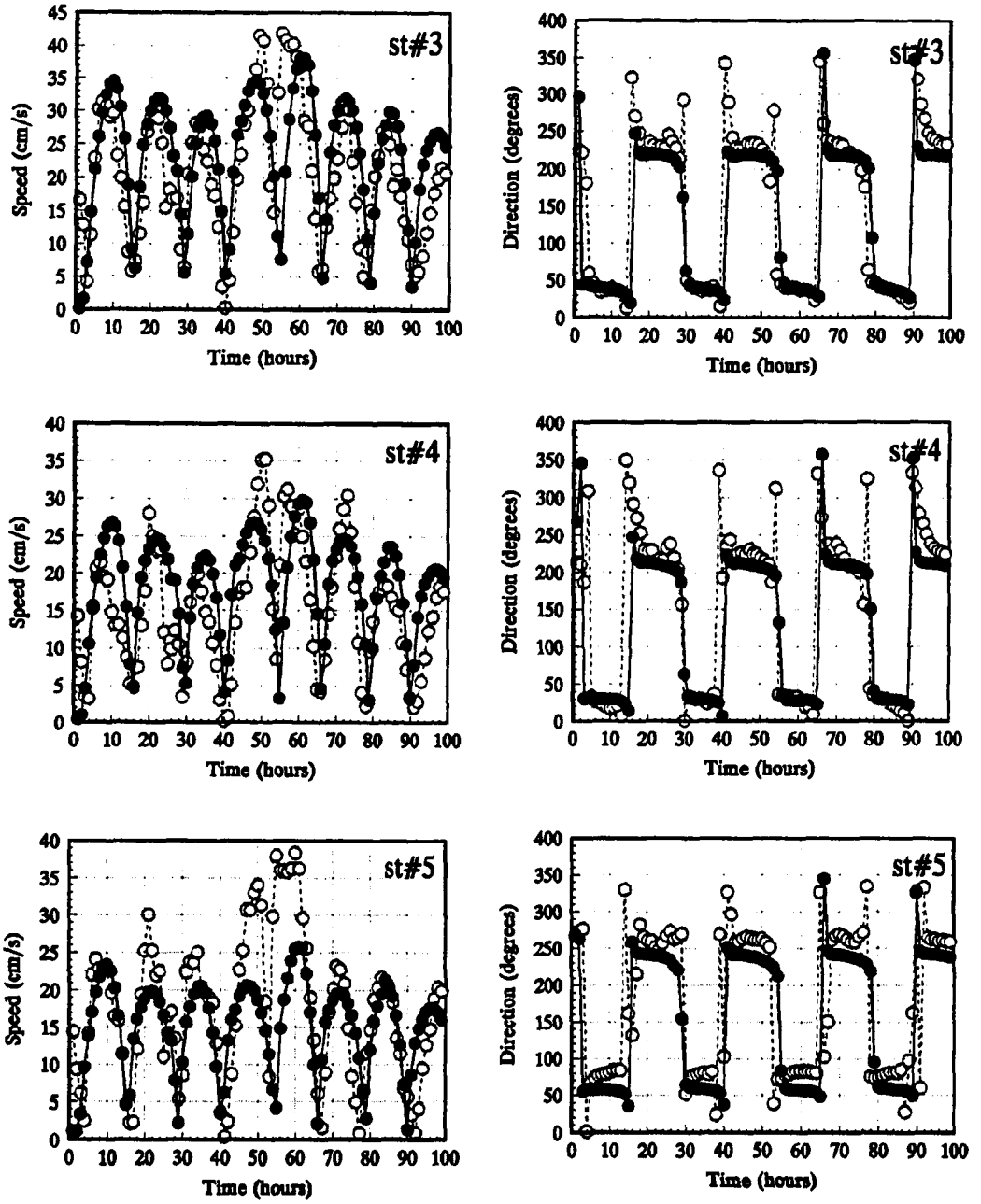

Figure 39: Observed (o) flow at current meter stations #3, #4, and #5 and that at corresponding model locations (●) for April 1 - 4, 1990; speed is on the left and direction on the right.

and real-time data decreases (Fig. 40). Qualitative comparisons of both speed and direction of flow at each location indicate that overall trends are similar (Fig. 41). The most significant difference in the direction of flow occurs at station #5. This is not unexpected because at this site relatively fine-scale bathymetric

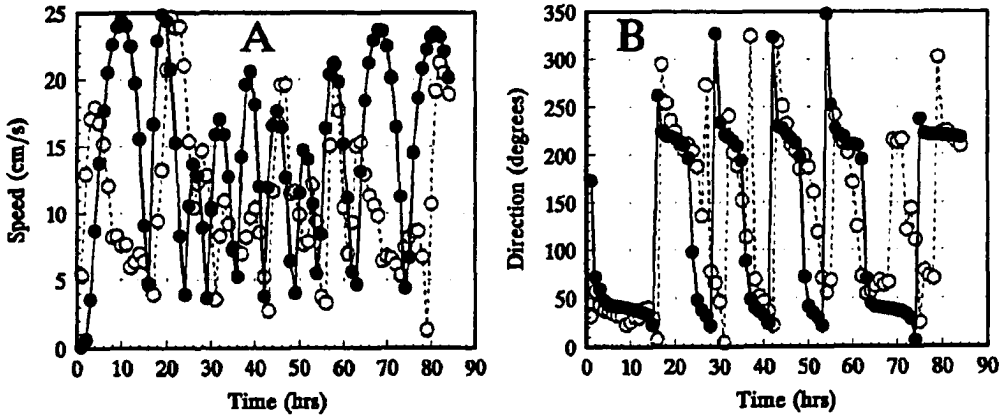

Figure 40: Modeled (●) versus observed (○) flow at station #3, March 24 - 27, 1990, speed (A) and direction (B).

changes probably play a strong role in controlling flow and may not be well represented in the model. Data from station #3, where two current meters were installed (one at 1.5 meters and the other at 2.5 meters below the surface), reveals that while the direction of flow is similar over a tidal cycle, near bottom currents tend to be slightly slower than those near surface (Fig. 42).

Comparisons between the observed Eulerian mean speed over one, two, and three tidal cycles, with the modeled rates reveals an error of less than 15% for each sequence (Table 6). Similarly, the error in averaged directions is approximately 15% over the comparison intervals.

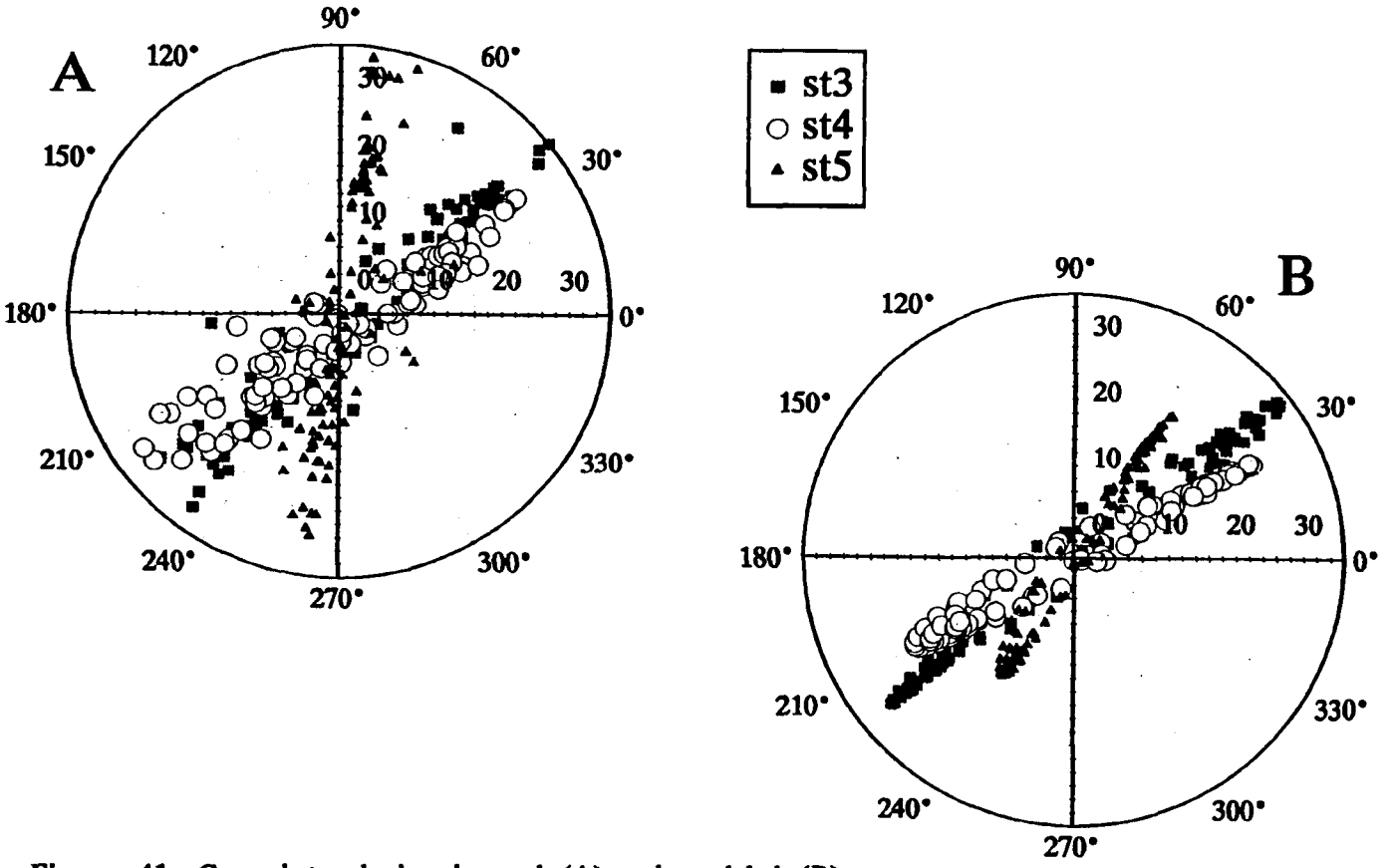

Figure 41: General trends in observed (A) and modeled (B) current speed and direction at each station during April 1 - 4, 1990 (reference axes based on model conventions, 90° is north and speed rings in cm/s).

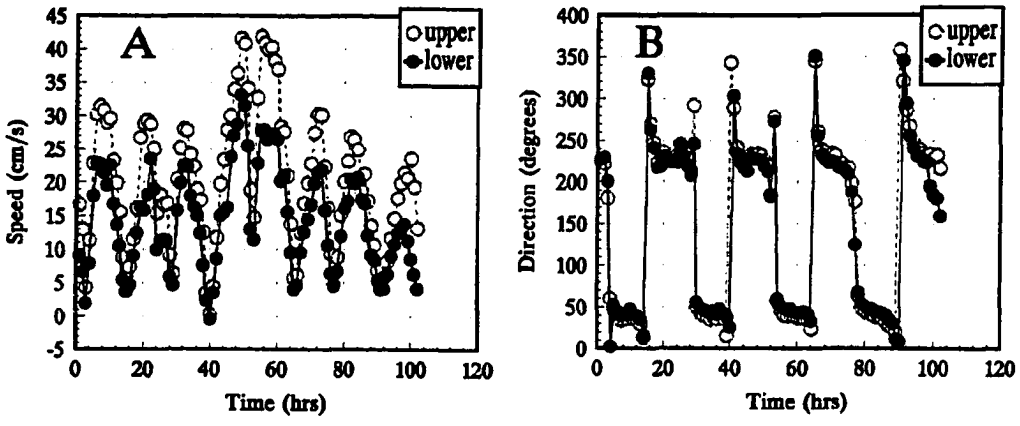

Figure 42: Surface versus near bottom flow, speed (A), direction (B), station #3, April 1 - 4, 1990.

Similar statistical measures and qualitative comparisons were performed for the September simulation period (Table 7; Figs. 43 - 45). The mean error in the unaveraged current speed is approximately 4.0 cm/s and directional differences are -10° to -17°. Qualitative evaluation of current meter data indicates that during the September simulation period there are more time intervals in which the normal ebb - flood cycle is poorly defined or irregular. The correlation between modeled flow and observed flow during these time intervals decreases. A particularly good example of deviations from the usual flood - ebb alternation is exhibited in the September 16th record (Fig. 45). During the second tidal cycle of the interval, where the model predicts flooding currents, the current meter record shows a very brief flood and extended ebb. Correlated to this time interval, between 30 to 40 hours into the period, is the absence of a velocity peak at station #2 (Fig. 45). At this station which is mid-bay, relatively close to the Navigation Canal, the model also consistently

Table 7: Difference between the tidally averaged observed and modeled flow at current meter stations for the September simulation period.

1 Tide		Speed (cm/s)			Direction (degrees)		
Model run	Station	$\overline{U_p}$	$\overline{U_o}$	D_u	$\overline{D_p}$	$\overline{D_o}$	D_d
9/8	2	17.76	11.44	6.31	137	149	-12
	3	19.68	15.48	4.21	123	124	-1
	4	15.34	11.79	3.56	116	132	-16
9/12	2	21.53	13.74	7.79	136	152	-16
	3	23.81	17.6	6.21	121	133	-12
	4	18.51	13.72	4.79	113	136	-23
9/16	2	13.74	8.1	5.64	154	189	-36
	3	15.38	18.19	-2.81	140	149	-9
	4	12.68	13.11	-0.44	139	150	-10
9/18	2	10.56	11.48	-0.92	134	155	-21
	3	11.82	4.75	7.05	124	160	36
	4	9.4	4.24	5.16	121	153	-32
Avg.		15.85	11.97	3.88	130	149	-13
Std. Dv.		4.30	4.26	3.28	12	16	17
2 Tides							
9/8	2	19.02	12.17	6.85	142	152	-10
	3	21.12	16.35	4.77	128	129	-1
	4	16.51	12.29	4.22	121	133	-12
9/12	2	21.26	13.32	7.93	142	154	-12
	3	23.58	17.34	6.24	129	143	-14
	4	18.43	13.28	5.15	122	140	-18
9/16	2	12.67	5.59	7.08	161	201	-40
	3	14.22	23.37	-9.15	148	175	-27
	4	11.29	13.04	-1.75	146	154	-8
9/18	2	11.73	11.46	0.27	135	156	-21
	3	13.13	5.61	7.52	125	160	-35
	4	10.48	4.81	5.67	121	132	-11
Avg.		16.12	12.39	3.73	135	152	-17
Std. Dv.		4.28	5.11	4.78	12	19	11
3 Tides							
9/8	2	20.17	13.04	7.12	143	154	-11
	3	22.38	16.79	5.58	130	130	-0.75
	4	17.52	13.17	4.35	122	137	-15
9/12	2	20.66	12.67	7.99	144	154	-9
	3	22.96	17.07	5.89	132	141	-9
	4	17.99	13.50	4.49	126	134	-8
9/16	2	11.34	4.67	6.67	170	201	-31
	3	12.73	20.98	-8.26	157	162	-5
	4	10.10	13.32	-3.22	154	143	12
9/18	2	12.85	10.34	2.51	140	167	-27
	3	14.38	6.57	7.81	129	154	-26
	4	11.48	5.78	5.69	124	125	-1
Avg.		16.21	12.33	3.89	139	150	-11
Std. Dv.		4.42	4.65	4.66	14	20	12

($\overline{U_p}$ = tidally averaged model speed, $\overline{U_o}$ = tidally averaged observed speed, $D_u = U_p - U_o$, $\overline{D_p}$ = tidally averaged model direction, $\overline{D_o}$ = tidally averaged observed direction, and $D_d = D_p - D_o$)

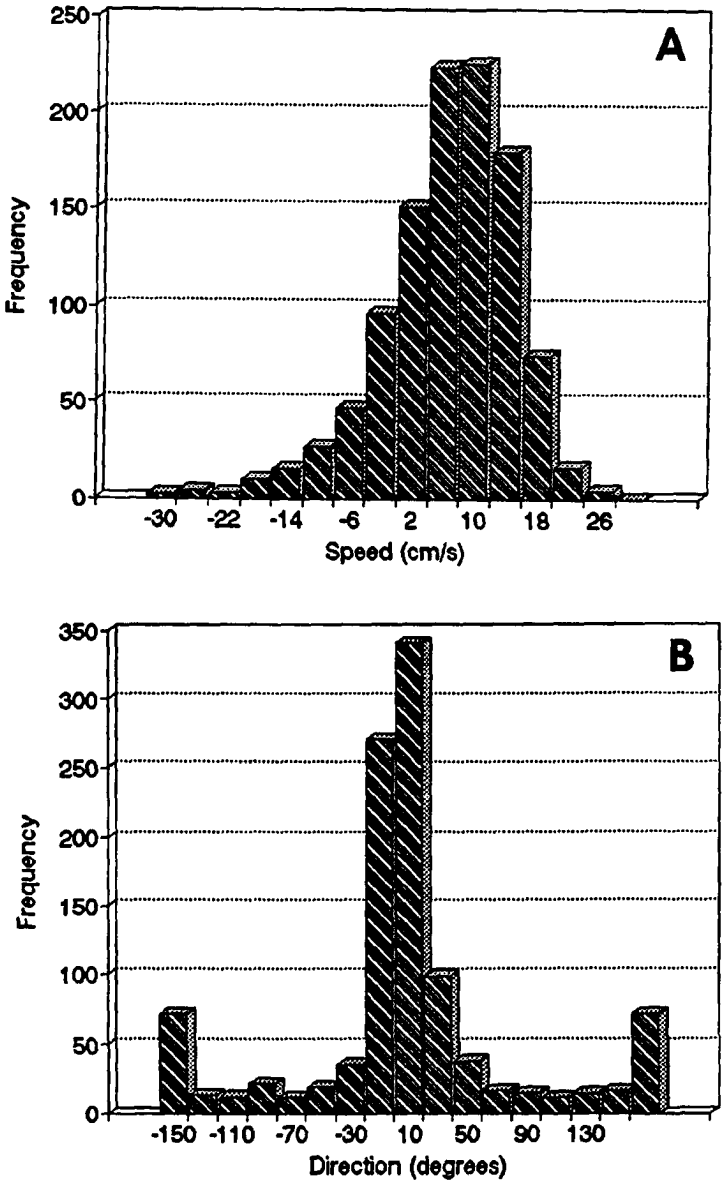

Figure 43: Difference between unaveraged observed and modeled speed (A), and direction (B) of flow at current meter station locations, September 8 -22, 1990.

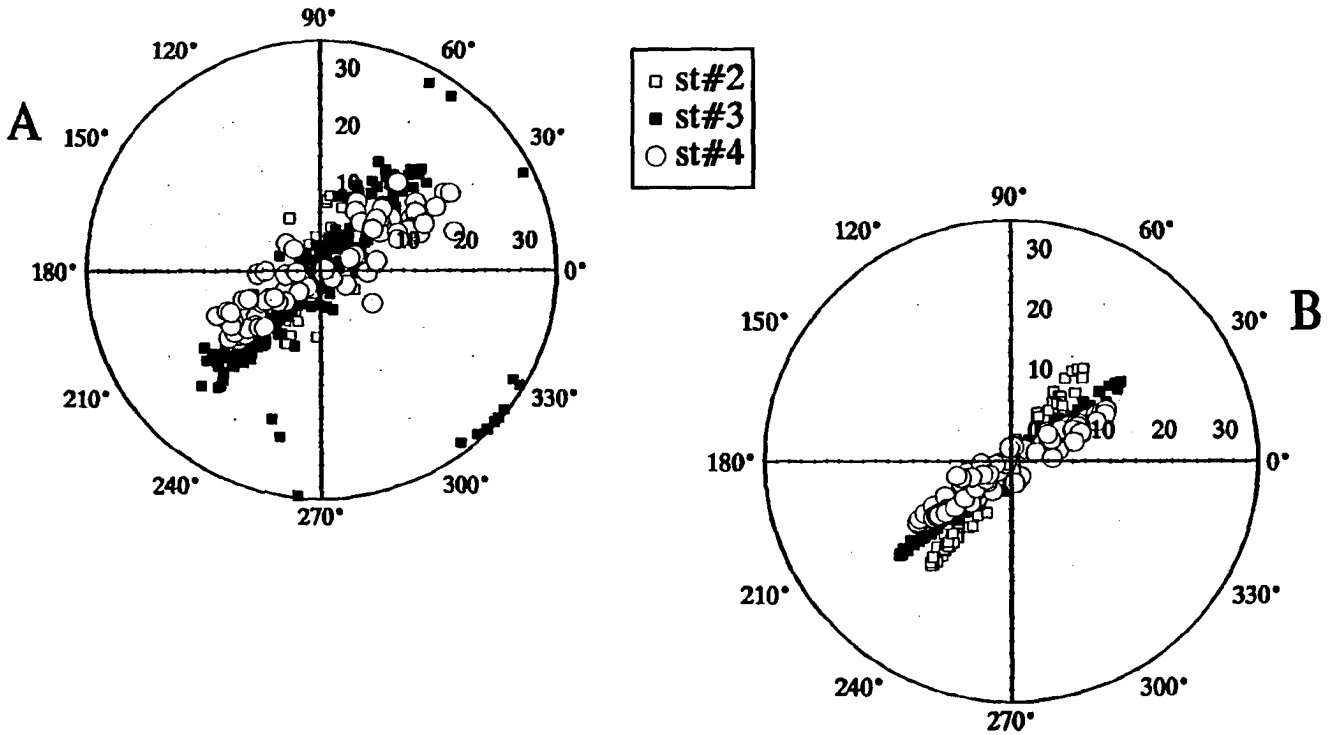

Figure 44: General trends in observed (A) and modeled (B) current speed and direction at each station during September 16 - 20, 1990 (reference axes based on model conventions, 90° is north and speed rings in cm/s).

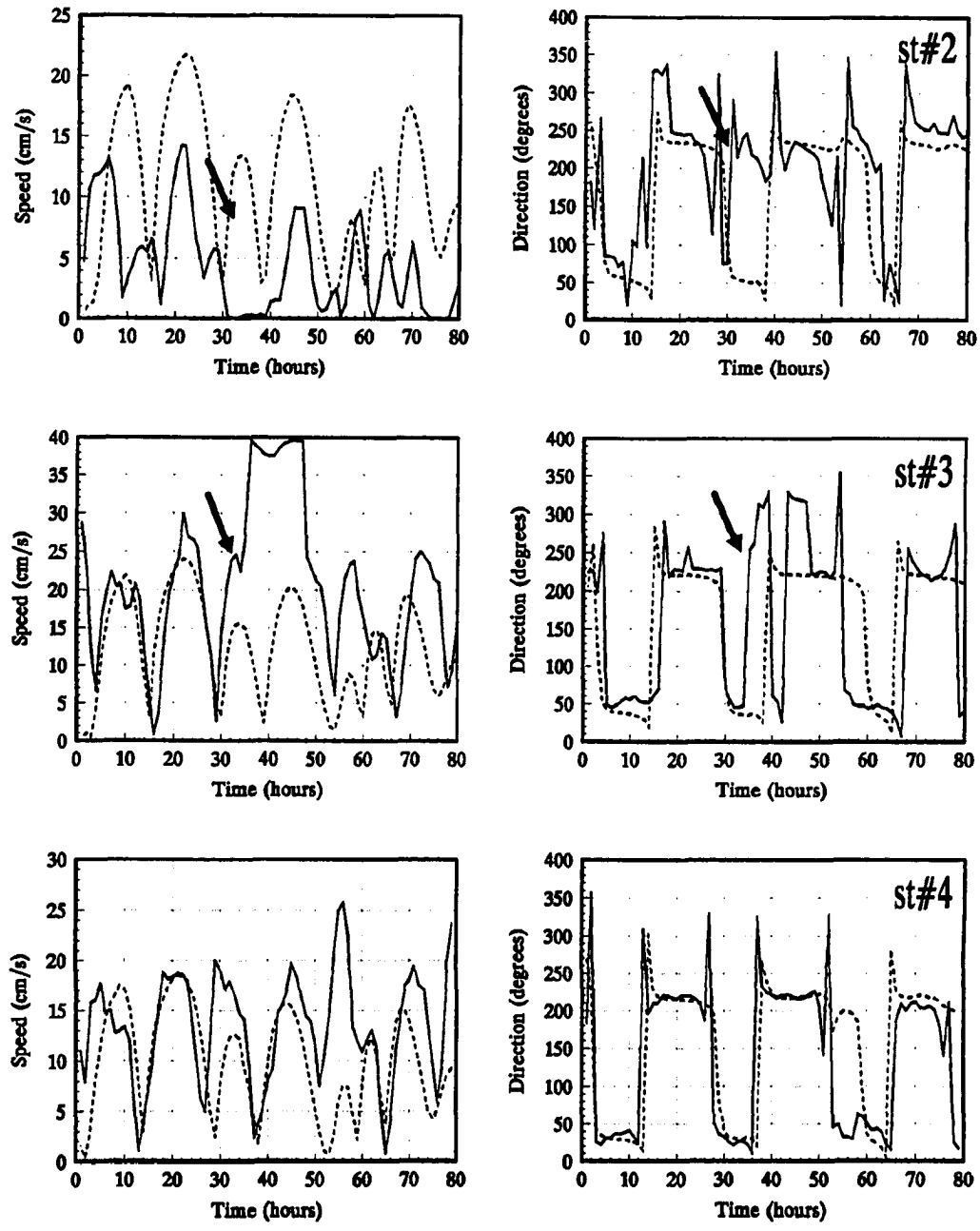

Figure 45: Observed (—) flow at current meter stations #2, #3, and #4 and that at corresponding model locations (▪▪▪) for September 16 - 20, 1990; speed is on the left and direction on the right. Arrow denotes hypothesized runoff event.

overestimates flow during the September 16th interval. While a better fit occurs at station #4, the correlation in velocities at station #3 is disrupted by a strong signal at about 40 hours (Fig. 45).

Discussion

Comparison between patterns of observed flow and those generated by numerical modeling techniques suggest that the model is relatively accurate for the oceanographic and meteorologic conditions during the March - April simulation period, and less accurate for conditions which occurred during September of 1990. Although the average error is only about 10 - 20% greater in current speed during the September period, the correlation in the alternating ebb and flood flow is visually much less accurate. A portion of the error in both cases may be explained by the use of a vertically integrated scheme. As results from the two meters at station #3 during the March simulation suggest, even during periods when the water column appears to be relatively well-mixed, bottom friction gives rise to a vertical velocity profile which tends to increase upward. Hence, current measurements near surface tend to be greater than an integrated average, and observations near-bottom less than the average.

It is suggested that the increased error which occurs during the September modeling period is primarily a result of increased runoff combined with weak winds, producing a weakly stratified water column. In partially mixed estuaries with significant river discharge, stratification and velocity shear with depth at the mouth are common (Bowden, 1967; Pritchard, 1967). In

Terrebonne Bay, when strong runoff occurs in combination with weak winds and/or tides, buoyancy driven flow may result in a similar gravitational-type circulation. With a lack of mixing and augmentation of the ebb flow by runoff, flow within the water column may become subject to the effects of strong shear. Because the data from stations with more than one current meter were lost, it is difficult to discern stratification and/or velocity shearing with the available records. However, ongoing studies of salinity within the bay and adjacent environments indicate that during local freshets, short-term stratification can occur (McKee, pers. comm.; Lee et al., 1990). Increased runoff during this period is suggested by both the water budget/discharge comparisons (Fig. 46), and the current meter data. Although it is not clear exactly when runoff increases, discharge from Bayou Grand Caillou increases sharply between September 13 and 16. Additionally, current meter records reveal damped flood tide currents and

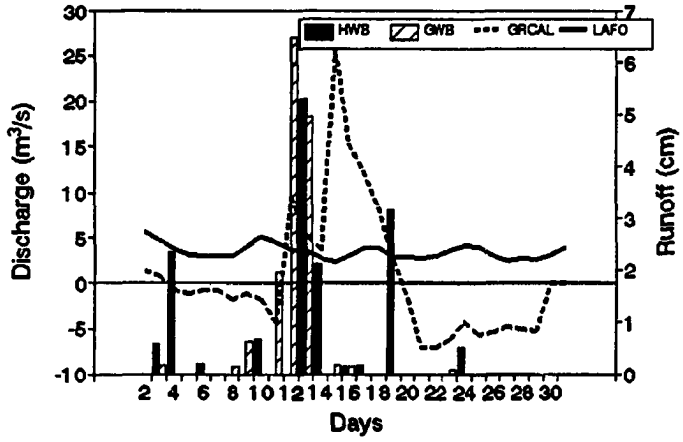

Figure 46: Discharge and water budget runoff, September 1990, note the increase in flow of Bayou Grand Caillou around the 16th.

augmented ebb currents around September 18th (Fig. 45). If increased freshwater discharge caused stratification during this period it is likely that its effects would be strongest in the vicinity of Cat Island Pass and associated with the Navigation Canal. Not only is the Canal a relatively deep conduit for more saline Gulf waters to flow up-bay, but it also is a major channel by which freshwater is discharged seaward. Therefore, if stratification is present, the current meter station closest to the Canal should exhibit the greatest effects of vertical shear relative to the other stations. Current meter records support this hypothesis. Data from station #2 which is in close proximity to the Navigation Canal, exhibits the greatest deviation during the September 16th modeling period from the earlier observed alternation of flood and ebb currents, as well as from the predicted variations. The reduced current speeds at this station and the overall tendency for positive speed differences during this period (refer to Fig. 43A) may reflect the effects of shear within the water column. Less of an effect is observed at the stations further away from the Canal. These results suggest that during periods characterized by weak wind and/or tidal mixing, and increased freshwater runoff, the validity of using a vertically integrated approach is diminished. The increased error in modeling under weak wind/tide conditions (March 24 - 27) also supports the findings of up-estuary water level variation comparisons; under weak forcing conditions, the model's accuracy decreases.

Results indicate that during periods of weak forcing, particularly when combined with strong freshwater runoff this

model cannot accurately reproduce the true patterns of flow within Terrebonne Bay. However, it should be recognized that on an annual basis, the conditions which appear to result in stratification are relatively infrequent.

24 - Hour Experiment

Much of this research focuses on the northwest quadrant of Terrebonne Bay; due to the intensity of local boating, fishing, and barge activity, this is also the most difficult area in which to work. Because it was not possible to install a moored current meter for any extended period of time within this region, in order to estimate the magnitude of flow, a 24 - hour period of current monitoring was undertaken. Unfortunately, due to logistical difficulties and bad weather, the experiment was conducted after the 1990 instrument deployment/modeling period had ended. One of the major obstacles while attempting to conduct this research was the presence of a dredging barge within the area.

Three stations were established as close as possible to the Navigation Canal (refer to Fig. 25). Each station was marked with an anchored buoy bound with reflective tape for location during night measurements. Approximately once per hour for 24 hours, current strength and direction were measured at each station using an Endeco Current meter with real-time logging capabilities on a shipboard computer. Where possible, current measurements were taken from the surface, mid-depth, and near bottom. Additionally, water temperature and salinity, as well as wind

speed and direction were determined. A tide gage was placed in the bay to record water level variations, and a fourth, moored current meter station was also established (Fig. 25).

Meteorologic and oceanographic conditions as similar as possible to those observed during the 24 - hour experiment were input into the model. Qualitative comparisons were then made between the observed flow and modeled flow at points most representative of the station locations. The correlation between the direction of water movement was extremely good (Fig. 47), however the model consistently underestimated the magnitude of flow at all stations (Fig. 48). This discrepancy may be explained by the recent dumping of dredge spoil in the area. If the amount of water flowing over the area remains constant, a decrease in depth via the input of dredge spoil would tend to increase the velocity of flow in the overlying waters. Since depths used in modeling were pre-dredging values, velocities should be, as observed, lower than those post-dredging. In addition, the apparent error in model output may be partially a function of numerical smoothing in the modeling process. Simulated velocities are actually representative of average flow within an elemental area versus that at an exact point. This is particularly true in areas where bathymetric changes occur on a finer scale than represented by gridding, such as in close proximity to the Navigation Canal.

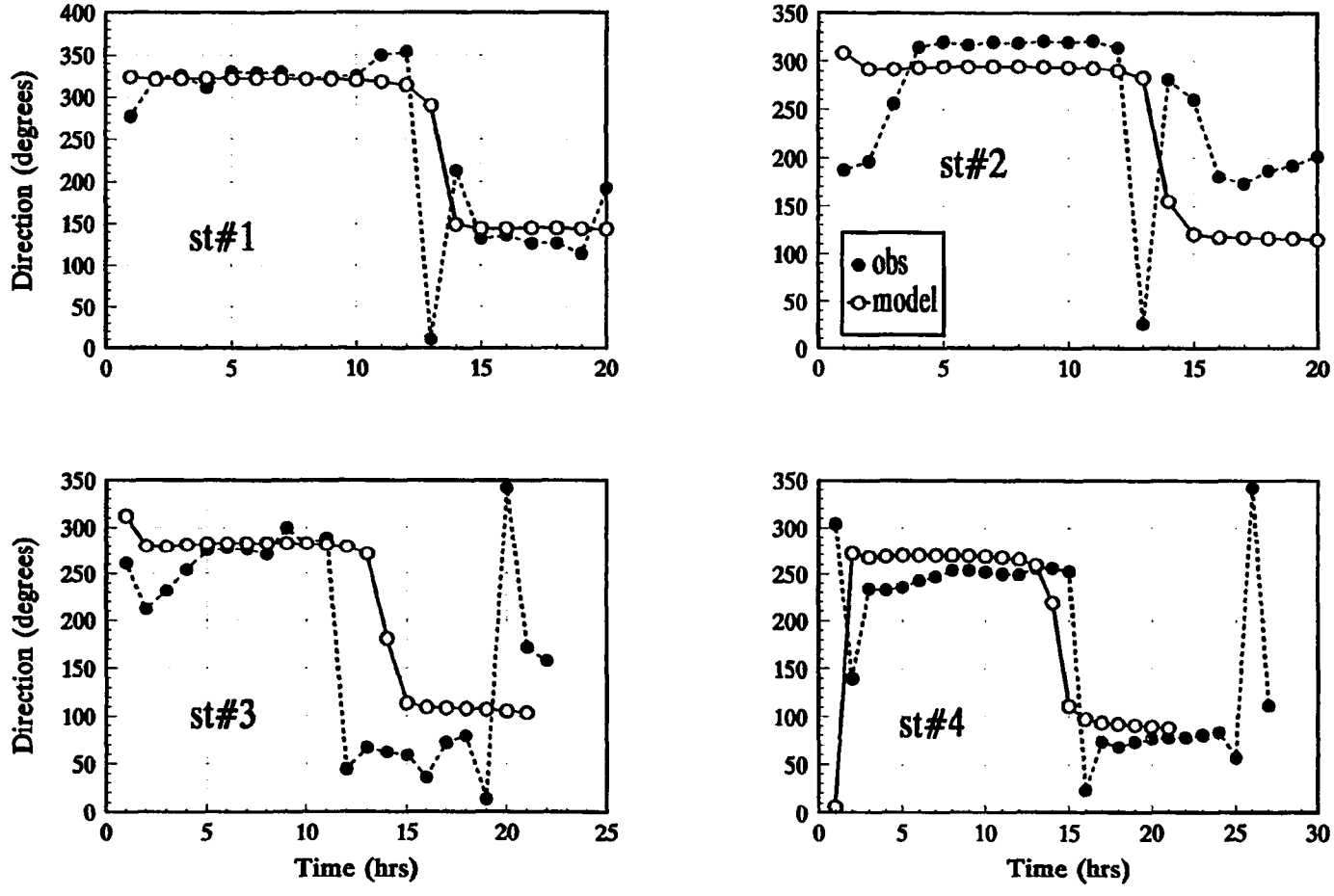

Figure 47: Results of 24 - hour experiment as compared to model output, direction.

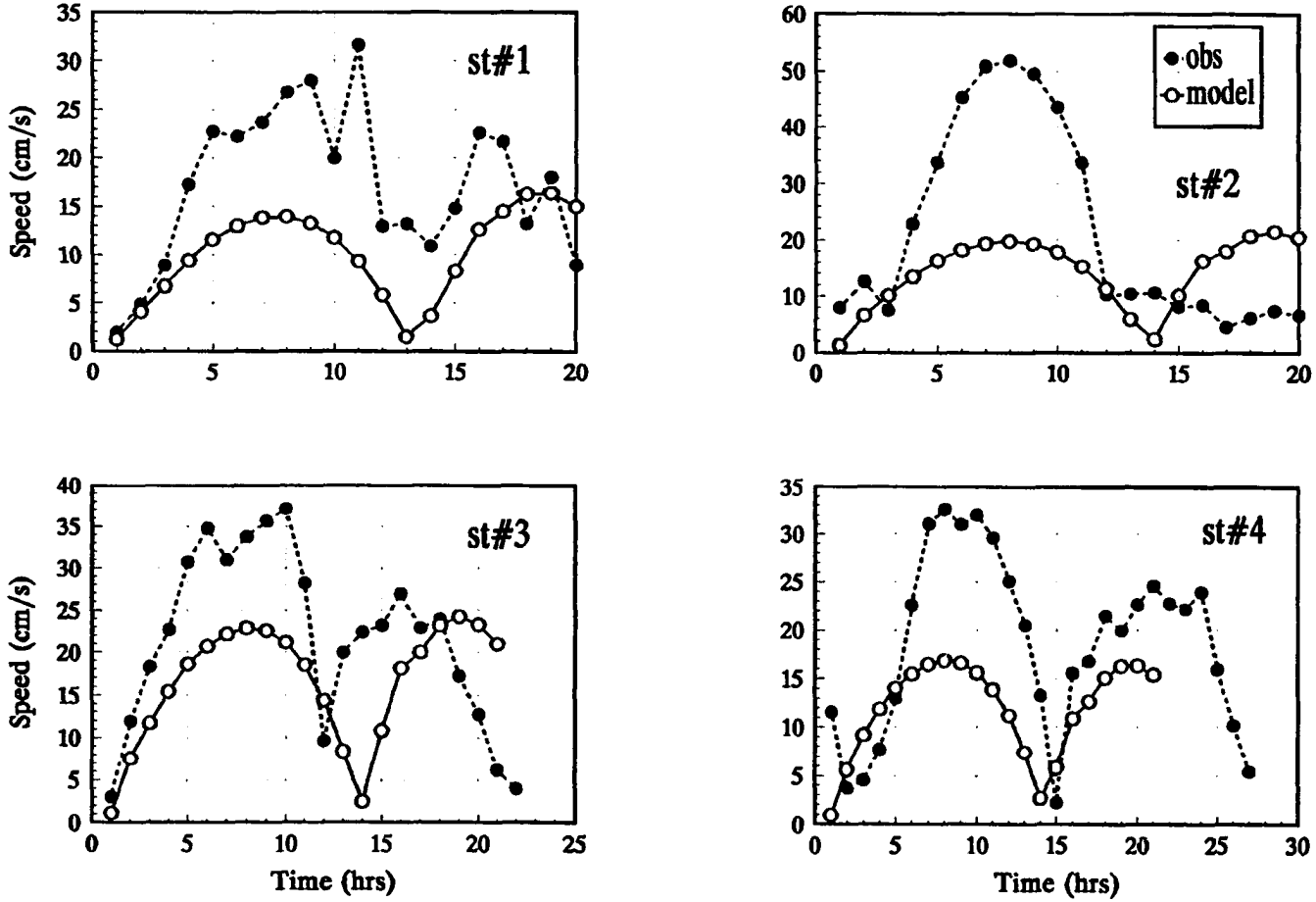

Figure 48: Results of 24 - hour experiment as compared to model output, speed.

CHAPTER 5

TRANSPORT PROCESSES

Methods

To evaluate the patterns of water-borne transport in the northwest region of Terrebonne Bay Lagrangian-type tracking techniques were employed. For each simulation period, two groups of particles, each consisting of 9 computer generated drogues, were released from an upper and lower bay location (Fig. 49). Particles released into the simulated patterns of flow are calculated to move with a vertically averaged velocity which is proportional to that at the center of each element and a function of the actual position of the particle relative to each nodal point of the element.

Figure 49: Diagrammatic sketch of release points for particle tracking experiments.

Based on morphology of the bay and grid size, the scale of dispersion is expected to be greater at the lower bay location. Consequently, at the more southern site, the distance between particles was increased from 100 m to 500 m, such that the spread of the particles covers one grid element in each area. At the upper bay location particles were released at the beginning of ebb and tracked over one, two, and three tidal cycles for each simulation. At the lower bay location particles were tracked over similar time scales, but released at the beginning of ebb, mid-ebb, the beginning of flood, and mid-flood for each modeling run. The two major properties of transport investigated are 1) the Lagrangian residual transport velocity, and 2) the dimensions of the plume produced by the oscillatory motion of particle advection. The net displacement of the center of each particle group was used to determine the residual transport velocity, and the maximum east-west, north-south spread of particle tracks after three tidal cycles as a measure of plume spread. Particles that were advected out of the grid were noted, but not included in transport calculations. Because of the uncertain effect of numerical noise generated in these modeling techniques, and the use of an artificially introduced eddy viscosity, the spread of individual particles within each group which would normally represent small-scale turbulence, will not be quantitatively discussed.

Since the position from which each particle group is released will have a significant effect on its travel path, several tracking experiments were performed with slightly altered release points in

both the upper and lower bay areas. The final location chosen for use throughout the remainder of the tracking experiments was one in which particle trajectories were most representative of the general paths taken from releases at all of the locations, except where particles hit islands or grid boundaries. On several of the releases from the upper bay group, one particle was transported down the bayou leading into Tambour Bay (Fig. 49). Because of the narrowness of the grid in this area each of these particles was usually advected out of the grid after one to two tidal cycles. Since the main focus of this project is the area where the Navigation Canal enters the Bay, these trajectories will not be discussed.

In addition to the four, approximately two-week modeling intervals, as previously described, several cases were modified to better delineate the effects of wind, tide, and runoff. Two separate simulations were conducted to examine the effect of tides in the absence of wind or additional runoff; one with an equatorial tidal range (0.12 - 0.4 m) and another with a tropic tidal range (0.5 - 0.7 m). The early April input conditions were also altered and run several times; 1) under the actual conditions with winds predominantly from the north to northeast, 2) with winds of the same strength from the south, 3) with no wind at all, and 4) with increased runoff. Additionally, since the amount of runoff appropriate to the September 16th modeling interval was unclear from the data, the model was run separately with different runoff conditions. To investigate the influence of cold front passage simulations were run with the actual oceanographic and meteorologic conditions which occur during a frontal passage (Fig.

50). Additionally, to evaluate the effects of local and remote wind forcing, the model was also run under these conditions without wind stress over the bay.

Results

Particle trajectories and their spread over a period of three tidal cycles without wind and either an equatorial or tropic tidal range are shown in Figs. 51 - 52. Within the upper bay, transport trends NNW to SSE in a linear fashion, and particle tracks are relatively parallel and overlapping from one tidal cycle to the next. Several of the particles in this area were advected northwest and out of the grid during a flood tide within the interval incorporating the larger tidal variation. Within the lower bay group, particles also move primarily in the north - south direction, however there appears to be a net drift towards the southwest and the rate of advection increases relative to the upper bay group. The cause of these differences is discussed later. Particle position after three tidal periods in the absence of wind with either an equatorial or tropic tidal range is shown in Fig. 53. Quantitative measures of transport for the particle group center in the upper bay group after one, two, and three tidal periods is described in Table 8, and for the lower bay group in Table 9.

Net movement of the upper bay particle group is to the southeast at an average residual transport velocity of about 0.8 - 1.0 cm/s during the equatorial tidal range, and in the same direction or to the northeast at 0.2 - 0.7 cm/s with the tropic tidal range. In the

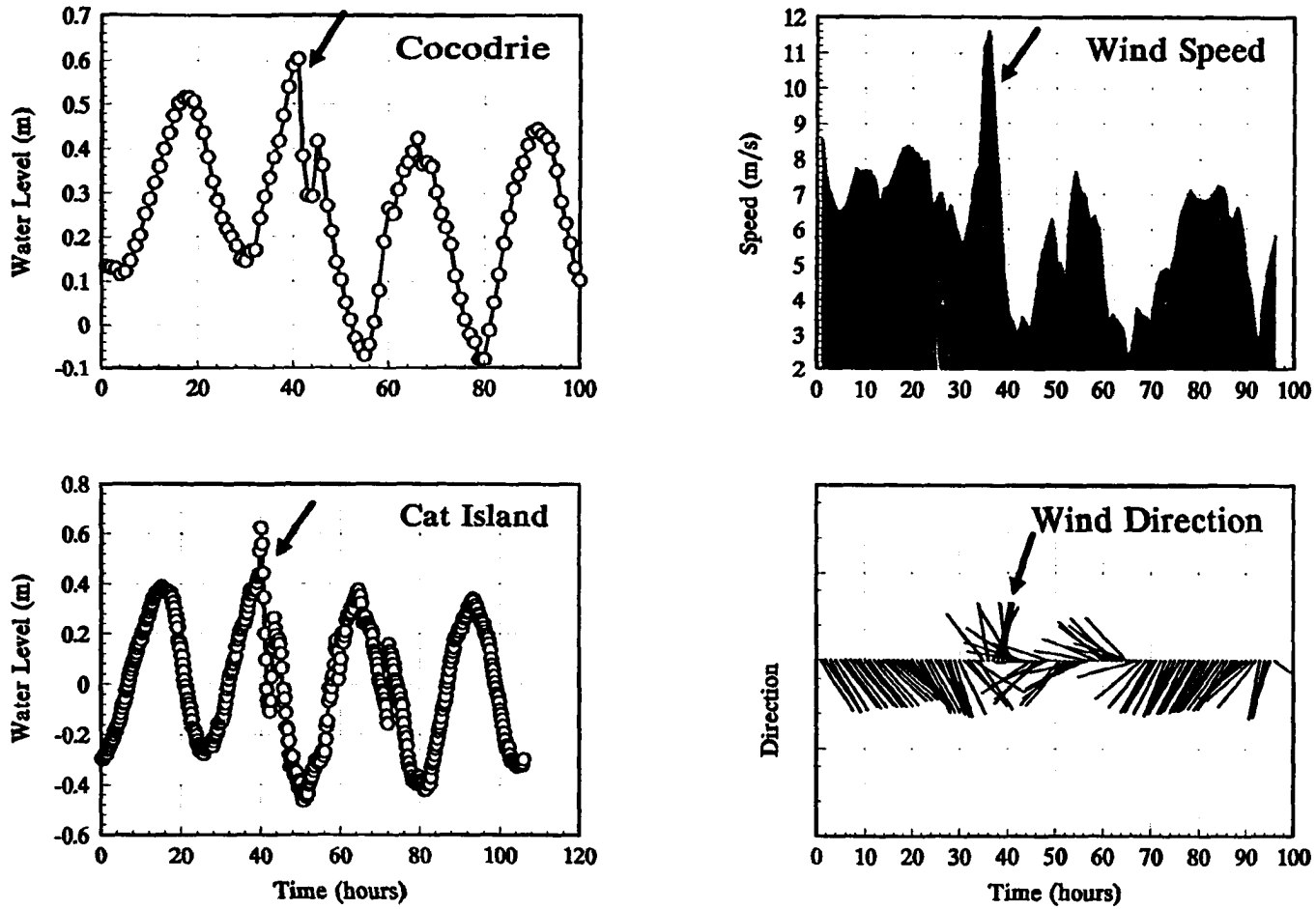

Figure 50: Input conditions during April 24 - 26, 1990; arrows indicate the time of a cold - front passage.

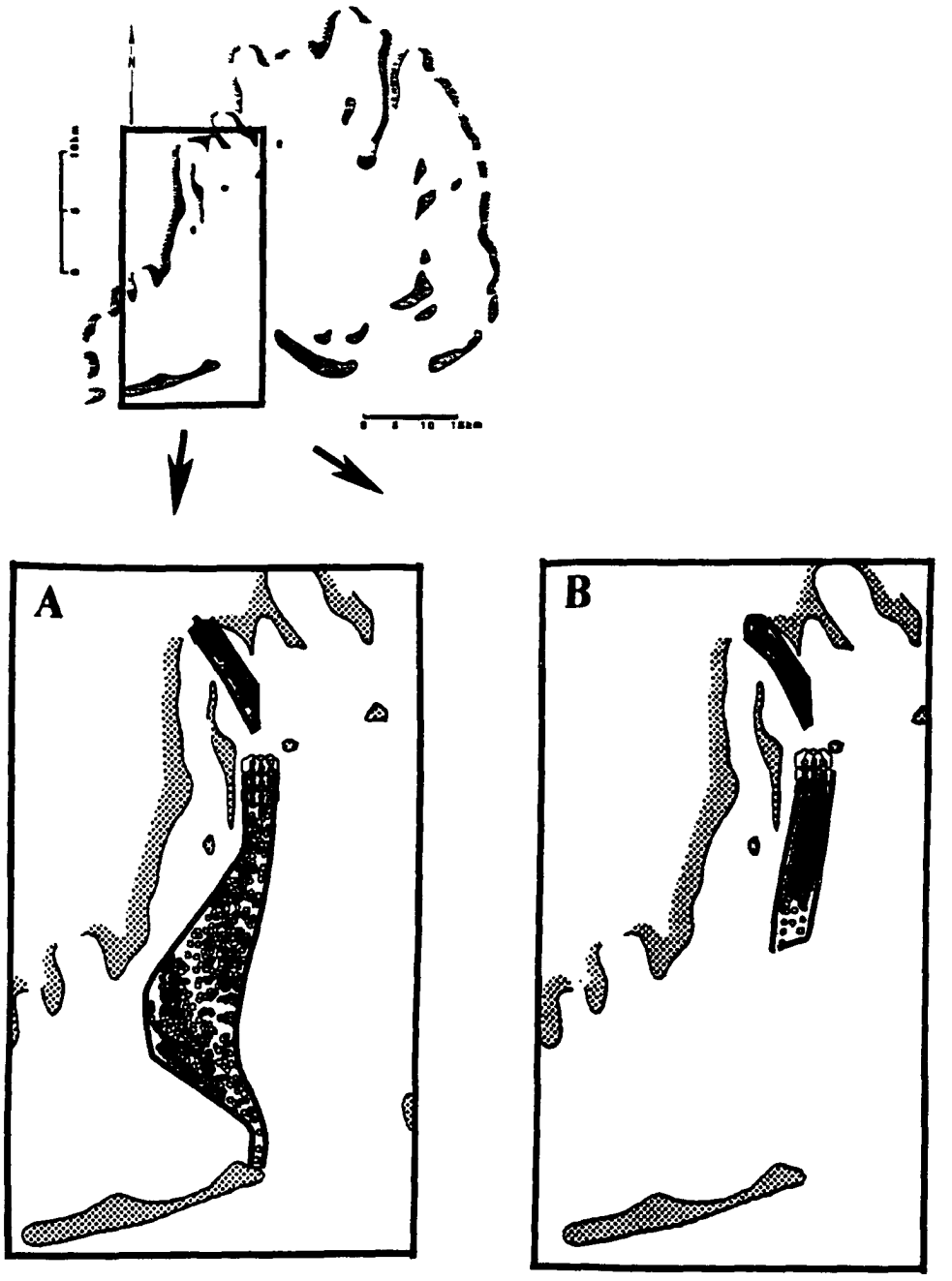

Figure 51: Particle tracks and plume spread after three tidal cycles without wind and either a tropic (A) or equatorial (B) tidal range.

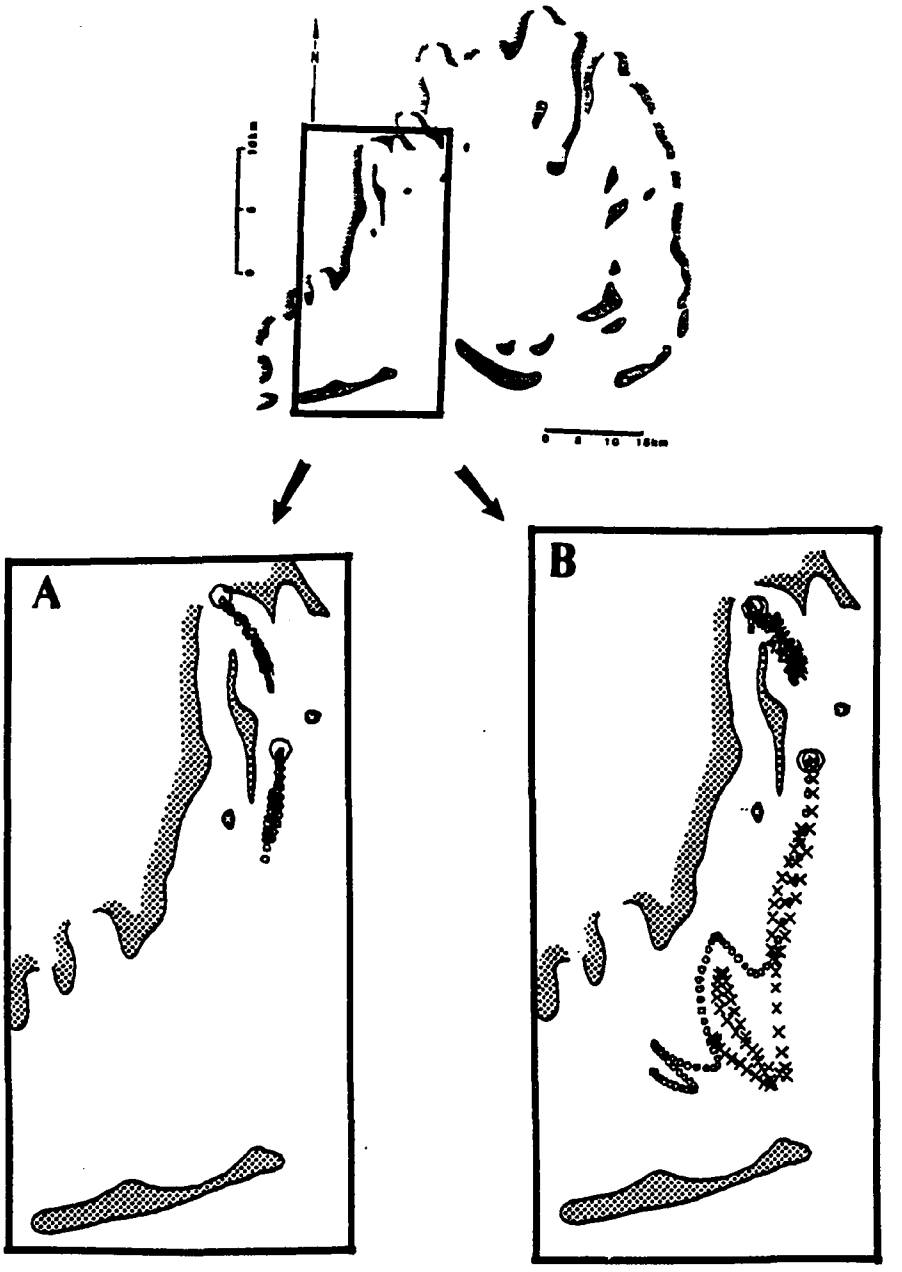

Figure 52: One particle track given an equatorial tidal range and no wind (A), and (B) two tracks with a tropic tidal range and either no wind (x), northeasterly wind (o).

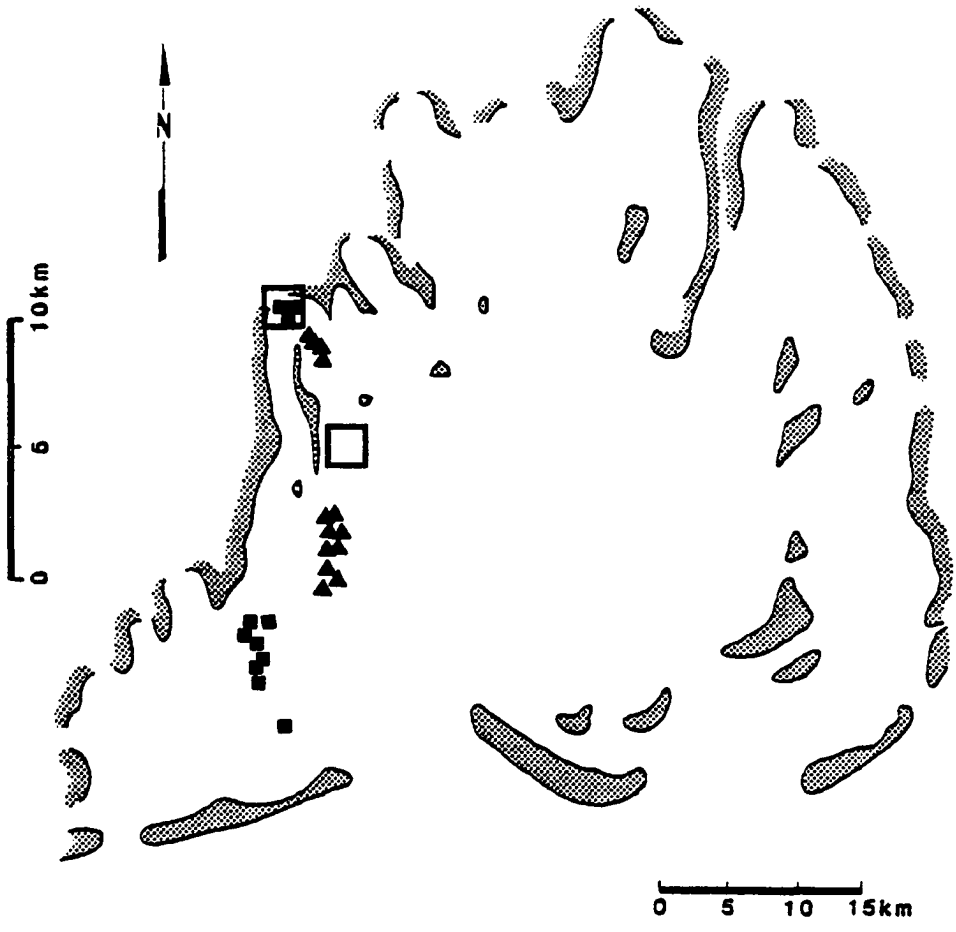

Figure 53: Position of particles following three tides with no wind and either an equatorial (▲) or tropic (■) tidal range, open boxes denote release points for the upper and lower bay particle groups.

Table 8: Upper bay transport given no wind, and either a tropic or equatorial tidal range.

TRANSPORT*					
Tidal Range	East (+)/ West (-) (m)	North (+)/ South (-) (m)	Total (m)	Rate (cm/s)	Direction
(1 Tide) Tropic	545	-169	650	0.72	SE
Equat.	743	-380	842	0.94	SE
(2 Tides) Tropic	437	37	620	0.34	NE
Equat.	1186	-700	1389	0.77	SE
(3 Tides) Tropic	331	104	427	0.16	NE
Equat.	1938	-1779	2631	0.97	SE
PLUME DIMENSIONS (m)					
		East - West		North - South	
Tropic		3119		3615	
Equatorial		2811		3298	

* Based on the position of the particle group center following one, two or three tidal cycles

lower bay particle group net transport is to the southwest, with an average residual transport velocity of 2.2 - 2.9 cm/s under tropic tide conditions, and 0.8 - 1.7 cm/s under the equatorial tidal range. As would be expected, the extent of both north-south, and east-west dispersion is greater with the larger water level variations (Tables 8 and 9). In the tropic tide case, as well as in the majority of runs to be described later, particles in the lower bay released during flood initially move farther north, travel less distance southward after three tidal cycles, and qualitatively tend to be dispersed in a greater variety of directions than those released during ebb (Fig. 54).

With addition of wind and runoff, distinct changes occur in the net displacement and pattern of particle dispersal throughout the

Table 9: Lower bay transport given no wind, and either a tropic or equatorial tidal range.

TRANSPORT* **					
Tidal Range	East (+)/ West (-) (m)	North (+)/ South (-) (m)	Total (m)	Rate (cm/s)	Direction
(1 Tide) Tropic	-1573	-353	1975	2.19	SW
Equat.	6	-312	451	0.50	SE
(2 Tides) Tropic	-2402	-4586	5271	2.93	SW
Equat.	-218	-1014	1484	0.82	SW
(3 Tides) Tropic	-3852	-6562	7665	2.84	SW
Equat.	-407	-1688	2127	0.79	SW
PLUME DIMENSIONS (m)*					
		East - West		North - South	
Tropic		5361		10761	
Equatorial		2047		4980	

* Values are averaged from four releases at various tidal phases, data from individual runs are given in Appendix B

** Based on the position of the particle group center following one, two or three tidal periods

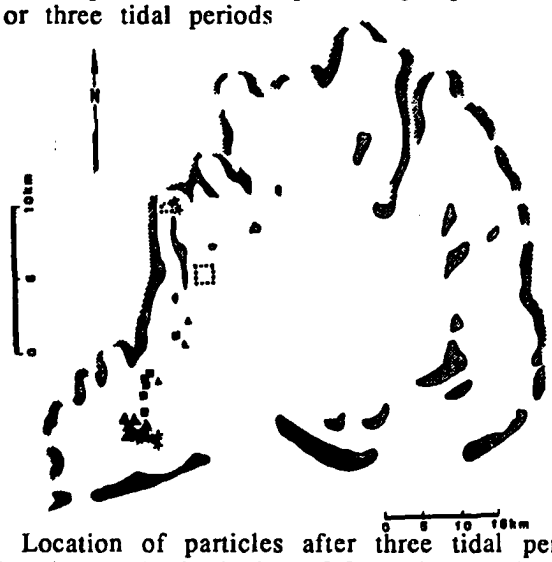

Figure 54: Location of particles after three tidal periods, given release at mid-bay location at the beginning of flood (▲), mid - flood (■), beginning of ebb (✱), or mid-ebb (▲).

bay. Results of the modified early April run exemplify some of these changes. The tropic tide case as described above is the April

first run without wind; when wind is included the results are as depicted in Fig. 55 and Tables 10 - 11. With moderately strong winds from the north to northeast, the average position of the upper bay particle group is displaced consistently southeast at a rate of about 0.6 - 0.9 cm/s over three tidal cycles, and the lower bay group

Table 10: Upper bay transport with various wind conditions added to the tropic tide case (4/1 - 4/4).

TRANSPORT*					
Wind	East (+)/ West (-) (m)	North (+)/ South (-) (m)	Total (m)	Rate (cm/s)	Direction
(1 Tide)					
No Wind	545	-169	650	0.72	SE
North	168	-431	570	0.63	SE
South	922	-404	1014	1.13	SE
(2 Tides)					
No Wind	437	37	620	0.34	NE
North	650	-1370	1755	0.98	SE
South	1228	-691	1412	0.78	SE
(3 Tides)					
No Wind	331	104	427	0.16	NE
North	112	-1597	1932	0.72	SE
South	849	-498	997	0.37	SE
PLUME DIMENSIONS (m)					
		East - West		North - South	
No Wind		3119		3615	
North Wind		3943		3615	
South Wind		3892		5171	

* Based on the position of the particle group center

southwest at a rate of 3.7 - 5.1 cm/s. With winds modified to blow out of the south, residual flow in the upper bay group ranged from 0.37 to 1.13 cm/s and in the lower bay group 0.74 to 1.88 cm/s.

Two separate cases were specifically modified to evaluate the influence of increased runoff: 1) during 48 hours within the April 1 - 4 run without wind, the average flow of bayous entering the bay was increased three times its original value, and 2) flow was

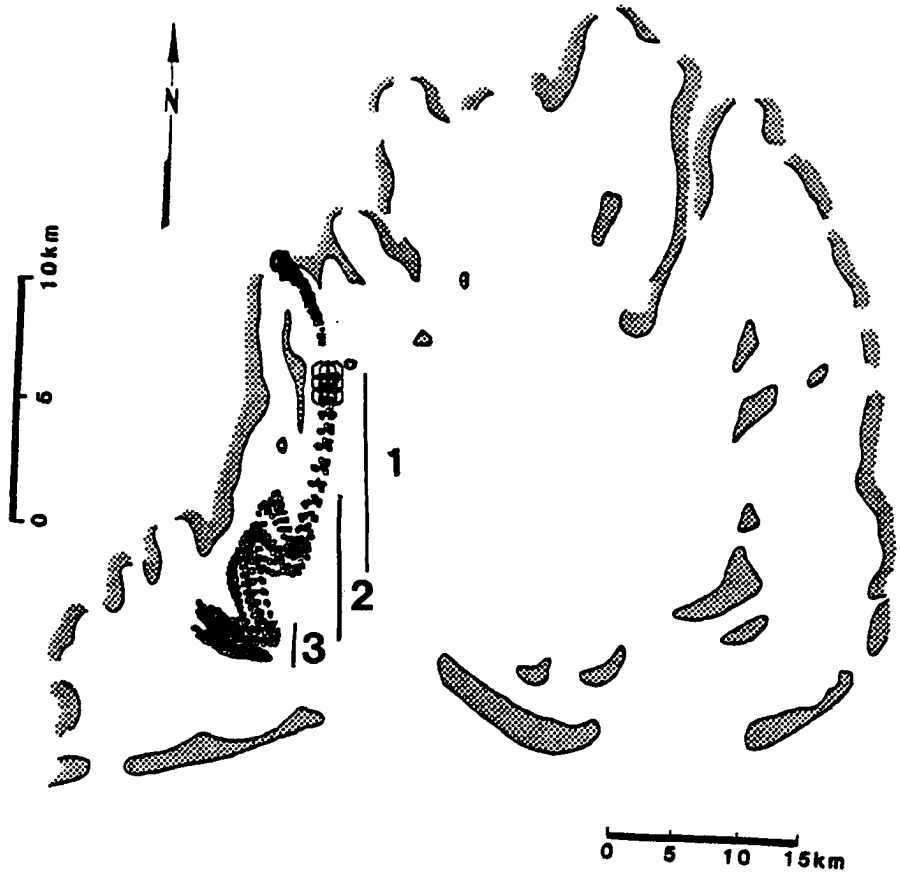

Figure 55: Particle trajectories over three tidal periods given a tropic tidal range and moderate northeasterly winds. Numbers show paths during the first, second and third tidal cycles.

increased approximately 4 times its original value for 72 hours in the September 16 - 20 run. The results of both the April and September particle tracking runs with added runoff are described in Table 12. In the lower bay area, after three tidal cycles all of the particles released were advected strongly to the south and moved out of the bay through Cat Island Pass.

Table 11: Lower bay transport with various wind conditions added to the tropic tide case (4/1 - 4/4).

TRANSPORT * **					
Wind	East (+)/ West (-) (m)	North (+)/ South (-) (m)	Total (m)	Rate (cm/s)	Direction
(1 Tide) No Wind	-353	-1873	1975	2.19	SW
North	-2857	-3494	4593	5.10	SW
South	251	-462	666	0.74	SE
(2 Tides) No Wind	-2042	-4586	5271	2.93	SW
North	-5187	-7153	8926	4.96	SW
South	-314	-2511	2749	1.52	SW
(3 Tides) No Wind	-3852	-6562	7665	2.84	SW
North	-6603	-7544	10135	3.75	SW
South	-2106	-4421	5078	1.88	SW
PLUME DIMENSIONS (m)*					
		East - West		North - South	
No Wind		5361		10761	
North		8524		11585	
South		4907		11281	

* Values are averaged from four releases at various tidal phases, data from individual runs are given in Appendix B

** Based on the position of the particle group center

In general, these results are indicative of the magnitudes and direction of transport, as well as the general patterns of dispersal, observed throughout the majority of simulations (Tables 13-15). The particle group released from the upper northwest quadrant of the bay tends to be transported southeast with an average residual

Table 12: Particle transport in model runs with added runoff (note that due to the length of the modeling period tracking from release during ebb in the September 16th interval is only possible for up to two tidal periods).

TRANSPORT *					
Model Run	East (+)/ West (-) (m)	North (+)/ South (-) (m)	Total (m)	Rate (cm/s)	Direction
(Upper bay, 1 tide) April 1	447	-173	559	0.62	SE
Sept. 16	1794	-1399	2276	2.53	SE
(2 Tides) April 1	561	-235	681	0.76	SE
Sept. 16	2553	-2751	3765	2.09	SE
(3 Tides) April 1	631	-430	923	0.70	SE
(Lower bay, 1 tide) April 1	-495	-1512	1725	1.29	SW
Sept. 16	-872	-2728	2887	3.21	SW
(2 Tides) April 1	-2412	-4625	5360	2.98	SW
Sept. 16	-1613	-4766	5040	2.80	SW
(3 Tides) April 1	-3210	-6241	7090	2.62	SW
PLUME DIMENSIONS					
		East - West		North-South	
(Upper bay group) April 1		3320		4795	
Sept. 16		3341		6531	
(Lower bay group) April 1		5570		12006	
Sept. 16		2720		8516	

* Based on the position of the particle group center

flow velocity of 0.6 - 0.9 cm/s. Exceptions occurred during the March 24th, June 25th, and July 4th runs where displacement to the northeast occurred. Additionally, during tracking experiments representative of conditions on September 16 - 20, the majority of

Table 13: Results of particle tracking for upper bay group.

TRANSPORT*					
Model Run	East(+)/ West (-) (m)	North(+)/ South (-) (m)	Total (m)	Rate (cm/s)	Direction
(1 Tide)					
3/24	336	65	491	0.55	NE
3/28	616	-302	691	0.77	SE
4/1	168	-431	570	0.63	SE
6/25	82	47	358	0.40	NE
6/27	1364	-864	1617	1.80	SE
7/1	284	-88	406	0.45	SE
7/4	67	157	388	0.43	NE
9/8	806	-293	861	0.96	SE
9/12	466	-209	715	0.79	SE
9/16	635	-444	800	0.89	SE,(most out NW)
9/18	1360	-826	1597	1.77	SE
12/5	650	-542	1029	1.14	SE
12/9	611	-315	752	1.84	SE
12/13	516	-133	765	0.85	SE
Avg.	567	-298	789	0.88	SE
Std. Dev.	390	297	383	0.43	
(2 Tides)					
3/24	242	258	578	0.32	NE
3/28	1112	-708	1330	0.74	SE
4/1	650	-1370	1755	0.98	SE
6/25	887	-225	916	0.51	SE
6/27	2114	-1579	2640	1.47	SE
7/1	627	-155	737	0.41	SE
7/4	199	32	569	0.32	NE
9/8	825	-256	869	0.48	SE
9/12	835	-364	916	0.51	SE
9/16	960	-239	1005	0.56	SE (most out NW)
9/18	1497	-924	1766	0.98	SE
12/5	1451	-1011	1776	0.99	SE
12/9	733	-396	889	0.49	SE
12/13	1028	-515	1153	0.64	SE
Avg.	940	-532	1207	0.67	SE
Std. Dev.	484	507	564	0.31	
(3 Tides)					
3/28	1719	-1281	2160	0.80	SE
4/1	112	-1597	1932	0.72	SE
6/27	2543	-1938	3199	1.18	SE
7/1	844	-269	928	0.34	SE
7/4	130	284	825	0.31	NE
9/8	673	-132	704	0.26	SE
9/12	999	-493	1125	0.42	SE
9/18	1635	-1005	1924	0.71	SE
12/9	863	-564	1121	0.42	SE
12/13	1419	-848	1656	0.61	SE
Avg.	1094	-784	1557	0.58	SE
Std. Dev.	713	652	734	0.27	

* Based on the position of the particle group center following one, two or three tidal periods

Table 14: Averaged* results of particle tracking for release at various tidal phases for lower bay group.

	TRANSPORT**				
Model Run	East (+)/ West (-) (m)	North (+)/ South (-) (m)	Total (m)	Rate (cm/s)	Direction
(1 Tide)					
3/24	-415	-166	1658	1.84	SW
3/28	-849	-1917	2196	2.44	SW
4/1	-2857	-3494	4593	5.10	SW
6/25	-53	-834	1063	1.18	SW
6/27	-242	21	397	0.44	NW
7/1	-771	-2348	2525	2.81	SW
7/4	-1042	-2156	2532	2.81	SW
9/8	427	-533	854	0.95	SE
9/12	-402	-1150	1247	1.39	SW
9/16	-103	-758	1035	1.15	SW
9/18	-942	-1765	692	0.77	SW
12/5	-1090	-2171	3699	4.11	SW
12/9	-170	-1029	1261	1.40	SW
12/13	-264	-581	1364	1.52	SW
Avg.	-592	-1348	1794	1.99	SW
Std. Dev.	776	953	1154	1.28	
(2 Tides)					
3/24	-602	-1492	2655	1.48	SW
3/28	-3503	-5059	6304	3.5	SW
4/1	-5187	-7153	8926	4.96	SW
6/25	-534	-1615	2095	1.16	SW
6/27	242	-502	1154	0.64	SE
7/1	-2135	-3757	4435	2.46	SW
7/4	-2615	-3845	4788	2.66	SW
9/8	824	-732	1363	0.76	SE
9/12	-1313	-2562	3056	1.70	SW
9/16	-431	-736	1989	1.10	SW
9/18	39	-820	1242	0.69	SE
12/5	-3807	-4336	6309	3.50	SW
12/9	-597	-2239	2344	1.30	SW
12/13	-1422	-2474	2998	1.67	SW
Avg.	-1503	-2666	3547	1.97	SW
Std. Dev.	1671	1880	2230	1.24	
(3 Tides)					
3/28	-4962	-6969	8683	3.22	SW
4/1	-6603	-7544	10136	3.75	SW
6/27	452	-1088	1784	0.66	SE
7/1	-3371	-5119	6181	2.29	SW
7/4	-3286	-5125	6267	2.32	SW
9/8	-514	-2569	2886	1.07	SW
9/12	-2352	-3961	4801	1.78	SW
9/18	-306	-1582	2168	0.80	SW
12/5	-268	-867	1534	0.57	SW
12/9	-1269	-3362	3783	1.40	SW
12/13	-2393	-4009	4240	1.57	SW
Avg.	-2261	-3836	4769	1.77	SW
Std. Dev.	2081	2136	2685	0.99	

* Results of releases at various tidal stages are given in Appendix B

** Based on the position of the particle group center following one, two or three tidal periods

Table 15: Maximum dimensions of particle tracks after 3 tides in meters.

	Upper Bay Group		Lower Bay Group									
			Ebb		Mid-Ebb		Mid-Flood		Flood		Avg.	
Model Run	East-West	North-South	East-West	North-South	East-West	North-South	East-West	North-South	East-West	North-South	East-West	North-South
3/24*	2678	3356	2795	7157	2601	6405	1667	6054	2137	5383	2300	6250
3/28	3156	5373	9470	12016	8861	11232	7054	12286	3792	11386	7294	11730
4/1	3943	3615	9442	11666	9598	11183	8162	12731	6894	10758	8524	11585
6/25*	3411	4197	4116	8741	3734	8251	1894	6158	2431	5568	3044	7180
6/27	3369	3609	1772	6019	3652	4202	1514	5434	3149	3759	2521	4854
7/1	3525	4781	6901	9931	6469	8971	4602	11053	3725	11739	5424	10424
7/4	3236	3963	7416	11397	6923	10834	4383	10638	3037	8019	5440	10222
9/8	3705	4491	5756	11844	4499	10465	2515	9103	2821	7909	3898	9830
9/12	3167	4494	6262	10668	5689	9776	3046	8413	2942	8600	4485	9364
9/16*	3176	3477	3387	5718	2898	5461	1773	4691	1924	4682	2496	5138
9/18	3464	3974	2366	6880	2562	6879	2522	7109	2202	7329	2413	7049
12/5*	3473	4752	8436	9905	6639	9285	5685	10539	3495	9539	6064	9817
12/9	3520	4151	5242	8186	4378	7894	3060	7938	2680	7834	3840	7963
12/13	3228	3537	6783	10778	6215	10555	2365	7567	2548	6683	4478	8896
Avg.	3311	4043	5585	9331	5177	8486	3472	8426	3173	7768	4444	8593
Std. Dev.	303	582	2284	2284	2234	2347	1927	2437	1236	2550	1848	2268

* Only 2 tidal cycles completed during tracking due to length of run and phase of release

particles within the upper group were advected out of the grid to the northwest. Several particles were also advected out of the grid to the northwest during modeling of flow on April 1st, July 4th, September 8th, and December 5th. The strongest rate of transport, 1.2 - 1.8 cm/s, occurred during the June 27 - July 1 simulation period and the lowest rate, 0.2 - 0.3 cm/s, during the September 8th and July 4th simulations. The average spread of the particle paths in the upper bay area was approximately 3 km in width and 4 km in length.

The particle group released in the more southern region of the bay exhibited net movement predominantly in a southwest direction. The average velocity of residual transport over one to three tidal cycles was approximately 1.8 - 2.0 cm/s. Consistently lower rates of transport occurred for the June 27th and September 8th runs, and higher rates during the April 1st and December 5th runs. The maximum spread of the particle paths averaged approximately 6 km in the east - west direction and about 9 km in the north - south direction.

Cold Front Passage

Results of particle tracking during the passage of a cold front are shown in Table 16 and Fig. 56. Following one tidal period and frontal passage, transport of the upper bay particle group is southeast at a relatively high rate of 1.2 cm/s. After frontal passage, over the next two tidal cycles, net movement continues to be in the southeast direction at speeds decreasing to 0.3 to 0.35

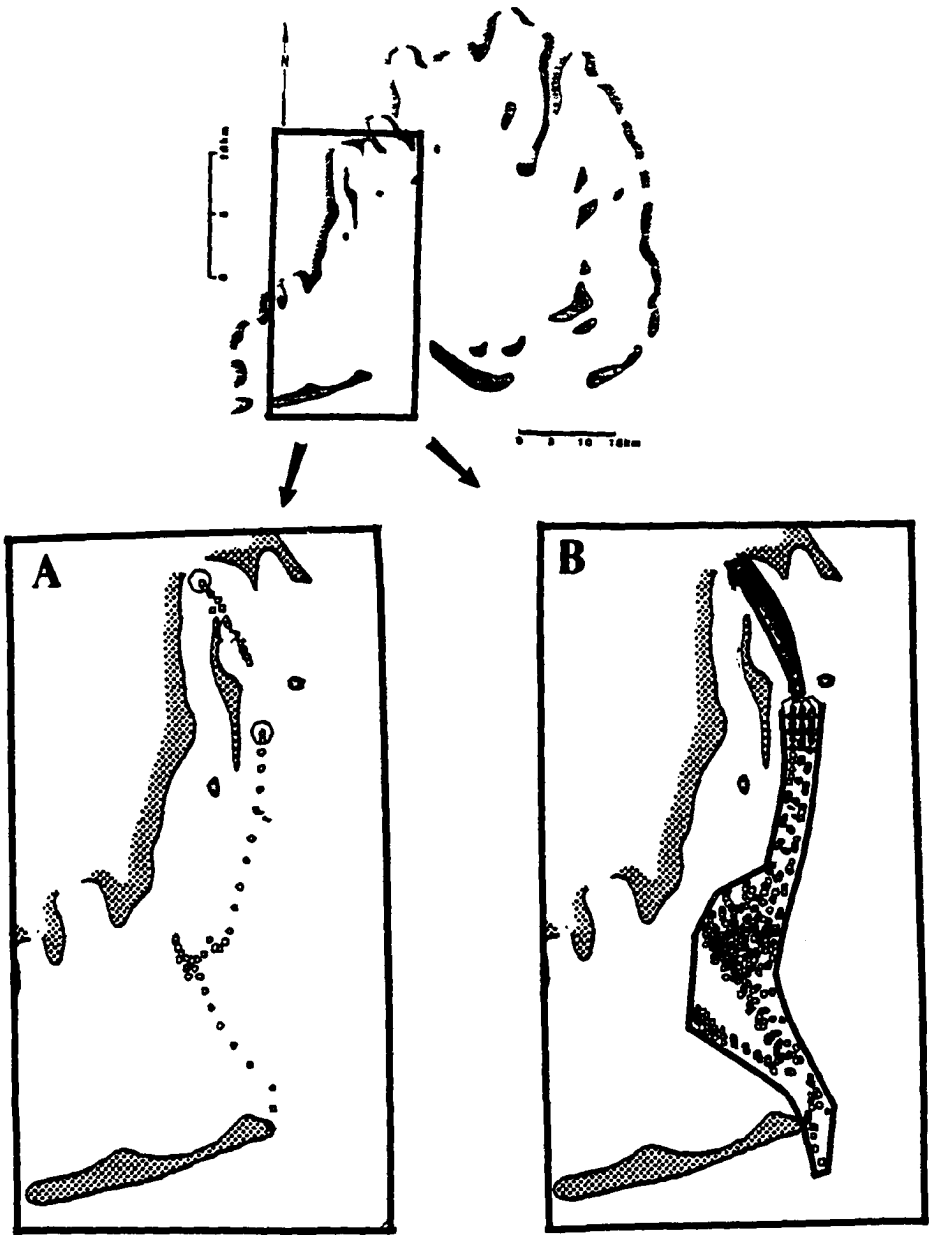

Figure 56: Particle tracking post-frontal passage, (A) one track, and (B) all tracks and plume spread.

Table 16: Particle transport following cold front passage.

TRANSPORT*					
Model Run	East (+)/ West (-) (m)	North (+)/ South (-) (m)	Total (m)	Rate (cm/s)	Direction
(Upper bay, 1 tide)	-794	-794	1054	1.17	SE
No Wind	519	-165	631	0.70	SE
(2 Tides)	573	-98	634	0.35	SE
No Wind	-18	243	402	0.22	NW
(3 Tides)	661	-201	802	509	SE
No Wind	47	160	573	0.21	NE
(Lower bay, 1 tide)	-1200	-4833	5290	5.88	SW
No Wind	-589	-1867	2042	2.27	SW
(2 Tides)	-3737	-7881	8774	4.87	SW
No wind	-2345	-5321	5242	2.91	SW
PLUME DIMENSIONS					
		East - West		North-South	
(Upper bay group)		3675		4889	
No Wind		3246		5031	
(Lower bay group)		6756		13947	
No Wind		5504		12828	

* Based on the position of the particle group center

cm/s. While the lateral spread of the plume is near to the overall average, the longitudinal spread is approximately 1000 m greater than the average. When the local wind patterns specific to cold-front passage are neglected, but the forcing provided by non-local winds are included via actual water level variations at the mouth, the magnitude of transport in the upper bay is decreased to 0.2 - 0.7 cm/s. The direction of residual flow varies over three tidal cycles from southeast after the first tidal period, to northeast following the third tidal cycle.

In the lower bay region, particle tracks and the calculated position of the particle group following one tidal cycle and frontal

passage indicate that transport is southwest at a relatively high rate of 5.8 cm/s. Several of the particles are advected out of the bay via Cat Island Pass during the second tidal cycle, and by the third tidal period, all of the particles have exited the bay. Based on only two tidal cycles, the longitudinal spread of the plume is greater than during all other runs. When run without wind stress over the bay, the results indicate that net movement remains southwesterly, but at a slower rate (2.3 - 2.9 cm/s). Particles are still advected out of the bay, but only during the third tidal cycle.

Discussion

Model results suggest that both the oscillatory motion of advective transport and the patterns of residual flow within Terrebonne Bay are strongly influenced by the combined effects of tidal forcing, bay morphology, bathymetry, runoff, wind stress, and changes in mean sea level within the Bay. It is not apparent that one of these factors is the dominant forcing mechanism throughout the year or within a given season, but rather that under varying meteorologic and oceanographic conditions the predominance of forcing shifts from one mechanism to the other.

Particle tracking experiments indicate that under the majority of environmental conditions studied, there is a tendency for residual flow to transport suspended material seaward at an average rate of about 0.8 cm/s in the upper bay, to 2.0 cm/s in the lower bay. Both the Lagrangian residual transport velocities as determined via particle tracking and the Eulerian residual flows calculated by the

averaging of current meter data suggest that residual flow is seaward, and that transport velocities increase towards Cat Island Pass. The residual flow found in this study is similar in magnitude to that found by previous workers in other coastal bay systems (Smith, 1990). Stronger flow in the more southern region of the bay probably results from decreasing bottom friction and the proximity of Cat Island Pass. Additionally, whereas the tendency for transport to veer westward in the lower bay may be a function of the opening up of the lower bay to the west, the eastward nature of seaward flow in the upper region is probably a result of the bay's narrow morphology and confining bathymetry within the area.

During periods of heavy rainfall, circulation within Terrebonne Bay and therefore the residual transport of water-borne materials may be dominated by the effects of bayou runoff. Discharge may also partially explain the prevalence of seaward transport in many of the modeled scenarios. Both groundwater and overland flow which drain into the bayous of the Terrebonne basin eventually flow into the upper reaches of Terrebonne Bay. Consequently, runoff which enters the Bay counteracts tidal forcing during flood and augments it during ebb. Thus in the absence of additional forcing, one would expect Terrebonne Bay to be an ebb-dominated system. When average flow increases as a result of precipitation over the drainage basin, the strength of the outgoing ebb relative to the incoming flood should be greater, thereby intensifying net flow seaward. The two simulation runs which were modified to incorporate increased runoff illustrate the effects of bayou drainage on transport within the bay. In both the upper and lower areas of

the Bay under investigation, increased runoff results in stronger advection towards Cat Island Pass, and an increase in the longitudinal dispersal of particles. Thus during and/or following heavy precipitation within the Terrebonne area, high bayou discharge may produce strong seaward transport and extensive north-south dispersal of particulates within bay waters. These effects may be furthered by buoyancy driven flow which is not considered by the model.

Previous research indicates that tidal asymmetries, variations in the tidal range, tidal phase, and spatially varying pressure gradients established by tidal propagation up estuary can affect the transport of suspended matter within coastal bays (Postma, 1967; van Leussen, 1991). Results of this study suggest that these tide-related and complex forcing mechanisms also significantly influence transport processes within Terrebonne Bay. The fortnightly periodicity of the tidal range appears to have the simplest effect on the dispersal of particulate materials within bay waters: as the range of the water level variation increases from the equatorial to tropic tide, both the longitudinal and lateral dispersion increases in the upper and lower regions of the bay (Fig. 57). In the upper bay region, all of the periods except the September 16th in which several particles were advected out of the northwest grid boundary were characterized by a relatively large tidal range. In the more southern area of the bay, stronger tides also correlate with stronger residual flow. However, in the upper northwest region of the bay, findings suggest that in the absence of wind or additional runoff, the stronger tidal forcing of the tropic tide does not necessarily produce

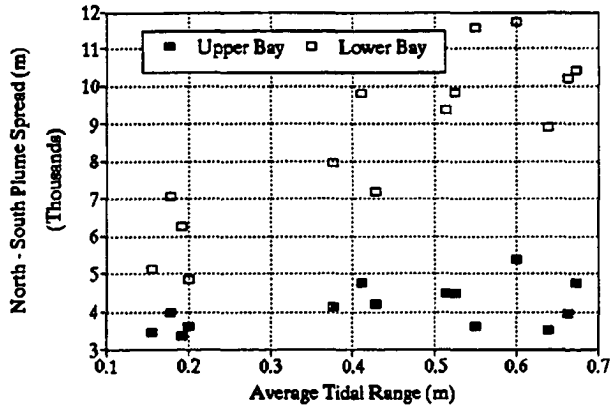

Figure 57: North-south plume spread versus average tidal range of a model period for both upper and lower bay simulations.

greater net movement than the weaker forcing of the equatorial tide. In the bay's upper reaches, tidal asymmetry and spatially varying pressure gradients due to tidal propagation, as well as changes in mean sea level may overshadow the effects of the varying tidal range (Fig. 58). The tidal records from Cat Island

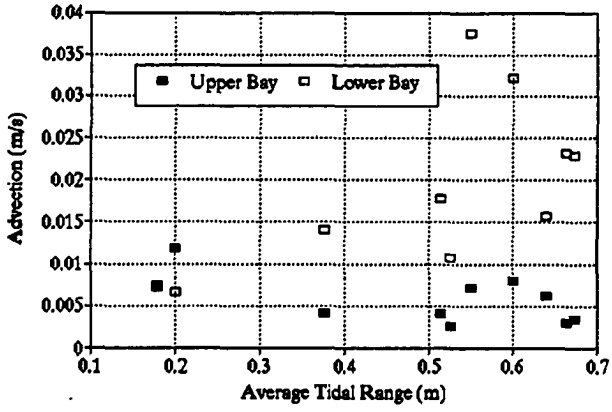

Figure 58: Advection versus average tidal range of a model period for both upper and lower bay simulations.

Pass and Cocodrie indicate that tidal asymmetries can occur either as a function of mean sea level change, or as a result of the interaction

of the tide with shelf and inlet bathymetry, bay morphology, and runoff. The short-term effect of tidal asymmetry on transport is exemplified by the first tidal cycle of particle release in the tropic tide - no wind case. The falling tide is one hour shorter and 0.08 m greater than the previous rising tide, consequently, unless there is net storage of water up-estuary, flow during the outgoing tide must exceed that of the flood. Modeling shows that net particle movement over this tidal cycle, as would be expected, is seaward. However, if we extend the reference time to several tidal cycles, changes in mean sea level become apparent. Following the first tidal cycle it appears that over the next 48 hours there is a lowering and then rising of the mean water surface (Fig. 59). Hence, as mean sea level rises during the third tidal cycle we would expect, as the model predicts, transport to be northward. The strong influence of changes

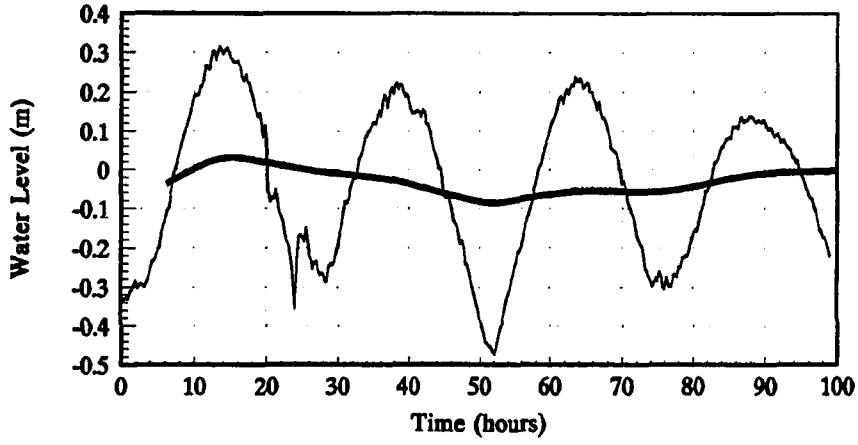

Figure 59: Estimated mean sea level changes at Cat Island Pass, April 1 - 4, 1990.

in mean sea level, is exemplified by the September 16th modeling period. Although winds are not significantly stronger, nor is runoff weaker than at any other interval, this is the only period in which

net advection in the upper bay was consistently northwest. Qualitative examination of the water level variations at Cat Island Pass reveals that the mean water level over this period is increasing with time (Fig. 60); suggesting that water level setup up-estuary is in progress. Over this four day interval, water level variation appears to be the dominant factor controlling the pattern of residual flow within the Bay. The rise of the mean water level during the September 16th interval, as indicated by the tidal curve, could be a result of prolonged southerly winds (refer to Fig. 20) or interaction with the coastal ocean. As indicated by model results, the dispersal of particulate material mid-bay is also influenced by the phase of

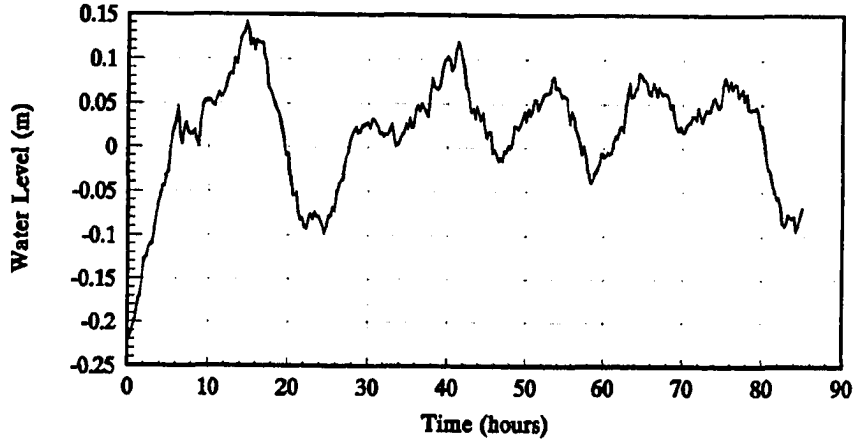

Figure 60: Observed water level variation at Cat Island Pass, September 16 - 20, 1990.

the tide upon its release. As would be expected, water-borne substances released during the ebb are more likely to be spread seaward than those discharged during flood.

The effect of wind stress on the patterns of water movement and transport appear even more complex than that of runoff and tides. Wind stress, which acts as a drag on the water surface, is

highly variable in magnitude, direction, and duration. Additionally, within shallow waters, wind may produce a build-up of water along the coast and generate a return flow (Elliott, 1978; Wang and Elliott, 1978). This return flow may move in a direction opposing that of the actual winds. North to northeasterly winds as used in the April 1st and December 5th simulations apparently result in transport seaward in both regions of the bay being examined. The most dramatic effect of northeasterly winds is in the lower region of the bay, where a strong westerly drift in particle motion occurs. We would in fact expect to see a greater effect of northerly winds in the more open southern reaches of the bay due to an increased fetch. In contrast, winds of the same strength blowing from the south have a significantly different effect on transport. Because wind stress is in the same direction as the rising tide and in opposition to the falling tide, in the lower bay advection seaward is decreased. The maximum extent of northward spread is increased in both particle groups. In the upper bay southerly winds seem to have a more variable effect on transport than in the lower region of the bay. Weak and/or relatively short-lived winds from the south decrease transport into bay waters. However, though model boundaries may intensify this effect, southerly winds which are strong enough, or prolonged in duration, appear to cause set-up along the coast and actually increase both transport seaward and the longitudinal spread of particles.

Results of tracking during modeled cold-front passage exemplify the influence of wind set-up and intensified seaward flow. Previous research indicates that prior to frontal passage, a

pressure gradient is established within the bay by relatively constant wind stress out of the south (Roberts et al., 1989). The model indicates that as the front passes, and the winds shift to blow from the north, set-up relaxes and particularly strong seaward transport of particulate material occurs. Due to Ekman-type transport along the coast, circulation during and following frontal passage may be more complex than the model reveals. However, it is clear that within the mid to lower bay region, transport seaward increases following cold-front passage and only two tidal cycles are needed for materials residing mid-bay to be advected into open Gulf waters. The model also suggests that during build-up prior to frontal passage, it is likely that materials will be advected up-bay into the oyster-rich shallow inlets along the northern shoreline.

The results of modeled transport under a variety of realistic combinations of tide, wind, and runoff exhibit further the interaction and complexity of forces which drive flow within the region. Because of the dynamic and variable nature of environmental forcing within south Louisiana, it is not clear that distinct patterns of transport characterize specific times of the year. Rather, that from day to day, the combination of forces or predominance of one or more force may change. For example, over the four, two-week periods modeled, the strongest transport seaward in the upper bay occurred during the June 27th simulation. Tides during this period were weak and irregular, with a relatively strong ebb as compared to the previous flood near the end of the simulation. Winds were out of the south at approximately 4 m/s for 64 of the approximately 85 hours modeled. Thus, seaward driven flow in the bay's upper

northwest reaches may be explained by the combined force of wind-driven buildup and an offshore flow responding to the ensuing setdown, and an ebb-dominated asymmetry of the tides. In contrast, during other days modeled within the summer, transport was weak and dispersal minimal.

In the mid to lower regions of the bay, strong transport seaward and dispersal occurred (1) following frontal passage, (2) with increased runoff, or (3) during periods of moderately strong north to northeasterly winds. Though more common in the winter months, on a short-term basis, over one to two tidal cycles, these conditions could also occur in the fall, summer, or spring. Furthermore, in the bay's upper reaches, strong advection up-estuary occurred due to rising sea level within the bay as well as during periods with a relatively high tidal range.

In summary, while there appears to be a relatively consistent seaward driven pattern of residual flow in Terrebonne Bay's nearshore waters, interactions among the environmental forces that drive flow and therefore transport are complex, highly variable, and do not lend themselves to seasonal classification. The direction and magnitude of the wind is important, but so is its duration in any one direction. Not only are variations due to the fortnightly tidal cycle important, but so is the phase of the tide as well as the asymmetry of the rise and fall of water levels. Sea level changes within the bay resulting from prolonged wind-driven flow, or forcing from the coastal ocean, appear to overshadow other forces driving advective transport. Furthermore, for simplification purposes other factors such as seasonal steric effects, changes in the coastal ocean, and

stratified flow, were neglected, but probably complicate circulation and transport patterns within the bay even further.

CHAPTER 6

ENVIRONMENTAL MANAGEMENT PERSPECTIVE

Results of this study indicate that because the predominance of environmental forcing varies and may include subtidal changes in sea level, it is not possible to predict the patterns of transport within the coastal waters of Terrebonne Bay by evaluating runoff, tides, and/or winds individually. It is not surprising then that previous research based on statistical comparisons of contamination levels and individual environmental parameters have been inconclusive. Because the processes controlling transport within the coastal environment of Terrebonne Bay vary at a frequency shorter than the seasonal signal, it may in fact not be possible to accurately predict trends in contamination on a seasonal basis. It may be helpful though to delineate the conditions most probable for high contamination and to determine, if possible, the combination of environmental forces that are likely to produce such conditions, and when those combinations are likely to occur.

As discussed earlier, studies suggest that the release of sewage-related wastes into Terrebonne Bay is discontinuous and relatively unpredictable. In addition, the survivability of potentially harmful bacteria and viruses once in estuarine waters is highly variable, but promoted by low water temperatures and salinities. Consequently, the tendency toward contamination of oyster-rich

areas should be high, particularly during the cold-water months, if 1) high discharge or bayou flushing occurs, and/or 2) transport and dispersal within bay waters is either minimal or directed into areas containing productive oyster grounds.

Relatively strong discharge into Terrebonne Bay's oyster-rich upper reaches occurs following heavy rains over the drainage basin and after frontal passages. Bayou drainage associated with the relaxation of set-up following cold-front passages in south Louisiana may be particularly hazardous with regard to oyster-bed contamination. Results suggest that prior to a cold-front passage, materials entering bay waters may be transported landward during set-up. Once advected into a shallow bay or inlet, particulates may settle out of the water column and accumulate over time. As a cold-front passes, and set-down drives flow seaward, materials accumulated within these shallow regions may be resuspended, transported down estuary, and made available for uptake by filter-feeding organisms.

In the upper northwest region of the bay, even under the strongest of transport regimes, findings suggest that residual flow and therefore the transport of particles in suspension like sewage is on the order of 1 - 2 cm/s, and that the plume of dispersal produced by the oscillatory tidal flow is approximately 4 km in length. Consequently, if we consider that the upper bay area, rich in oyster beds, is approximately 4 -5 km in length, then sewage-related wastes could reside within the area for approximately 2 - 3 days. Because it is not clear how long bacteria and viruses survive in this water, these estimates are conservative. But even so, it appears that

within one tidal cycle, water-borne substances will remain within the bay's oyster-rich upper reaches. Furthermore, because of the shoreline irregularities prominent within this area, particulates may become trapped within the shallow inlets or bays as a result of interactions with the daily oscillation of the tide (Okubo, 1973). Thus even following a frontal passage and/or strong runoff, the residence time of particulate materials in the upper bay may be several days. Because of strong tidal forcing the likelihood of contamination post-frontal passage and following strong rains appears to be very high. It is recognized, however, that further research is necessary to confirm these findings and examine the effects of buoyancy-driven flow during periods of high bayou discharge.

Modeled transport also suggests that rising mean sea level not necessarily associated with a cold-front passage, and winds blowing from the south-southeast or north-northeast could produce conditions conducive to contamination. Southerly winds appear to decrease transport out of the more oyster-rich regions of the bay, except when associated with pressure-driven seaward flow. When combined with an equatorial tidal range, weak southerly winds may further decrease the spread of water-borne materials, thereby diminishing the potential for dilution that occurs under the stronger tropic tidal range. As mentioned earlier, climatic data indicate that during the winter months winds blow predominantly from the north to northeast. Model results suggest that winds of this orientation tend to drive transport seaward, but in the middle, western region of the Bay, a net drift to the west occurs. Because of the

configuration of the shoreline and the presence of productive fisheries in the area, under these conditions the probability for contamination along the western shore of the bay may be increased.

Forces that control transport of suspended materials within Terrebonne Bay are not a function of season, the predicted tide, or annual trends; thus it is the author's opinion that management based on seasonal contamination prediction is unrealistic and rather risky. Originally, as part of this study, coliform concentration data collected by the state and used as a basis for the management program was to be contoured for periods as close as possible to those modeled. However, with research, it was found that data from the necessary stations was not collected regularly, and that because of the logistics involved and dynamics of the system, collections were not synoptic enough to produce concentration contours on an appropriate time scale. Given the limited funds and personnel available to those responsible for oyster harvesting management in Louisiana, these problems are not surprising. Considering the documented effect of cold-water on sewage-related microbes, and because of the prevalence of frontal passages and strong, northeasterly winds in the winter months, the State's winter-month no-harvesting policies in the Terrebonne Bay area is a reasonable first approach to the problem. However, it really is not clear that at other times of the year, particularly in the spring and fall when frontal passages also occur, that harvesting is safe.

Obviously this is a difficult problem. In addition to the complexities of the physical system, economic concerns must be considered. The ongoing illegal harvest of oysters negates the

efforts of the State to protect human welfare, while restrictions on harvesting diminish the revenue available to local communities and those in south Louisiana who depend on oyster fishing for survival. As further studies are performed, even greater complexities in the dynamics of transport within this coastal system will be found. Changes in the configuration of the marsh-bay complex are constantly occurring due to subsidence, sea level change, storms, and human intervention. As these changes occur the patterns of water movement and transport will also be modified. Though modeled as a two-dimensional system here, it is likely that at times flow within the region is three-dimensional, complicating the matter even further. Who is willing to accept the liability for potential illness or death from tainted shellfish, and is the risk of collecting potentially contaminated oysters worth the monetary benefit?

The real solution to the problem does not lie in the management of a natural, ever-changing system, but in education and modifications to human behavior. If we desire to continue consuming raw shellfish, then the techniques previously developed for purification should be utilized. It has been shown that after collection, purification of oysters occurs within 48 hours provided there is constant flushing with clean water (Perkins et al., 1980). An approved purification plant has already been installed north of Terrebonne Bay. The use of this technique would in the long-term be economically sound, increasing the oysters available to harvest and reducing the need for strict harvesting enforcement, as well as greatly lowering the risk of illness to the public. The alternative is better and/or more efficient means of treating sewage wastes prior

to their release into natural waters. Use of both natural and constructed wetlands is now becoming a very viable means to further waste-water treatment. However, because some of the wastes in this case may be coming from private homes and fishing camps, this option may not solve the entire problem. Although more research is needed to confirm the findings reported here, it seems clear that rather than attempting to simplify and classify such a complex and dynamic system, environmental management should focus on practices to reduce the problem and/or repair its consequences.

Other Uses

Terrebonne Bay and its surrounding waters are heavily utilized by the oil and gas industry for transport as well as production. Although few spills have occurred in the region, the threat of such is very real. Whether for planning purposes or in response to a specific event, modeling of bay circulation offers rapidly available and useful information to aid clean up. If oil or other buoyant chemicals were released into the waters of Terrebonne Bay, it should be possible to predict then the primary directions of movement based on the patterns of water movement and residual flow within the bay. Knowledge of transport patterns allows for rapid deployment of containment and/or clean-up equipment within the appropriate area. The details of flow are probably not exhibited by modeled transport, but the main axes of dispersal and transport should be relatively accurate. For any spill,

if it is possible to readily obtain reasonable tidal information, wind data, and precipitation records, it is then possible to predict a trajectory of transport. Prior to this type of use however, it would be helpful to conduct tracer experiments throughout the bay to confirm the accuracy of model predictions.

CHAPTER 7

CONCLUSIONS AND RECOMMENDATIONS

Results of this study indicate that patterns of particle transport within the nearshore waters of Terrebonne Bay, Louisiana are highly complex and depend on the interplay of tides, wind, runoff, and changes in mean sea level within the bay. The following conclusions are based on circulation modeling and computer simulated tracking of particles released in the northwest and mid-west portions of the bay.

1. Use of a two-dimensional numerical model to simulate flow within Terrebonne Bay is relatively accurate for all but infrequent meteorological and oceanographic conditions. However, the correlation between model output and real-time flow decreases when tidal and/or wind forcing is weak.

2. Residual flow of materials entering the bay is commonly seaward at a rate of 0.8 to 5 cm/s depending on location within the bay and environmental conditions occurring at the time of release. Advection landward occurs on a daily basis during the flood portion of the tidal cycle, and residual transport up bay may occur when sea level is rising within the bay, and under a variety of wind/tide combinations. Strong flow seaward occurs with increased runoff and

following frontal passages within the area. Even under the strongest of flow regimes, the residence time within the upper reaches of the bay appears to be on the order of 2 or more days.

3. The patterns of transport indicated by this research are not a function of processes occurring on a seasonal, weekly, or even annual basis. Interactions among forcing mechanisms and the predominance of one or more forces fluctuates daily; consequently seasonal classification of properties which are strongly controlled by transport is difficult, if not impossible. Therefore, results suggest that the seasonal classification of oyster-growing waters as open or closed based on the probability for sewage dispersal and or concentration is not recommended. The highest probability for contamination in the bay's upper reaches appears to occur following cold-front passage and heavy precipitation over the drainage basin. However, interactions with the coastal ocean which could induce rising sea levels within the bay, and other combinations of wind and tide could also minimize dilution of materials entering the bay, as well as transport them back up into the highly productive shallow inlets up-estuary. The author recommends that management strategies, which have the goal of protecting the public and the oyster fishing industry, should focus more on purification processes following harvest and effective treatment of sewage prior to discharge, than in predicting processes dependent on the ever-changing and highly complex nearshore waters of coastal bay's in south Louisiana.

4. One of the difficulties in environmental management is its multidisciplinary nature. Research during this study exemplified both the advantages and disadvantages of multidisciplinary research. By combining techniques from mathematical modeling and oceanography, it is possible to better understand complex processes within the physical environment. However, during the research process the perspective of scientists with differing backgrounds may be difficult to integrate. For example, the theoretical oceanographer suggests the use of an eddy viscosity value as theory predicts whereas the modeler suggests that which makes the model stable. Without the proper background, the researcher cannot choose the appropriate value, or justify it once chosen. In a similar way, numerical models such as used here are not yet appropriate for use by environmental management personnel without a solid multidisciplinary background. One must not only understand the basic ecological and physical processes involved in a given problem, but also be able to decide if a model is appropriate for a particular environment, and if not, are simple modifications possible. In addition to learning how to run the model used here, it was necessary for the author to make modifications to incorporate the forcing mechanisms appropriate to the bay being studied. Furthermore, it is also essential that those using these types of techniques are aware of their limitations and weaknesses, e.g., though relatively infrequent, during periods of weak forcing and strong runoff when bay water may become stratified, two-dimensional modeling is unable to accurately simulate circulation within the bay which was studied. Therefore, the author also

concludes that while modeling techniques are potentially extremely useful for environmental management purposes, the user must have a broad, and solid background in the physical sciences involved to apply a model and interpret the results correctly.

REFERENCES

Anderson, I.C., Rhodes, M., and H. Kator, 1979, Sublethal Stress in *Escherichia coli*: a Function of Salinity, Appl. and Environ. Microbiology, v. 38(6): 1147-1152.

American Public Health Association, 1980, Standard Methods for Examination of Water and Waste Water, 15th ed., American Public Health Association, Washington, DC.

Berg, G., 1973, Viruses in Waste, Renovated, and Other Waters, U.S. Environmental Protection Agency Publ. EPA-670/9-74-005, Cincinnati Ohio.

Bonde, G.J., 1974, Bacterial Indicators of Sewage Pollution, In: Discharge of Sewage from Sea Outfalls, A.L.H. Gameson ed., Pergamon Press: 37-46.

Bowden, K.F., 1967, Circulation and diffusion, In: Estuaries, G.H. Lauff ed., American Association for the Advancement Science, Pub. No. 83: 15-36.

Brebbia, C.A., and Connor, J.J., 1973, Fundamentals of Finite Element Techniques, Butterworths, London, England.

Callaway, R.J., 1974, Subsurface Horizontal Dispersion of Pollutants in Open Coastal Waters, In: Discharge of Sewage from Sea Outfalls, A.L.H. Gameson ed., Pergamon Press: 297-307.

Cederwall, K., Goransson, C-G, and T.S. Svensson, 1974, Subsequent Dispersion-Methods of Measurement, In: Discharge of Sewage from Sea Outfalls, A.L.H. Gameson ed., Pergamon Press: 309-319.

Christensen, B.A.,1983, Hydrodynamics of Apalachicola Bay System, In: Apalachicola Oyster Industry: Conference Proceedings, S. Andree ed.: 10-17.

Cole, M.T., Kilgen, M.B., Reily, L.A., and C.R. Hackney, 1986, Detection of Enteroviruses and Bacterial Indicators and Pathogens in Louisiana Oysters and Their Overlying Waters, Jour. Food Protection, v. 49(8): 596-601.

Colwell, R.R, and J. Kaper, 1978, Distribution, Survival, and Significance of Pathogenic Bacteria and Viruses in Estuaries, In: Estuarine Interactions, Academic Press, Inc.: 443-457.

Dinnel, S.P., and W.J. Wiseman, Jr., 1986, Fresh water on the Louisiana and Texas shelf, Continental Shelf Research, v. 6(6): 765-784.

Dronkers, J.J., 1964, Tidal Computations in Rivers and Coastal Waters, North-Holland Publishing Co., Amsterdam, Netherlands.

Ellender, R.D., Mapp, J.B., Middlebrooks, B.L., Cook, E.W., and E.W. Cake, 1980, Natural Enterovirus and Fecal Coliform Contamination of Gulf Coast Oysters, Jour. Food Protection, v. 43: 105-110.

Elliott, A.J., 1978, Observations of the Meteorologically Induced Circulation in the Potomac Estuary, Estuarine Coastal Marine Science, v. 6: 285-300.

Faust, M.A., Aotaky, A.E., and M.T. Hargadon, 1975, Effect of Physical Parameters on the In Situ Survival of *Escherichia coli* MC-6 in an Estuarine Environment, Applied Microbiology, v. 30(5): 800-806.

Fischer, H.B., 1974, Numerical Modeling of Dispersion in Estuaries, In: Discharge of Sewage from Sea Outfalls, A.L.H. Gameson ed., Pergamon Press: 371-380.

Gunter, G., 1963, The Fertile Fisheries Crescent, Jour. Miss. Acad. Sci., v. 9: 286-290.

Gunter, G., 1967, Some Relationships of Estuaries to Fisheries of the Gulf of Mexixo, In: Estuaries, G.H. Lauff ed., AAAS Pub. No. 83: 621-638.

Kilgen, M.B., Dantin, T.J., and Kilgen, R.H., 1985, Assessment of sources of sewage contamination of Terrebonne Parish Oyster growing waters, Nicholls State University and Louisiana Universities Marine Consortium, Thibodaux, Louisiana.

Kilgen, M.B. and R.H. Kilgen, 1990, State of Louisiana Lower Atchafalya-Barataria Basin Sanitary Survey Report, Volume I, LA Office of Public Health, Oyster Water Monitoring Division, 76 p.

Kjerfve, B.J., 1973, Dynamics of the Water Surface in a Bar-Built Estuary, Ph.D. diss., Louisiana State University, Baton Rouge, 90 p.

Kjerfve, B., 1975, Tide and Fair-Weather Wind Effects in a Bar-Built Louisiana Estuary, In: Estuarine Research, Geology and Engineering, v. 2, L. E. Cronin ed.: 345-363.

Kolb, C.R., and J.R. Van Lopik, 1958, Geology of the Mississippi deltaic plain - southeaster Louisiana: Coastal Environments, Inc., Baton Rouge, Louisiana, 6 p.

Lee, J.M., Wiseman, W.J., and F.J. Kelly, Barotropic, Subtidal Exchange Between Calcasieu Lake and the Gulf of Mexico, Estuaries, v. 13(3): 258-264.

Leendertse, J.J., 1967, Aspects of a Computational Model for Long-Period Water-Wave Propagation, Memorandum, RM-5294-PR, Rand Corporation, Santa Monica, California.

Leendertse, J.J., 1970, A Water-quality Simulation Model for Well-mixed Estuaries and Coastal Seas: Vol. I, Principles of Computation, Memo. RM-6230-RC, The Rand Corporation, Santa Monica, Calif.

Limerinos, J.T., 1970, Determination of the Manning Coefficient From Measured Bed Roughness in Natural Channels, Geological Survey Water-Supply Paper 1898-B, 47 p.

Lousiana Universities Marine Consortium, 1989, Environmental Impact of Produced Water Discharges in Coastal Louisiana, D.F. Boesch and N.N. Rabalais eds., LA Div. Mid-Continent Oil and Gas Association, 287 p.

Metcalf, T.G., 1974, Evaluation of Shellfish Sanitary Quality by Indicators of Sewage Pollution, In: Discharge of Sewage From Sea Outfalls, A.L.H. Gameson ed., Pergamon Press: 75-83.

Munro, D., 1974, Observed and Predicted Coliform Distributions near a Sea Outfall, In: Discharge of Sewage from Sea Outfalls, A.L.H. Gameson ed., Pergamon Press: 353-362.

Murray, S.P., 1976, Currents and Circulation in the Coastal Waters of Louisiana, Technical Report No. 210, Coastal Studies Institute, Louisiana State University, Baton Rouge, Louisiana, 35 p.

National Oceanic and Atmospheric Administration, 1990, Tide Tables, east coast of North and South America, Ocean Survey, Rockville, MD.

Okubo, A., 1970, Oceanic Mixing, Technical Report No. 62, Chesapeake Bay Institute, The John Hopkins University, 120 p.

Okubo, A., 1973, Effect of Shoreline Irregularities on Streamwise Dispersion in Estuaries and Other Embayments, Netherlands Journal of Sea Research, v. 6(1-2): 213-224.

Okubo, A., 1975, Some Speculations on Oceanic Diffusion Diagrams, Rapp. P.-v Reun. Cons. Int. Explor. Mer, v. 167: 77-85.

Perkins, F.O., Haven, D.S., Morales-Alamo, R., and M. W. Rhodes, 1980, Uptake and Elimination of Bacteria in Shellfish, Jour. Food Protection, v. 43(2): 124-126.

Postma, H., 1967, Sediment Transport and Sedimentation in the Marine Environment, In: Estuaries, G.H. Lauff ed., Amer. Assoc. Advanc. Sci., Publication No. 83: 158-186.

Pritchard, D.W., 1967, Observations of Circulation in Coastal Plain Estuaries, In: Estuaries, G.H Lauff ed., American Association for the Advancement of Science, Publication. No. 83: 37-44.

Pritchard, D.W., 1971, Hydrodynamic Models, In Estuarine Modeling: An Assessment, Water Pollution Control Research Series, TRACOR, Inc., for EPA.

Reid, R.O., and B.R. Bodine, 1968, Numerical Model for Storm Surges in Galveston Bay, Jour. Waterways and Harbors Div., ASCE, v. 94(WWI): 33-57.

Roberts, H.H., Huh, O.K., Hsu, S.A, Rouse, L.J. Jr., and D.A. Rickman, 1987, Impact of Cold-Front Passages on Geomorphic Evolution and Sediment Dynamics of the Complex Louisiana Coast, American Society of Civil Engineers, Proceedings, Coastal Sediments '87: 1950-1963.

Roberts, H.H., Huh, O.K., Hsu, S.A, Rouse, L.J. Jr., and D.A. Rickman, 1989, Winter Storm Impacts on the Chenier Plain Coast of Southwestern Louisiana, Transactions-Gulf Coast Assoc. Geol. Sci., v. XXXIX: 515-522.

Schroeder. W.W., and W.J. Wiseman, Jr., 1986, Low-frequency shelf-estuarine exchange processes in Mobile Bay and other estuarine systems on the northern Gulf of Mexico, In: Estuarine Variability, D. A. Wolfe, ed., Academic Press: 355-367.

Smith, N.P., 1977, Meteorological and tidal exchanges between Corpus Christi Bay, Texas and the northwestern Gulf of Mexico, Estuarine and Coastal Marine Science, v. 5: 511-520.

Smith, N.P., 1990, Computer Simulation of Tide-Induced Residual Transport in a Coastal Lagoon, Jour. Geophys. Res., v. 95(C10): 18,205-18,211.

Sobsey, M.D., Hackney, C.R., Carrick, R.J., and M.L. Speck, 1980, Occurence of Enteric Bacteria and Viruses in Oysters, Jour . Food Protection, v. 43(2): 111-113.

Thornthwaite, c.W., 1948, An Approach Toward a Rational Classification of Climate, Geog. Rev., v. 38: 55-94.

van Leussen, W., 1991, Fine Sediment Transport under Tidal Action, Geo-Marine Letters, v. 11: 119-126.

Waldron, R.P., 1963, A Seasonal Ecological Study of Foraminifera from Timbalier Bay, Louisiana, United States Gulf Coastal Studies, Tech. Rep. No. 16 (Part B), Coastal Studies Institute, Louisiana State University, 188 p.

Wang, D-P., and A.J. Elliot, 1978, Nontidal Variability in the Chesapeake Bay and Potomac River: Evidence for nonlocal forcing, Jour. Phys. Oceanogr., v. 8: 225-232.

Wang, J.D., 1978, Real Time Flow in Unstratified Shallow Water, Jour. Waterway, Port, Coastal and Ocean Div., ASCE, v. 104: 53-68.

Wang, J.D., and Connor, J.J., 1975, Mathematical Modeling of Near Coastal Circulation, Report No. 200, R.M. Parsons Laboratory for Water Resources and Hydrodynamics, MIT, Cambridge, Massachusetts, 272 p.

Willmott, C.J., Ackleson, S.G., Davis, R.E., Feddema, J.J., Klink, K.M., D.R. Legates, J. O"Donnell, and C.M. Rowe, 1985, Statistics for the Evaluation and Comparison of Models, Jour. Geophys. Res., v. 90 (C5): 8995-9005.

Wiseman, W.J. Jr., Swenson, E.M., and F.J. Kelly, 1990, Control of Estuarine Salinities by Coastal Ocean Salinity, Coastal and Estuarine Studies, v. 38: 184-193.

Zienkewicz, O.C., 1971, The Finite Element Method in Engineering Sciences, McGraw-Hill Book Co., Inc., New York, N.Y.

APPENDIX A

Procedure to convert water level recorder pressure measurements to depth

Raw pressure data taken from the tide gage in the mouth of Terrebonne Bay was in mbars. The first step of the procedure was to convert the values to atmospheres and remove the effect of atmospheric pressure:

$$1 \text{ mbar} = 9.8692 \times 10^{-3} \text{ atm.} - 1 \text{ atm}$$

Variability in atmospheric pressure is neglected for simplicity, and because the time scales being considered are relatively short as compared to weather time scales, but long compared to tidal time scales.

The pressure values were then converted to feet of seawater:

$$1 \text{ atm.} = 0.29499 \text{ feet} * \frac{1025}{1000}$$

To determine the variation about the mean water level, an average value was then calculated over the time period being considered, and then subtracted from each value. Because it was this variation that was important and not absolute values, the depth of the instrument was not removed. The final value was then converted to meters and used as input for open boundaries at the mouth of the Bay.

APPENDIX B

Tables 17 - 20

Table 17: Results of particle tracking for release at the beginning of ebb for lower bay group.

	TRANSPORT*				
Model Run	East (+)/ West (-) (m)	North (+)/ South (-) (m)	Total (m)	Rate (cm/s)	Direction
(1 Tide)					
3/24	-659	-2020	2127	2.36	SW
3/28	-1561	-2732	3178	3.53	SW
4/1	-5274	-6127	8086	8.98	SW
6/25	-325	-1676	2238	2.49	SW
6/27	173	-103	316	0.35	SE
7/1	-1467	-3130	3500	3.89	SW
7/4	-2440	-3702	4475	4.97	SW
9/8	572	-135	648	0.72	SE
9/12	-1087	-2402	2261	2.51	SW
9/16	-429	-1571	1636	1.82	SW
9/18	3	-611	629	0.70	SE
12/5	-4021	-4686	6220	6.91	SW
12/9	-127	-1223	1239	1.38	SW
12/13	-1065	-2574	2811	3.12	SW
Avg.	-1265	-2335	2812	3.12	SW
Std. Dev.	1593	1643	2129	2.37	
(2 Tides)					
3/24	-1079	-4640	4771	2.65	SW
3/28	-6594	-7681	10147	5.64	SW
4/1	-7870	-9379	12246	6.80	SW
6/25	-1793	-3402	4324	2.40	SW
6/27	-204	-1615	1636	0.91	SW
7/1	-3942	-4806	6230	3.46	SW
7/4	-5397	-6322	8323	4.62	SW
9/8	1076	-249	1230	0.68	SE
9/12	-3321	-4657	5745	3.19	SW
9/16	-705	-2538	2654	1.47	SW
9/18	35	-1371	1392	0.77	SE
12/5	-6513	-7325	9808	5.45	SW
12/9	-815	-1954	2141	1.19	SW
12/13	-3929	-4917	6314	3.51	SW
Avg.	-2932	-4347	5497	3.05	SW
Std. Dev.	2743	2576	3446	1.91	
(3 Tides)					
3/28	-7526	-9173	11946	4.42	SW
4/1	-7604	-10245	12768	4.73	SW
6/27	-395	-2537	2575	0.95	SW
7/1	-5639	-6976	8896	3.29	SW
7/4	-6246	-8100	10247	3.80	SW
9/8	-1890	-3707	4248	1.57	SW
9/12	-5044	-6563	8284	3.07	SW
9/18	-384	-3220	3248	1.20	SW
12/9	-1956	-3991	4472	1.66	SW
12/13	-5394	-6528	8481	3.14	SW
Avg.	-3825	-5549	6264	2.78	SW
Std. Dev.	2805	2967	4231	1.29	

* Based on the position of the particle group center

Table 18: Results of particle tracking with release at mid-ebb for lower bay group.

TRANSPORT*					
Model Run	East (+)/ West (-) (m)	North (+)/ South (-) (m)	Total (m)	Rate (cm/s)	Direction
(1 Tide)					
3/24	-493	-1379	1469	1.63	SW
3/28	-1723	-2693	3268	3.63	SW
4/1	-5226	-5878	7866	8.74	SW
6/25	-101	-1152	1169	1.30	SE
6/27	74	-218	315	0.35	SE
7/1	-1090	-2577	2841	3.16	SW
7/4	-1618	-3337	3763	4.18	SW
9/8	712	-16	721	0.80	SE
9/12	-522	-1663	1774	1.97	SW
9/16	-382	-1576	1625	1.81	SW
9/18	-29	-674	685	0.76	SW
12/5	-3348	-4098	5317	5.91	SW
12/9	-95	-1286	1292	1.44	SW
12/13	-503	-1700	1787	1.99	SW
Avg.	-1074	-2052	2421	2.69	SW
Std. Dev.	1559	1586	2005	2.23	
(2 Tides)					
3/24	-659	-2859	2948	1.64	SW
3/28	-5719	-6627	8763	4.87	SW
4/1	-7733	-8821	11734	6.52	SW
6/25	-591	-2247	2357	1.31	SW
6/27	-257	-1159	1198	0.67	SW
7/1	-2926	-4050	5070	2.82	SW
7/4	-4356	-6161	7564	4.20	SW
9/8	1354	-104	1388	0.77	SE
9/12	-1715	-3584	4010	2.23	SW
9/16	-614	-2473	2559	1.42	SW
9/18	-73	-1733	1744	0.97	SW
12/5	-4536	-4495	6392	3.56	SW
12/9	-611	-1742	1862	1.03	SW
12/13	-1674	-3280	3719	2.07	SW
Avg.	-2150	-3524	4379	2.43	SW
Std. Dev.	2465	2280	3051	1.70	
(3 Tides)					
3/28	-7276	-8250	11026	4.08	SW
4/1	-9738	-7517	12313	4.56	SW
6/27	-306	-1819	1859	0.69	SE
7/1	-4518	-5744	7328	2.71	SW
7/4	-5327	-7866	9526	3.52	SW
9/8	-534	-2716	2894	1.07	SW
9/12	-3476	-5057	6159	2.28	SW
9/18	-384	-3220	3892	1.44	SW
12/9	-1533	-4053	4374	1.62	SW
12/13	-3392	-5066	6147	2.28	SW
Avg.	-3648	-5131	6552	2.43	SW
Std. Dev.	2999	2119	3320	1.23	

* Based on the position of the particle group center following one, two or three tides

Table 19: Results of particle tracking for release at the beginning of flood for lower bay group.

TRANSPORT*					
Model Run	East (+)/ West (-) (m)	North (+)/ South (-) (m)	Total (m)	Rate (cm/s)	Direction
(1 Tide)					
3/24	-551	2335	2437	2.71	NW
3/28	156	-688	728	0.81	SE
4/1	-105	-414	632	0.70	SW
6/25	100	-155	433	0.48	SE
6/27	420	130	508	0.56	NE
7/1	-69	-1399	1421	1.58	SW
7/4	94	-139	423	0.47	SE
9/8	200	-829	866	0.96	SE
9/12	14	-22	417	0.46	SE
9/16	74	-7	454	0.50	SE
9/18	68	-626	651	0.72	SE
12/5	-113	-1436	1455	1.62	SW
12/9	-47	-1206	1223	1.36	SW
12/13	11	251	571	0.63	NE
Avg.	18	-300	873	0.97	SE
Std. Dev.	207	907	557	0.62	
(2 Tides)					
3/24	-692	1961	2116	1.18	NW
3/28	156	-688	728	0.40	SW
4/1	-1359	-4021	4274	2.37	SW
6/25	148	86	763	0.42	NE
6/27	758	519	968	0.54	NE
7/1	-541	-2917	2987	1.66	SW
7/4	-112	-576	863	0.48	SW
9/8	366	-961	1133	0.63	SE
9/12	-61	-413	851	0.47	SW
9/16	-415	2119	2193	1.22	NW
9/18	68	-626	1180	0.66	NE
12/5	-1690	-4389	4732	2.63	SW
12/9	-401	-2755	2800	1.56	SW
12/13	14	-662	894	0.50	SE
Avg.	-269	-952	1892	1.05	
Std. Dev.	631	1893	1299	0.72	
(3 Tides)					
3/28	-1508	-4653	4925	1.82	SW
4/1	-3127	-5192	6082	2.25	SW
6/27	1293	254	1325	0.49	NE
7/1	-1376	-3843	4114	1.52	SW
7/4	-323	-1009	1540	0.57	SW
9/8	291	-1754	1909	0.71	SE
9/12	-238	-1080	1535	0.59	SW
9/18	-430	995	567	0.21	SW
12/5	-22	-159	2594	0.97	SE
12/9	-734	-2432	3185	1.18	SW
12/13	-728	-3079	937	0.35	SE
Avg.	-627	-1996	2610	0.97	SW
Std. Dev.	1078	1938	1690	0.63	

* Based on the position of the particle group center

Table 20: Results of particle tracking for release at mid-flood for lower bay group.

TRANSPORT*					
Model Run	East (+)/ West (-) (m)	North (+)/ South (-) (m)	Total (m)	Rate (cm/s)	Direction
(1 Tide)					
3/24	44	400	597	0.66	NE
3/28	-268	-1553	1609	1.79	SW
4/1	-824	-1556	1788	1.99	SW
6/25	115	-354	410	0.46	SE
6/27	300	276	450	0.50	NE
7/1	-461	-2286	2338	2.60	SW
7/4	-204	-1444	1465	1.63	SW
9/8	225	-1152	1182	1.31	SE
9/12	-14	-511	534	0.59	SW
9/16	31	-344	424	0.47	SE
9/18	-29	-778	804	0.89	SW
12/5	-492	-1723	1805	2.01	SW
12/9	-129	-1274	1291	1.43	SW
12/13	-1	14	287	0.32	NW
Avg.	-137	-919	1070	1.19	SW
Std. Dev.	302	800	633	0.70	
(2 Tides)					
3/24	22	-431	783	0.44	SE
3/28	-1856	-5239	5579	3.10	SW
4/1	-3785	-6390	7451	4.14	SW
6/25	102	-897	935	0.52	SE
6/27	670	247	812	0.45	NE
7/1	-1132	-3254	3453	1.92	SW
7/4	-597	-2321	2403	1.34	SW
9/8	499	-1615	1699	0.94	SE
9/12	-156	-1594	1618	0.90	SW
9/16	9	-50	551	0.31	SE
9/18	125	449	651	0.31	NE
12/5	-2488	-1136	4303	2.39	SW
12/9	-560	-2503	2572	1.42	SW
12/13	-97	-1038	1065	0.59	SW
Avg.	-660	-1841	2420	1.34	SW
Std. Dev.	1212	1925	2018	1.12	
(3 Tides)					
3/28	-3539	-5800	6835	2.53	SW
4/1	-5943	-7200	9380	3.47	SW
6/27	1215	-248	1375	0.51	SE
7/1	-1953	-3912	4386	1.62	SW
7/4	-1247	-3524	3755	1.39	SW
9/8	76	-2100	2493	0.92	SE
9/12	-650	-3142	3226	1.19	SW
9/18	-26	-881	966	0.36	SW
12/5	-1048	-3307	3540	1.31	SW
12/9	-850	-2973	3102	1.15	SW
12/13	-58	-1361	1394	0.52	SW
Avg.	-1275	-3133	3678	1.36	SW
Std. Dev.	-1885	1959	2390	0.89	

* Based on the position of the particle group center

VITA

Ellen Joyce Prager was born April 30, 1962 in Bethpage, New York. She is the second of two children born to Lawrence and Phyllis Prager of Sudbury, Massachusetts. She graduated from Lincoln-Sudbury Regional High School in June, 1980. In May, 1984 she received a Bachelor of Arts degree, majoring in environmental studies with a concentration in geology, from Wesleyan University in Middletown, Connecticut. She earned a Master of Science degree in marine geology and geophysics from the University of Miami in 1987, and wrote a thesis titled *The Growth and Structure of Calcareous Nodules on Florida's Outer Shelf.* In August, 1988 she entered the Ph.D. program at Louisiana State University

DOCTORAL EXAMINATION AND DISSERTATION REPORT

Candidate: Ellen J. Prager

Major Field: Geology

Title of Dissertation: Modeling of Circulation and Transport in Terrebonne Bay, Louisiana and Its Implications for Oyster Harvesting Management

Approved:

Major Professor and Chairman

Dean of the Graduate School

EXAMINING COMMITTEE:

Date of Examination:

April 3, 1992